eman ta zabal zazu
Universidad del País Vasco
Euskal Herriko Unibertsitatea

Fabrication and Characterization of Multilayered Assemblies based on Polyelectrolytes and Hybrid Systems with Carbon Nanomaterials for Applications in Nanofiltration and as Smart Surfaces

Joseba Irigoyen Otamendi

CIC biomaGUNE
Biomaterialetako Ikerkuntza Kooperatiboko Zentroa
Centro de Investigación Cooperativa en Biomateriales

Fabrication and Characterization of Multilayered Assemblies based on Polyelectrolytes and Hybrid Systems with Carbon Nanomaterials for Applications in Nanofiltration and as Smart Surfaces

Dissertation presented to the

Department of Ciencia y Tecnología de Polímeros

of the Basque Country (UPV/EHU), Donostia-San Sebastián

for the degree of

Doctor in Applied Chemistry and Polymeric Materials

Presented by

Joseba Irigoyen Otamendi

Thesis Supervisor: Dr. Sergio E. Moya

University Tutor: Dr. Antxon Santamaria

eman ta zabal zazu

Universidad del País Vasco Euskal Herriko Unibertsitatea

Donostia-San Sebastián 2016

Agradecimientos | Acknowledgments

En primer lugar me gustaría agradecer a mi director de tesis Dr. Sergio E. Moya por su apoyo, por abrirme las puertas al mundo de la investigación y por las oportunidades ofrecidas durante el desarrollo de este trabajo. Esta tesis no solo me ha dado la oportunidad de crecer profesionalmente sino personalmente; muchas experiencias vividas, los viajes, los diferentes entornos de trabajo, gente que he podido conocer y que me han hecho conocerme mejor a mi mismo y crecer como persona.

Realizar una tesis a caballo entre San Sebastián y múltiples lugares por todo el mundo no ha sido tarea fácil, aunque obviamente tiene muchos aspectos positivos también hay experiencias duras y momentos no tan placenteros, el apoyo de mi familia siempre ha sido un pilar en mi vida y saber que tengo su respaldo incondicional siempre ha sido un paracaídas para aventurarme a vivir nuevas experiencias. ¡Os quiero familia!

Tengo que agradecer como no a todos los compañeros del laboratorio, Soft Matter Nanotechnology Group. En especial a Gabriela Romero, la bigotes, aún me acuerdo cuando llegaste el primer día todo peripuesta recién llegada de México y te volviste hecha toda una vasquita a comerte el mundo, gracias por los momentos pasados juntos y el apoyo que has sido siempre. María Echeverria muchas gracias por compartir tu neurona conmigo, ese sentido del humor tan parecido que tenemos y las conversaciones escatológicas que nadie

entiende, he descubierto una amiga que espero sea para muchos años. Eleftheria Diamanti, quien iba a pensar que una griega nula en geografia iba a tener tantas cosas en común conmigo, aún recuerdo en Argentina cuando salimos a comprar la mochila mas barata del mundo, o en Berlin cuando me rescataste de mi vida de fantasma. Nikolaos Politakos, el futuro marido, y tu siempre sereis mis griegos favoritos, aunque él parezca mexicano. Richard Murray, ¿quién necesita a google translator si tienes un amigo irlandes con el que encima te puedes ir de cañas?, gracias por todo el apoyo en el trabajo pero especialmente por ser un buen amigo. Ane Escobar aunque por poco tiempo eres la mejor poligonera de Irun multifacetas que he conocido, te deseo muchos éxitos y que encuentres el mejor goxoki del mundo. Podría hacer una dedicatoria personalizada para todos ellos, pero entonces necesitaría otra tesis solo para eso, así que gracias también a Elena, Ángel, Yuan, Danijela, Guocheng, Patrizia, Dessire, Marija, Teodoro a quien se me olvide y como no a todas las visitas que hemos tenido tanto de Argentina, Brasil, Alemania y China. Os deseo muchos éxitos a todos.

También me gustaría agradecer especialmente a Mihaela, Jagoba e Ixi, Aitziber e Irantzu, amigos de otra epoca vivida en biomaGUNE pero que aún siguen estando ahí y con quien siempre puedo contar. Y a mis compañeros de Pamplona: Paula N., Luis, Sagrario, Iñaki, Paula C. y Uxua.

Por último me gustaría agradecer aquellas personas que me hicieron sentir como en casa durante los viajes realizados, Eduar Gutierrez en Argentina, Wang Bing en China y los Marcelos en Brasil, ¡gracias por todo!

Index

POLYELECTROLYTE MULTILAYERS

HYBRID SYSTEMS CARBON NANOMATERIALS/POLYELECTROLYTES

List of figures

Introduction

Chapter 1 | Materials and methods

List of tables

Abstract

This PhD thesis is mainly focused on the development of hybrid materials based on polyelectrolytes (PEs) and carbon nanomaterials assembled Layer by Layer, for the fabrication of membranes with applications for water treatment, for the templating of capsules and the development of smart surfaces. In parallel we have performed extensive physico-chemical characterization of the fabricated systems with emphasis on their permeability, ionic conductance and stability in different media.

This thesis is divided in two; the first section is purely focused on multilayered structures based in polyelectrolytes, while the second section pertains to hybrid systems of carbon nanomaterials and polyelectrolytes.

POLYELECTROLYTE MULTILAYERS

In chapter 2, a comparison between two polyelectrolyte multilayers (PEMs) with the same polyanion but different polycations with quaternary amines showing different growth regimes has been presented; poly (diallyl dimethyl ammonium chloride) (PDADMAC)/ poly (sodium 4-styrenesulfonate) (PSS) shows a supralinear growing regime while multilayers of poly (vinylbenzyltrimethylammonium chloride) (PVBTMAC)/PSS display a linear growing regime. Both multilayer systems are assembled in the same conditions. Contact angle measurements were made for both PEM systems as a function of the number of layers. Cyclic voltammetry and impedance spectroscopy studies reveal that although both multilayer systems show similar

insulating responses, the way the electrons are transferred along the film to the surface of the electrode for the redox reaction between $K_4Fe(CN)_6$ and $K_3Fe(CN)_6$ is different. A particular phenomenon of complexation between PDADMAC/PSS and the ferro species occurs once 11 layers are assembled; the multilayer behaves as an electron regulating interface modifying the way the charge transfer is produced.

In chapter 3, regenerable polyelectrolyte membranes have been prepared on the basis of di-block polyelectrolyte multilayers (PEM) with a sacrificial top block of polyelectrolytes on top of a non-removable PEM. The di-block PEM fabrication is envisaged as a strategy for foulant removal and surface cleaning and regeneration. Different protocols for PEM removal have been followed according to the specific polyelectrolyte combination employed for the fabrication of the top block.

Non removable supporting PEM blocks were fabricated with polyelectrolyte combinations not affected by the stimuli used to remove the top block.

Bovine Serum Albumine (BSA) was used as a model foulant. For all di-block PEMs coated with BSA on top, the BSA was removed with the top block or with part of the top block, which could later be regenerated.

In chapter 4, responsive PEMs of PDADMAC and PSS with thicknesses between 350 nm and 400 nm for 11 deposited polyelectrolyte layers were fabricated by assembling polyelectrolytes at 3 M NaCl. When the bulk solution

(3 M NaCl) is exchanged for water, the PEMs release water, approximately 46 % of the total mass, and experience a reduction in thickness of more than 200 nm. These changes in thickness and water content are fully reversible. The film recovers its original thickness and water content when it is exposed again to a 3 M NaCl solution. A responsive polymer film is achieved with the capability of swelling at high ionic strength and collapsing in water with variations in thickness of hundreds of nanometers. Such a film could have applications as a nanoactuator or for the fabrication of responsive barriers.

HYBRID SYSTEMS CARBON NANOMATERIALS/POLYELECTROLYTES

In chapter 5, a PEM of PDADMAC and PSS has been deposited on top of a thick layer micrometer range of multiwalled carbon nanotubes (MWCNTs) assembled on a porous SiC tubular membrane support. MWCNTs are assembled "Layer by Layer" (LbL) by alternately depositing oxidized carbon nanotubes (CNTs) and poly (allylamine hydrochloride) (PAH) modified CNTs. The MWCNT layer is crosslinked by annealing after assembly. The MWCNT layer acts as a spacer between the PDADMAC/PSS PEM and the SiC support. The MWCNT support increases water permeability by 42% compared to the PEMs deposited without MWCNTs. Hybrid MWCNT-PEM membranes show high rejection for divalent ions, which increases directly with flux. A rejection rate of up to 92 % was measured for $MgSO_4$ and up to 60 % rejection rate difference between $MgCl_2$ and NaCl, making the hybrid MWCNT PEMs highly appealing for nanofiltration and mono and divalent ion separations.

In chapter 6, a novel and facile method was developed to produce hybrid graphene oxide (GO)-polyelectrolyte capsules using erythrocyte cells as templates. The capsules are easily produced through the Layer by Layer technique using the alternating deposition of polyelectrolyte layers of PAH as the polycation and PSS as the polyanion and GO sheets. The amount of GO, and therefore its coverage, in the resulting capsules can be tuned by adjusting the concentration of the GO dispersion during the assembly. The capsules retain the approximate shape and size of the erythrocyte template after the latter is fully removed by oxidation with NaOCl in water. The PE/GO capsules maintain their integrity and can be placed or located on other surfaces such as in a device. When the capsules are dried in air, they collapse to form a film that is approximately twice the thickness of the capsule membrane. AFM images in the present study suggest a film thickness of ~ 30 nm for the capsules in the collapsed state implying a thickness of ~ 15 nm for the layers in the collapsed capsule membrane.

Resumen

El contenido de esta tesis está principalmente enfocado al desarrollo de materiales híbridos basados en polielectrolitos y nanomateriales de carbono ensamblados mediante la técnica "capa a capa" con el objetivo de fabricar membranas con aplicaciones en tratamiento de agua, el desarrollo de superficies inteligentes y la producción de cápsulas. En paralelo se ha realizado una extensa caracterización fisico-química de los sistemas fabricados con un especial énfasis en su permeabilidad, conductividad iónica y estabilidad en diferentes medios.

Esta tesis la hemos agrupado en dos partes; una primera parte enfocada en estructuras multicapa únicamente basadas en polielectrolitos y una segunda parte en la que se discuten los sistemas híbridos compuestos por materiales basados en carbono en combinación con polielectrolitos.

MULTICAPAS DE POLIELECTROLITOS

La caracterización fisico-química de multicapas de polielectrolitos es fundamental para poder ensamblarlos en condiciones óptimas que permita controlar posteriormente su desempeño en las aplicaciones requeridas.

En el capítulo dos se ha realizado un estudio comparativo de dos tipos de multicapas fabricadas "capa a capa"que presentan regímenes de crecimiento diferente. Se han comparado dos pares de polielectrolitos con un mismo polianión, PSS, pero que difieren en el policatión, por un lado poly (diallyl

dimethyl ammonium chloride) (PDADMAC) que en combinación con poly (sodium 4-styrenesulfonate) (PSS) presenta un régimen de crecimiento supralineal y por otro lado poly (vinylbenzyltrimethylammonium chloride) (PVBTMAC) cuyo crecimiento es lineal. Se estudió la variación del ángulo de contacto con el número de capas ensambladas. Mediante estudios electroquímicos de voltametría cíclica y espectroscopía por impedancia se ha observado que ambas multicapas presentan una capacidad aislante bastante similar, sin embargo la manera en que la transferencia de electrones se produce para dar lugar a la reacción de oxidación-reducción entre las especies $K_4Fe(CN)_6$ y $K_3Fe(CN)_6$ utilizadas como sonda es diferente. A partir de la onceava capa en el sistema PDADMAC/PSS se produce la formación de un complejo entre las especies electroquímicas usadas como sonda y el policatión, PDADMAC, la multicapa empieza a actuar como una interfaz reguladora de electrones, modificando así la manera en que se produce la transferencia de carga.

En el capítulo tres se han efectuado estudios de estabilidad de la multicapa frente a agentes externos con el efecto de producir membranas de polielectrolitos regenerables y con propiedades "antiincrustantes"; adherencia de material orgánico que inhabilita o perjudica el desempeño del proceso de filtrado.

La metodología de trabajo seguida se basó en la preparación de di-bloques de multicapas de polielectrolitos; un primer bloque sobre el que el estímulo externo no es eficaz y un segundo bloque depositado sobre este primero que sea

total o parcialmente removido ante el estímulo. Este segundo bloque puede ser reconstruido a posteriori. Se han seguido diferentes protocolos de deconstrucción y regeneración de este segundo bloque en función de la combinación de polielectrolitos elegida para cada sistema. Como test antiincrustante se ha depositado albumina de suero bovino, como modelo de incrustación, sobre la multicapas y se ha comprobado que es posible remover la proteína con el bloque superior o parte de él aplicando el estímulo apropiado.

La fuerza iónica es una de los parámetros que influyen de manera más relevante tanto durante el ensamblado de las multicapas como al ser aplicado a posteriori sobre las mismas.

En el capítulo cuarto se han fabricado multicapas de polielectrolitos responsivas constituidas por PDADMAC y PSS que alcanzan espesores entre 350 nm y 400 nm para 11 capas depositadas al ser ensambladas bajo condiciones de fuerza iónica altas como 3M NaCl. Tras el ensamblado al someterlas a agua pura sin ningún contenido en sal, se produce un efecto de colapso de la multicapa por efecto de la liberación del agua que contenía internamente, aproximadamente un 46% del agua total retenida es liberada produciendo una disminución de alrededor de 200 nm en el espesor de la multicapa. Estos cambios en el contenido de agua y por consiguiente en su espesor son totalmente reversibles, volviendo a su estado original una vez se somete a una solución de 3M NaCl nuevamente. Este tipo de films puede ser utilizado como nano interruptor o en la fabricación de barreras responsivas.

SYSTEMAS HÍBRIDOS EN BASE A NANOMATERIALES DE CARBONO Y POLIELECTROLITOS

En el capítulo quinto se han utilizado nanotubos de carbon multicapa para el desarrollo de membranas de nanofiltración. Partiendo como soporte de una membrana tubular porosa de SiC se ha depositado sobre esta una multicapa de nanotubos de carbono mediante la técnica "capa a capa" alternando nanotubos multicapas oxidados y nanotubos modificados con un policatión, PAH. Sobre esta multicapa de nanotubos se ha depositado una multicapa de polielectrolitos PDADMAC/PSS.

La multicapa de nanotubos de carbono actúa como espaciador entre el soporte y la multicapa de polielectrolitos en contacto con la solución a filtrar, este espaciador provoca un efecto de embudo durante el proceso de filtración favoreciendo en un 42% la permeabilidad al agua y aumentando por tanto la cantidad de solución que se puede filtrar. Estas membranas híbridas presentan una alto rechazo frente a iones divalentes, el cual aumenta directamente con el aumento de flujo de la solución. Un rechazo de hasta un 92% se ha medido frente a $MgSO_4$ y se ha observado una diferencia de hasta un 60% entre el rechazo a $MgCl_2$ y NaCl por lo que este tipo de membranas resultan atractivas para su uso en aplicaciones de separación de iones mono y divalentes de soluciones en las que coexisten.

En el capítulo sexto se ha desarrollado un método sencillo y novedoso para la producción de cápsulas híbridas de oxido de grafeno y polielectrolitos utilizando como plantilla eritrocitos (glóbulos rojos).

Para la producción de estas cápsulas se ha utilizado el método "capa a capa" alternando polielectrolitos PAH a modo de policatión y PSS como polianión intercalando láminas de oxido de grafeno. La cantidad de óxido de grafeno y por lo tanto el recubrimiento de las cápsulas por el mismo es ajustable en función de la concentración de oxido de grafeno utilizada durante el ensamblado. Las cápsulas mantienen el tamaño y forma del eritrocito que se ha usado como plantilla, una vez la multicapa se ha ensamblado completamente el eritrocito es eliminado mediante oxidación con hipoclorito sódico, dejándolas huecas.

Estas cápsulas huecas mantienen su integridad y debido al tamaño del eritrocito son fácilmente manipulables para poder situarlas en otro tipo de superficie a modo de dispositivo. Cuando las cápsulas se secan y pierden su contenido acuoso, colapsan formando un film de ~ 30 nm, el doble del espesor de la pared de una cápsula individual.

Abbreviations

Å	Amstrong
AC	Alternating current
AFM	Atomic force microscopy
BSA	Bovine serum albumine
cm	Centimetre
CMM	Capillary membrane model
CNT	Carbon nanotubes
D	Energy dissipation
d	Space between planes diffraction planes (in x-ray diffraction)
dn/dc	Refractive index increment
$E^{1/2}$	Formal redox potential (in electrochemistry)
$E_{binding}$	Electron binding energy
EDS	Energy dispersive x-ray spectroscopy
EIS	Electrochemical impedance spectroscopy
$E_{kinetic}$	Electron kinetic energies
E_{lost}	Energy lost during one oscillation
E_{photon}	Energy of the photon of x-ray source
Eq.	Equation
ESCA	Electron spectroscopy for chemical analysis
E_{stored}	Energy stored in the oscillator
eV	Electron volts
$f(K_a)$	Henry´s factor
Fig.	Figure
f_0	Resonant frequency of the quartz crystal (QCM-D)
FT-IR	Fourier transform infrarred
FWHM	Full with at half maximum
G	Graphene
g	Grams
GO	Graphene Oxide
h	Hour
HMM	Homogeneous membrane model
Hz	Hertz
i	Harmonic number
ITO	Indium tin oxide
K	Spring force constant
kV	Kilovolts

L-B	Langmuir-Blodgett
LbL	Layer by Layer
m	Meter
M	Molar
MEMS	Micro electrical mechanical systems
mg	Milligram
MHz	Mega hertz
ml	Millilitre
mM	Millimolar
MPS	3-mercapto-1-propanesulfonic acid
mV	Millivolts
MWCNT	Multiwalled carbon nanotubes.
MΩ	Megaohms
n	Integer (in x-ray diffraction)
N	Newton
NEMS	Nano electrical mechanical systems
ng	Nanogram
NHE	Normal hydrogen electrode
nm	Nanometer
Pa	Pascal
PAA	Poly (acrylic acid)
PAH	Poly (allylamine hydrochloride)
PBS	Phosphate buffered saline
PDADMAC	Poly (diallyl dimethyl ammonium chloride)
PEG	Polyethylene glycol
PEI	Poly(ethyleneimine)
PE	Polyelectrolyte
PEM	Polyelectrolyte membrane/multilayer
PMAA	Poly (methacrylic acid) (PMAA)
PSS	Poly (sodium 4-styrenesulfonate)
PVBTMAC	Poly (vinylbenzyltrimethylammonium chloride)
PWP	Pure water permeability
QCM-D	Quartz crystal microbalance with dissipation
R_a	Average roughness
R_{et}	Electro transfer resistance
rGO	Reduced graphene oxide
rpm	Revolutions per minute
R_s	Solution resistance
s	Second
SCE	Saturated calomel electrode
SDS	Sodium dodecyl sulfate
SEM	Scanning electron microscope
SWCNT	Single walled carbon nanotubes

TanΨ	Change in the amplitude ratio (in ellipsometry)
TCF	Transparent conducting films
TEM	Transmission electron microscopy
t_q	Thickness of the quartz crystal (QCM-D)
TTAB	(1-tetradecyl) trimethylammonium bromide
UHV	Ultra high vacuum
UV	Ultraviolet
V	Volts
W	Watts
wt.	Weight
XPS	X-ray photoelectron spectroscopy
Δ	Phase difference (ellipsometry)
Δf	Frequency change
Δm	Adsorbed mass (QCM-D)
ε	Dielectric constant
ζ	Zeta potential
η	Viscosity
θ	Incident angle (in x-ray diffraction)
θ_γ	Contact angle
λ	Wavelength
μ_e	Electrophoretic mobility
μl	Microlitre
ρ_q	Density of the quartz crystal (in QCM-D)
Φ	Phase (EIS)
γ_{lv}	Liquid-vapor interface tension
γ_{sl}	Solid-liquid interface tension
γ_{sv}	Solid-vapor interface tension

Objectives and aim

This thesis has three main objectives:

1) To advance the knowledge on the assembly and physico-chemical properties of layer by layer films, in particular those related to the use of polyelectrolyte multilayers as nanofiltration membranes: i.e. the ionic permeability.
2) To present a novel approach to remove foulants and regenerate layer by layer films by using sacrificial top layers in PEM, which can be applied for PEMs used for nanofiltration in situ under real operation conditions.
3) To assemble hybrid films based on polyelectrolytes and carbon nanomaterials, carbon nanotubes and graphene oxide for the development of nanofiltration membranes and capsules.

The first objective, the physico-chemical characterization of the PEMs performed in the thesis, was fundamental for the two other objectives of the work. Studies of PEM stability in different media were necessary to determine the right conditions to develop films with sacrificial top layers with stable bottom layers. The study of the assembly of the multilayers at high ionic strength adds to the knowledge of how the quality of the layers can be tuned with ionic strength as well as on the limits for the ionic strength at which PEMs can be assembled. The electrochemical characterization of the layers is important with regards to the use of the PEMs as nanofiltration membranes. The comparison of the properties of PEMs with the same polyanion and similar

polycation with a quaternary amine but a different backbone structure for the polymers let us advance the understanding of how the properties of the film are influenced by its architecture.

The second objective has a strong practical goal. We want to address a different approach for removing foulants from PEMs. Foulant accumulation is a common problem in applications such as nanofiltration as all kinds of charged organic molecules can attach to the PEMs. Very often these molecules are very difficult to remove and in the case of nanofiltration devices they may eventually block the pores of the membranes thereby limiting their application for filtration and their lifetime. In this thesis, we propose to develop PEMs fabricated with two blocks. A top block with a PEM that can be removed under certain stimuli, such as pH or the presence of a surfactant, and a bottom block that is stable under the conditions at which the top block is removed. In this way, when the multilayer is covered by foulants we will be able to remove the top layers with the foulants without affecting the whole PEM, and then reassemble the top layers to reconstitute the original foulant free PEM. This approach could be easily applied under operating conditions in reactors and could significantly extend the lifetime of nanofiltration membranes.

The third objective of the thesis is to explore the use of carbon materials with polyelectrolytes in hybrid layer by layer assemblies. We have selected two possible applications: the generation of nanofiltration membranes using films of carbon nanotubes as supports, and the development of capsules with graphene oxide as layer constituent.

A problem with the use of PEMs as nanofiltration membranes is that they have to be deposited on a support for practical applications. If the support is a porous structure and these pores have dimensions larger than the polyelectrolyte being assembled, the polyelectrolyte will pass through the pores and deposit on the pore walls reducing the pore size, affecting the flux and producing a membrane with defects. To avoid this situation we have assembled a film of carbon nanotubes in a layer by layer fashion using positively and negatively charged nanotubes and used it as a spacer between the membrane support and the PEM. The nanotubes will not penetrate the porous support thereby creating a porous structure but with smaller pores, on top of which we will assembly the PEMs. We will show that PEMs supported on nanotube films have improved ion separation properties while retaining high flux.

Finally, we want to show a different approach to use graphene oxide in assemblies leading to capsules, with potential applications in delivery or controlled deposition of layered hybrid graphene/polyelectrolyte composites in the dry state. For this purpose we have coated red blood cells with multilayered films based on polyelectrolytes and graphene oxide which, are later oxidized in order to remove the core biological material. This results in empty capsules with high graphene oxide content.

This thesis aims to explore practical applications of PEMs: antifouling films, nanofiltration membranes, and delivery systems based on hybrid assembly concepts: blocks of polyelectrolytes, films of carbon nanotubes supporting

polyelectrolyte multilayers and graphene oxide assembled with polyelectrolytes. In parallel, we have performed a careful physicochemical characterization in order to understand fundamental issues related to the assembly and properties of PEMs that are highly relevant for practical applications.

This dissertation has been divided into two sections; the first section focuses on multilayered structures based on polyelectrolytes and a second section focussing on hybrid systems of carbon nanomaterials and polyelectrolytes. The work is divided into six chapters.

POLYELECTROLYTE MULTILAYERS

In the first chapter the different techniques used during the course of this work are briefly explained, together with a list of the materials employed.

In the second chapter, differences in the structural conformation of two multilayered membranes assembled in a layer by layer fashion using the same polyanion but a different polycation are studied by electrochemical techniques. The comparison is measured in terms of permeability to cyanoferrate electrochemically active molecules.

In the third chapter, di-block multilayered membranes with antifouling properties are analysed. The di-block system consists of a permanent block with a sacrificial block on top which is removable under an external stimulus. The performance, with a protein simulating organic fouling on top, and their regeneration afterwards is analysed.

In the fourth chapter smart surfaces that change their content in water and therefore their thicknesses following changes in the ionic strength of the surrounding media are produced by assembling the polyelectrolytes at 3 M NaCl.

HYBRID SYSTEMS BASED ON CARBON NANOMATERIALS AND POLYELECTROLYTES

In the fifth chapter, hybrid carbon nanotubes/polyelectrolyte structures are assembled in between porous substrates and PEMs with nanofiltration purposes. Acting as a spacer, they enhance the ion retention and flux parameters of nanofiltration membranes.

In the sixth and final chapter, hybrid capsules of graphene oxide and polyelectrolytes using erythrocytes as templates are produced.

Introduction

"Nanotechnology is the technology based on the manipulation of matter with at least one dimension in the nanometer scale, from 1 to 100 nm", definition established by the National Nanotechnology Initiative a United States federal government program.

In 1959 the physicist Richard Feynman gave a talk entitled "There is Plenty of Room at the Bottom", in which he predicted the ideas and concepts that years later would become defined as Nanotechnology. The term was coined by Professor Norio Taniguchi in 1974 in his work in ultraprecision machining. With the appearance of the electron microscope in 1937 and afterwards with the scanning tunnelling microscope in 1981, it became possible to visualise individual atoms, material and structures at the nanoscale. A new revolutionary period in science had started.

In the intervening years, material science has developed into an interdisciplinary field that encompasses all kinds of organic and inorganic materials such as polymers, metals, biological components, inorganic and organic molecules to be used in multiple applications in medicine, biotechnology, engineering, physics, biology and/or chemistry.

Due to the unique properties of material at the nanoscale massive interest has been generated regarding the use of these materials to create nanostructured functional materials and assembly techniques for the preparation of molecular assemblies with tuneable compositions, structures and enhanced properties.[1]

Pioneering work on synthetic nanoscale heterostructures based on organic molecules was carried out by Kuhn in the 1960s using the Langmuir-Blodgett (L-B) technique.[2] These experiments are often considered as the first true nanomanipulation experiments performed involving the mechanical handling of individual molecular layers with angstrom precision.

In the early 1980s Sagiv et al., were able to produce layered films via covalent adsorption of organic molecules with specific functional groups onto a solid substrate as an alternative to the L-B method.[3]

In 1992, Decher and collaborators developed a technique capable of producing nanostructured films mostly independent of the nature, size and topology of the substrate provided that it is charged or can interact with the absorbing molecules by any other interaction i.e. hydrogen bonding, hydrophobic interactions, coordination chemistry, etc. This technique was called "Layer by Layer" (LbL) and it is mainly based on the electrostatic attraction of oppositely charged molecules.[4,5]

Layer by Layer.

In the layer by layer technique positively and negatively charged polyelectrolytes are alternately assembled on top of charged surfaces, planar or colloidal. Polyelectrolytes are polymers with charged or chargeable groups within the monomer repeating units. We can distinguish between:

- Strong polyelectrolytes: display permanent charges in solution for most reasonable pH values.

- Weak polyelectrolytes: charge is pH dependent.

The electrostatic interaction between the oppositely charged polyelectrolytes is the main driving force leading to the assembly of LbL films. Besides electrostatics, the increase in entropy resulting from the liberation of counter ions plays an important role in the assembly. As mentioned above other interactions can lead to the formation of LbL film such as hydrogen bonding, coordination chemistry, charge transfer and host interactions.[6–12]

Schlenoff et al. describe the polyelectrolyte assembly through a charge overcompensation mechanism.[13,14] Polyelectrolyte multilayer (PEM) formation involves an overall electroneutrality during the building up of the layers. This mechanism for LbL is based on intrinsic and extrinsic charge overcompensations and competitive ion pairing, see Fig. 1.

- Intrinsic charge compensation: pairing of the charges between oppositely charged polyelectrolytes or segments of them. There are no counterions within the bulk of the polymer layers and all non-compensated charges are located at the surface.
- Extrinsic charge compensation: pairing of the polyelectrolyte charges with oppositely charged counterions if dissolved salt is present in the surrounding medium
- Competitive ion pairing: competitive ion exchange due to the addition of a new oppositely charged polyelectrolyte at the moment of creating a new layer during assembly.[14]

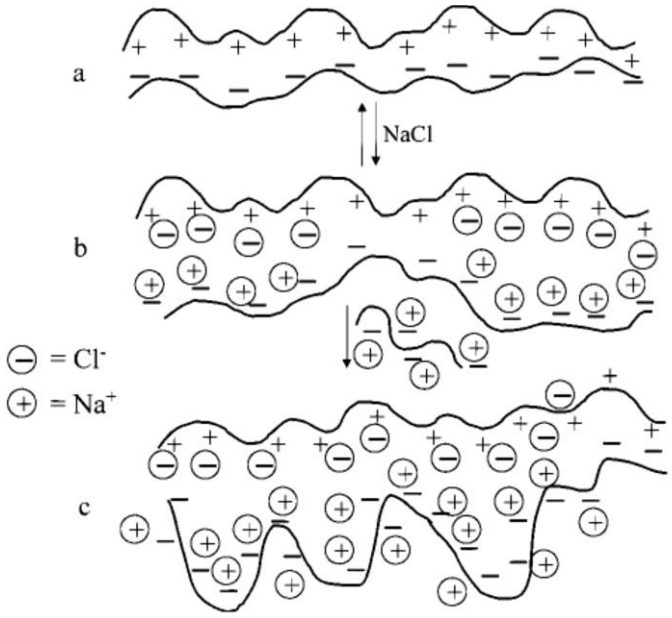

Figure 1. a) intrinsic charge compensation between two oppositely charged polymer strands. b) extrinsic compensation occurs with the addition of salt. c) Competing for polymer charge in the presence of additional polyelectrolyte during the assembly of a new layer.[14]

Upon assembly, when an oppositely charged polyelectrolyte approaches the extrinsic charge on the surface becomes intrinsically compensated by the interaction with the depositing polyelectrolyte chains. Due to the interaction with the new polyelectrolyte layer counter-ions are released from the bulk creating an entropic driving force for the LBL assembly.[15]

LbL is an easy and robust technique, representing a powerful, effective and simple strategy for modifying surfaces and endowing them with specific properties. From a practical point of view, LbL assembly only requires the dipping of a charged substrate into a solution of polyelectrolyte with a charge opposite to that of the substrate. The procedure is repeated a number of times

alternating between polycations and polyanions, including water or salt rinsings between layer deposition, until a film of the desired thickness is obtained.[5,16,17]

The dipping method of deposition is simple to implement and can even be automated. It is, however, time consuming since adsorption time and rinsing steps for each layer are required, see Fig. 2. Alternative methods have been developed to speed up the process, such as spray deposition and spin coating.[18–20]

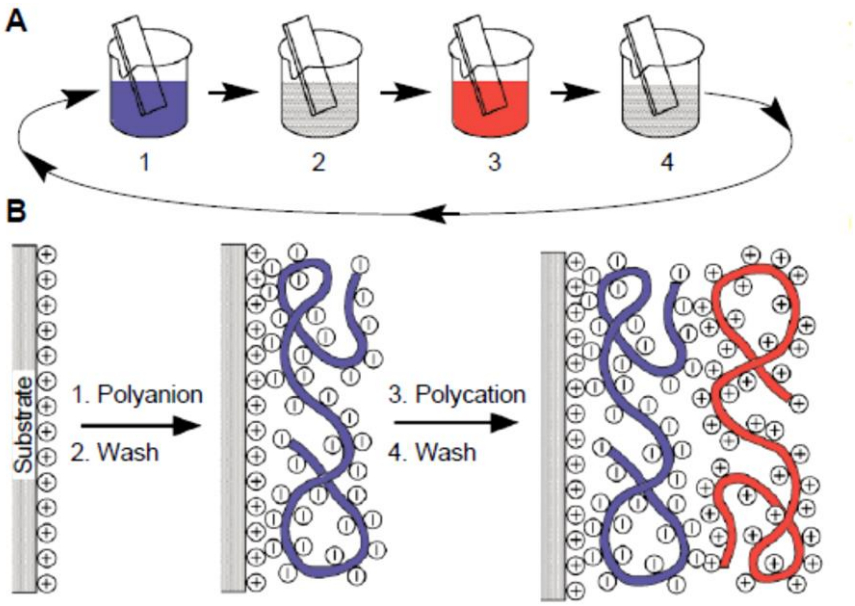

Figure 2. a) Scheme of the film deposition process using flat substrates and beakers, step 1 and 3 represent the adsorption of a polyanion and a polycation respectively, while 2 and 4 are rinsing steps. b) Simplified picture of the first two adsorption steps, counterions are omitted for clarity.[16]

Alternatively, if working with colloids, these are alternately suspended in polycation and polyanion solutions with several rinsing steps by centrifugation

in between until a film of the desired thickness is obtained. In the case of colloids, the core can be removed after PEM assembly in order to create capsules, see Fig. 3.

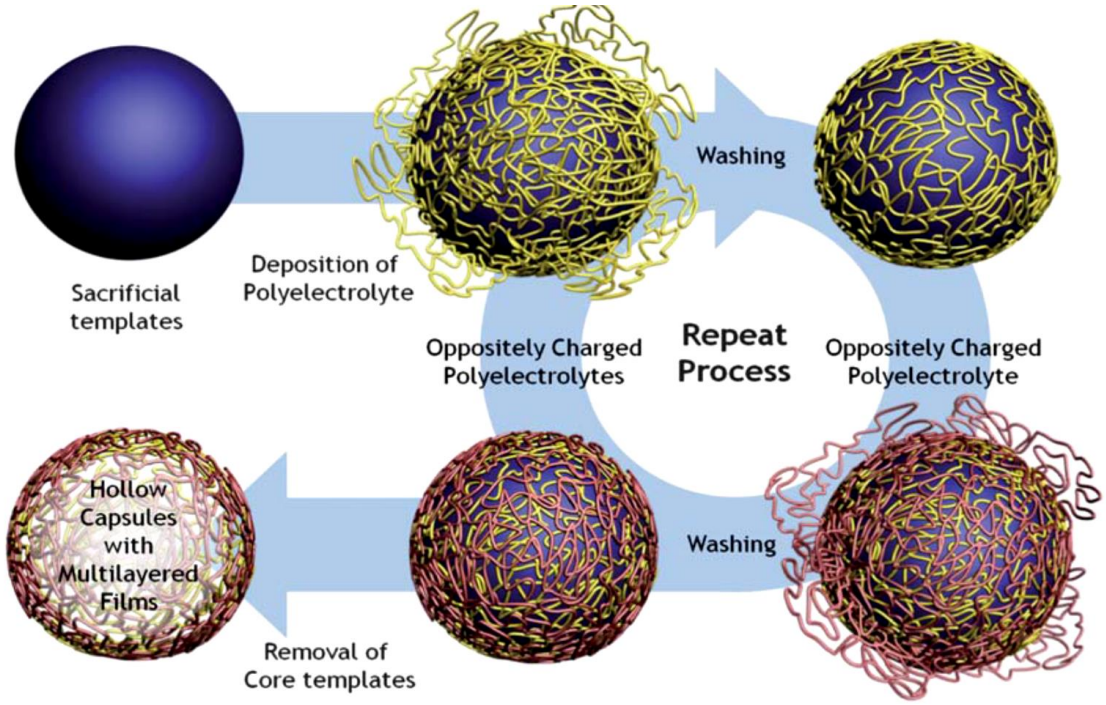

Figure 3. Schematic illustration of polyelectrolyte multilayer films on colloids and capsule creation by core removal afterwards.[21]

The practical procedures applied by the different groups working in LbL assembly varies, regarding the number of rinsing steps between the deposition of layers, the use of salt or water for the washings, assembly time, pH, and the ionic strength of the polyelectrolyte solution amongst others.[22–25] For some of these parameters, variations in the conditions of assembly can have a strong impact on the quality of the assembled PEMs.

For example, the thickness of the PEMs can be tuned by adjusting the charge density of the polyelectrolytes involved. In the case of strong polyelectrolytes the charge is not affected by changes in pH however, it is possible to modify the intramolecular interactions by screening the electrostatic interactions by adjusting the salt concentration of the polyelectrolyte solution.[26] A charged polyelectrolyte in solution without salt adopts a more extended conformation due to intramolecular repulsive interactions between the charges of its own chain.

When the ionic strength is increased, the charges in the polyelectrolyte are screened causing the chain to adopt a more coiled conformation. The polyelectrolyte assembled in coiled conformations will result in thicker layers compared to assembly in an extended conformation. If the polyelectrolyte is weak, the pH will affect the charge of the polyelectrolyte and consequently its conformation in solution and the thickness of assembled layers.

LbL films can be deposited onto a huge variety of substrates and, as already mentioned, different combinations of molecules or objects are possible, not only polyelectrolytes. Small molecules, proteins, vesicles, and nanomaterials can be assembled in LbL films. The characteristics of the LbL assembly and the large variability in the composition of the films make PEMs suitable for many applications. Among them we can cite the fabrication of polyelectrolyte capsules for biomedical applications,[23,27,28] sensors,[29] optical lenses,[30] membranes for nanofiltration[31–33], reverse osmosis,[34] anticorrosion coatings,[35] and antireflection coatings[36] to mention some examples.

- ***Principal parameters that influence LbL assembly.***

There are some parameters that must be taken into account in order to create a desired multilayer film.[15]

- Choice of polyelectrolyte pair: the multilayer formation depends on the properties of the constituent polymers and the strength of the polymer-polymer interaction. The characteristics of the polymers and their interaction will determine the growth mechanism, the resultant thickness, roughness, porosity, hydrophilicity, swellability and mechanical properties. For example: pairs that assembly preferably by intrinsic compensation will produce thinner, less permeable films that are less prone to swelling.[37,38]
- The ionic strength of the polyelectrolyte solution: the ionic strength of the polyelectrolytes during the assembly has a direct impact on the quality of the assembled layers. High salt concentration causes the screening of polyelectrolyte (PE) chains, and results in more coiled polyelectrolytes and therefore thicker layers.
- pH: the charge density of weak polyelectrolytes can be tuned by changing the pH which, in turn affects the polymer conformation and the resulting layer thickness. pH changes after LbL assembly can lead to the reorganization of the multilayer.[22,39,40]
- Temperature: It can have both a negative and positive impact on the assembly. On one side high temperatures play against electrostatic

attraction giving more mobility to the polymer chains; on the other hand temperature enhances the entropic gain by releasing counterions improving the polyelectrolyte assembly.[41]

All these parameters will influence the structure of the resultant film and therefore the physico-chemical properties. A general overview of the main properties to be studied in LbL films will be outlined next.

Film Growth and Thickness.

An important factor to take into account in multilayer formation is the growth rate of the multilayer. If the growth rate is linear, the film grows as a linear function of the pairs deposited which means that the amount of polyelectrolyte deposited per pair is approximately constant. The degree of interpenetration between layers is low, meaning that each new adsorbed layer neutralises almost all of the charges of the previous layer; the charge overcompensation is mainly intrinsic.[13] A small amount of excess charge through polymer loops, or tails, becomes the driving force for growth.[42] These films usually behave from a mechanical point of view, more like elastic solids.[43,44]

On the other hand, if the growth is supralinear the mass of each polymer layer increases as the number of layers increases. In this type of growth the interaction between the PEs is not so strong and both intrinsic and extrinsic charge compensation coexist, there is a high degree of chain mobility between assembled layers. Typically, if one of the polyelectrolytes has a low charge density and is highly swollen in water it can diffuse into the film and results in

supralinear growth.[45] This results in thick films following a relatively small number of deposition steps.[46,47] Films are highly hydrated and from a mechanical point of view they can be thought of as having more viscolelastic behaviour.[48]

Roughness.

It is generally accepted that roughness is related to the thickness. The thicker the film the rougher it will be. The characteristics of the substrate on which the PEM is deposited will strongly influence the final roughness but all factors affecting film thickness will also impact on film roughness, such as the polyelectrolyte pair chosen, film growth, salt content, pH.[49]

As explained, high ionic strengths induce a more coiled conformation of the polyelectrolytes resulting in thicker films displaying greater surface roughnesses.

Polyelectrolyte combinations, or conditions that produce thin and glassy films, usually with linear growth, are less rough, while supralinear, or exponentially, grown films will yield rougher films.[50]

Hydration and Swellability

Film hydration refers to the content of water which is trapped in the films. A general rule is that films composed of polysaccharides and polypeptides retain more water than synthetic polyelectrolytes, at comparable salt concentrations.

This is due to the hydrophobic character of the backbone in synthetic polyelectrolytes.[51]

Film hydration and the film swelling capability are strongly associated to the pair of polyelectrolytes selected and also to the conditions of assembly such as ionic strength, pH, and the swelling solvent. It has already been reported that responsive PEMs with the capability of modifying thickness via the release or uptake of water under changes in ionic strength or pH of the medium.[52–54]

Stability

An important aspect regarding the use of PEMs is their stability in the environment/conditions in which the PEMs will be applied.

For example, if the PEM is to be applied in cell cultures it must be stable in physiological conditions and in cell media. If the PEM is to be built in specific acidic conditions, e.g.: collagen/hyaluronic acid, which are assembled at low pH, they cannot be exposed to solutions of pH 7 because as Johansson et al. found these films dissolve under these conditions.[55]

One possible application of PEMs is their use as nanofiltration membranes in combination with commercial membranes for water treatment. Typically these types of membranes are cleaned in industrial applications with a bleach treatment. Then, for this application the use of polyelectrolytes with primary amines must be avoided as these oxidize and degrade in the presence of bleach as shown by Gregurec et al.[56]

Consequently, this instability may be advantageous for other applications. As we will see in chapter 4, instability of multilayers in certain conditions can be used to selectively remove polyelectrolyte layers, which can be used for antifouling treatments. The stability of polyelectrolyte multilayers has been studied in different conditions such as high ionic strength, pH, and the presence of surfactants amongst others.[57–59]

Mechanical Properties

Mechanical properties of polyelectrolyte multilayers vary significantly depending on the PE pair used and on the deposition conditions. Depending on these conditions PEMs can behave as rubber like or glassy materials.[60]

It has been shown that the elastic modulus will be different if PEMs are stabilised mainly by electrostatic interactions, or by hydrogen bonding. In the case of PEMs stabilised by electrostatic interactions such as PAH/PSS or PDADMAC/PSS it has been found that the elastic modulus decreases with increasing salt concentration after PEM assembly. A high ionic strength causes instability in the ion pairings. It provokes the swelling of the PEM leading to absorption of both water and ions thus producing a reduction in the elastic modulus. Saline solutions act as plasticizers, turning glassy like multilayers into more rubber like films.[44] On the other hand for films stabilised by hydrogen bonding interactions the elastic modulus increases with increasing salt concentration. Regardless, there is a limit at which the structure begins to

relax and the modulus decreases. In the case of PAH/DNA microcapsules this effect happens at concentrations above 1 M NaCl.[61]

Mueller et al. in 2005 reported some kind of glass transition for PDADMAC/PSS at temperatures above 35 ^{o}C, there was a reversible decrease in the elastic modulus of 2 orders of magnitude. The material appears to be melting above 35 ^{o}C going from a glassy to a viscoelastic fluid state and returning to the original state at room temperature. However, there was no evidence of glass transition by calorimetric methods.[62]

Film stiffness is extremely important in biological applications regarding cell adhesion. There are several studies regarding this issue which highlight that film stiffness can be adjusted by simply tuning the crosslinking between the PEs in the PEM. This can be done by simple adjustment of the crosslinker concentration if the crosslinking is done by carbodiimide chemistry between carboxylic and amine groups, the polyanion and polycation respectively, or by temperature changes if the crosslinking is thermal, pH control during assembly and ultraviolet treatments.[63,64]

Permeability

Film permeability is one of the most interesting properties to control in PEMs. Permeability is very important for several applications such as drug delivery,[65,66] water purification,[67] solvent separation,[68] gas barrier, etc .[69]

When discussing permeability we have to take into account different aspects of permeability. Firstly, let us consider the case of PEM permeability to liquids,

like pure water. In this case, the porosity of the film can be controlled by choosing the appropriate assembly conditions. In general, more compact structures show lower water permeability than less compact ones. Linearly growing PEMs result in thinner and more compact structures than supralinearly growing PEMs. Also, the degree of swelling of the films will affect its porosity and compactness.

On the other hand, we have to consider the permeability to molecules, ions, or particles. Different mechanisms can apply for the molecular permeability. One of them is sieving, due to size exclusion, applicable also for neutral molecules. Molecules or compounds bigger than the pore size will not pass through it. Another possible mechanism is related to the electrostatic interaction of the permeating species with the charges of the polyelectrolyte in the PEMs. The positive or negative character and extent of the charge of the permeating molecule or ions together with the character and charge density of the outer layer of the film will influence the permeability. A negatively charged outer layer PEM would be more effective at preventing negatively charged ions or molecules to go through than a positively charged one. This effect has been thoroughly studied by electrochemical techniques. Usually, for these experiments a gold electrode is modified with a polyelectrolyte multilayer, and exposed to an electroactive probe. The cyclic voltammetry or impedance response is measured, obtaining information on the diffusion of the electroactive probe.

One of the latest studies published in this field from Elżbieciak-Wodka et al. in 2015, studied the permeability of potassium hexacyanoferrate II and III in multilayers with different growing regimes, i.e.: PAH/PSS and PDADMAC/PSS.[70] Consequently, work performed during the completion of this thesis will also follow in a similar vein. However, in this case the study will analyse the permeability in films with polycations with similar chemical structures, quaternary amines, but different growing regimes, i.e.: PVBTMAC and PDADMAC in combination with PSS.

Polyelectrolytes in Membrane Separation Systems.

A membrane is a selective barrier between two phases that allows some elements to transit through and stops others. Membranes based on PEs have been considered suitable for building separation membranes with high selectivity and permeability. PEMs are exquisitely suitable for nanofiltration membranes. These membranes are usually consisting on a thin layer on top of a porous support. PEMs are good candidates for this thin layer; the deposition procedure is rather simple, it affords control of the membrane thickness at the nanoscale by the addition of more or less layers, it also allows the use of a wide range of different PEs which should permit the tailoring of the flux, selectivity and even fouling rates.[71]

PEM based nanofiltration membranes are especially attractive for separation of ions, their multipolar structure favours separation by Donnan exclusion of mono and divalent ions.[72] The charges on the surface of dense PEMs restrict

permeation through the membrane of ions that have the same charge as the last layer deposited on top and it is more efficient with multivalent ions.

For example, coated porous alumina with 5 bilayers of PAH/PSS on top exhibits a rejection rate of 95 % for Mg^{2+} and Ca^{2+} and a high selectivity for Na^{+}/Mg^{2+} and even higher for Na^{+}/Ca^{2+} with a better performance than NF 270 commercial membranes.[33] The properties of PEMs in regards to nanofiltration applications can be optimised by choosing the appropriate PE and deposition conditions. It has to be taken into consideration that imperfections in the film can reduce the selectivity of the membranes and produce convective transport of ions thus reducing the overall efficiency of the membrane.

Nanomaterials.

Nanomaterials can be defined as objects displaying a size lower than 100 nm in at least one of their three dimensions.[73] However, when dealing with nanomaterials it is important to take into consideration the state of aggregation.

There are different classifications for nanomaterials with respect to their origin, dimensionality, morphology, composition, uniformity and agglomeration, etc.

- ***Classification According to Composition:***

  Nanomaterials can be classified on the basis of their chemical composition into: [74]

  - Metal and metal oxide based: metallic nanoparticles, e.g. Au, Ag.., metal oxides such as titanium oxides, zinc oxide, iron oxide, etc

- Carbon based: Nanomaterials that display carbon atoms in sp^2 configurations: fullerenes, carbon nanotubes, buckyballs, graphene.
- Organic based: fabricated upon organic molecules: dendrimers formed by branched polymer units, micelles, vesicles, etc…
- Nanocomposites: materials made from two or more constituents at the nanoscale that, when combined, produce a material with characteristics different than those of the original components.

- ***Classification According to Dimensionality:***[73,75]

This classification is based on the number of dimensions that are non-nanoscale. As said before the nanoscale is considered below 100 nm.

- 0D: all the dimensions are nanoscale. E.g.: quantum dots, fullerenes, nanoparticles, dendrimers and so on.
- 1D: only one of the dimensions is non-nanoscale, needle like shaped materials, e.g.: nanotubes, nanowires and nanorods.
- 2D: two of the dimensions are non-nanoscale, plate like shape nanomaterials, e.g.: nanofilms, nanolayers and nanocoatings.
- 3D: all of the dimensions are non-nanoscale. It refers to bulk materials that possess nanocrystalline structure or the presence of features at the nanoscale, i.e.: nanoballs with dendritic structures, nanoflowers, nanopillars, etc.

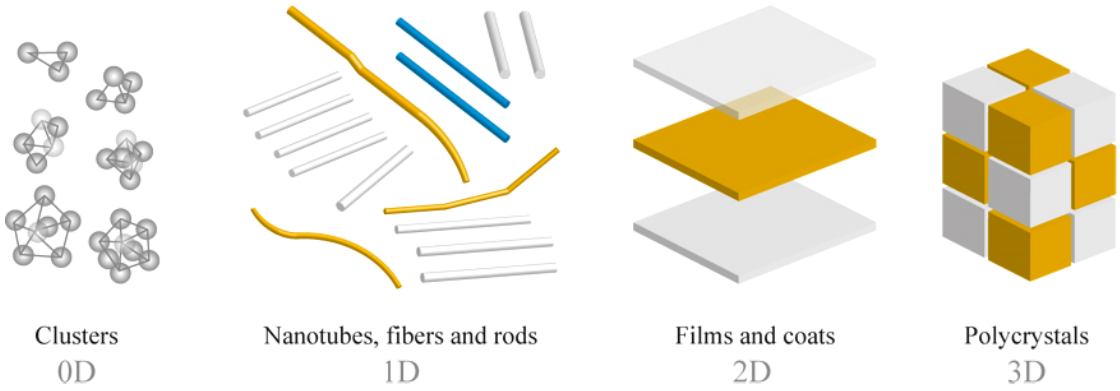

Figure 4. Schematic of nanomaterials classified by dimensionality. *(Image taken from http://eng.thesaurus.rusnano.com).*

Nanomaterials have different properties compared to their bulk materials which make them appealing for multiple applications. There are two principle factors responsible of the nanoscale properties:

- Surface effects: The fraction of atoms at the surface of the nanomaterial is very high compared to microparticles or bulk materials. They present a large surface area to volume ratio and therefore a high particle number per mass. Due to this large surface area they present an enhanced reactivity compared with bulk materials.
- Quantum effects: when the size of a particle is comparable or smaller than the Bohr radius of that material, electric dipoles are formed due to spatially confined holes and electrons producing discrete electronic energy levels, not continuous as in bulk material. Separation between adjacent energy levels increases with decreasing size producing transformations in the density of the energy levels.

These factors result in variations in the properties of the materials with respect to the bulk material. Some of the most common and general changes are listed below:[76–78]

- Structural properties: crystal structure, lattice parameters, bonds and bond strength at the nanoscale can differ from the bulk. For example, gold nanoparticles are icosahedral while in bulk gold is face-centered cubic.
- Thermal properties: melting point of nanomaterials decreases with size reduction and is lower than for bulk material, also the melting point of bulk material occurs at a specific temperature while at the nanoscale it occurs over a broad temperature range.
- Chemical reactivity: chemical reactivity of nanomaterials can be altered with respect to bulk material due to the different crystallographic structure and also due to the high surface to volume ratio. Ionization energy is generally higher for nanomaterials than for the bulk material.
- Mechanical properties: in the case of nanomaterials the ratio of grain boundaries is really high increasing the amount of atoms close to or related to incoherent interfaces or lattice defects such as dislocations, vacancies and so on. Dislocations have a direct effect on the strength of nanomaterials. Also, nanomaterials with different atomic structural arrangements to bulk will show different mechanical properties.
- Magnetic properties: a large proportion of atoms on the surface lead to different magnetic coupling between neighbouring atoms.

Ferromagnetic materials show multiple magnetic domains, however below a critical size, specific for each material, the spin of the electrons of the atoms orient in the same direction to form a single domain, displaying a super-paramagnetic behaviour. For example Fe, Co, Ni y Gd are ferromagnetic in bulk but paramagnetic in the nanoscale.

Also non-magnetic material in bulk can display magnetic behaviour in the nanoscale.

- Optical properties: these properties are connected to the electronic structure. In bulk materials electrons are free to move but in nanomaterials they are restricted, reacting differently with light. For example, gold in bulk is yellow coloured but nanoscale gold particles can be orange, purple, red or green depending in their size.
- Electronic properties: due to quantum effects, energy bandwidth and conductivity of materials change at the nanoscale with respect to bulk material. For example, silicon is an insulator in bulk but it is a conductor in nanoscale. In metals, by reducing the size, energy bands become narrower and ionisation potential energy increases causing a decrease in conductivity.

Carbon Nanomaterials

Carbon is the basic element of life, from the chemical point of view it is special not only from the multiple ways it can bond to other atoms but because it can bond to itself in many different ways too. This tendency allows the formation of different carbon network structures.

Before the 1980's only three carbon allotropes were known; graphite, diamond and amorphous carbon. While the structure of fullerenes was postulated in 1965 it was not until 1985 when Kroto et al. discovered a cage formed by 60 carbons displaying unique stability and symmetry proving their existence.[79] Thus, a new path for carbon nanotechnology was opened.[80]

In 1991, Sumio Ijima discovered carbon nanotubes, single or multi concentric graphene cylindrical hollow tubes with high aspect ratios.[81] Graphene (G), a 2D single layer of graphite, even if it was already theoretically predicted since 1947, was first produced and isolated in 2003.[82]

- ***Graphene.***

  Graphene is undoubtedly one of the most exciting materials generated in the last decade. It has unique mechanical, optical, thermal and electrical properties that may lead to the next generation of optoelectronic devices, while its properties can be used in parallel applications.[83,84]

  The unique properties of graphene, which form super strong sheets of carbon a single atom thick, result from its planar nature and the sp^2 hybridization of its carbon atoms.[85]

  Single, bi and multi-layer graphene, is itself difficult to work with in soft matter or wet chemistry applications because of dispersibility issues and its tendency to form multi-layered agglomerates, which begin to acquire the properties of graphite.[86–88] Because of these difficulties, most studies of graphene, whether for layered assembly or other investigations, have

been performed on graphite oxide or its exfoliated form, GO, which bears a mix of sp^2 and sp^3 hybridized carbons in an overall planar structure. These derivatives of graphene have the potential to be reduced to what is called a reduced form of graphene oxide, rGO, by chemical or physical means, which can lead to materials with properties more like G than GO, see Fig. 5.[89–92] The derivation of G to form GO leads to easily dispersible and stable systems containing GO with an overall surface charge while exfoliated, for example, in water.[93] The use of GO sheets in the formation of hierarchical structures and assemblies is a subject of current interest and, if done by procedures involving wet chemistry techniques, offers much potential for the development of advanced and composite layered materials.

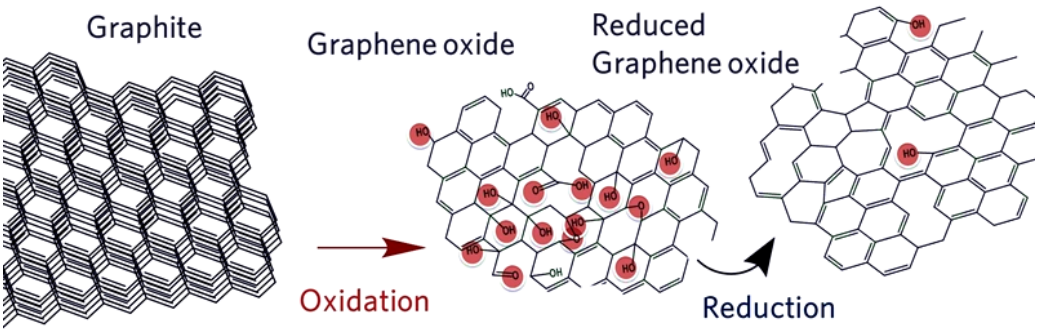

Figure 5. Graphite can be exfoliated in single sheets of graphene that after oxidation became graphene oxide and a posteriori reduction derivatizes in reduced graphene oxide.

- ***Carbon Nanotubes***

Carbon nanotubes, as previously mentioned, are tubular structures that can be considered to be rolled sheets of graphite, of nanometer diameter and large length/diameter ratio. Nanotubes can be formed by a single sheet of carbon atoms called single walled carbon nanotube (SWCNT) or they can be formed by several sheets one inside the other called multi walled carbon nanotubes (MWCNT).

The properties of the carbon nanotubes are determined by the chirality of the graphite sheet, it depends on how the graphite sheet is rolled; the orientation of the hexagonal network with respect to the long axis of the nanotube. Depending on this, there are three different types, armchair, zig-zag or chiral nanotube, see Fig.6).[94]

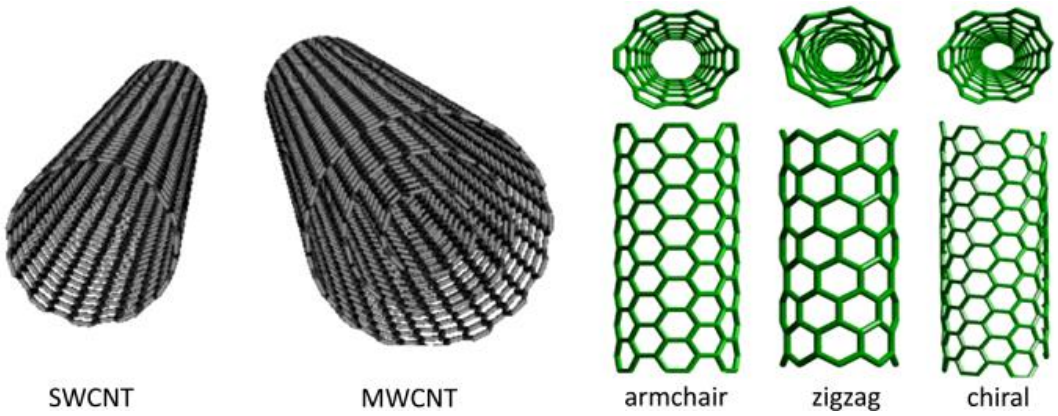

Figure 6. Representation of SWCNT and MWCNT and the three types of conformations for carbon nanotubes. *(Image taken from http://www.nano-reviews.net).*

MWCNTs have similar properties to SWCNTs but in the case of MWCNTs the outer walls can protect the inner walls from chemical interactions with outside molecules. Also, in terms of reactivity the MWCNTs show more reactivity due to multiple graphene edges at the surface. Depending on the chirality they can behave as metallic or as semiconducting materials. In terms of mechanical properties they present very high strength, elastic modulus and resiliency, as well as good compression and extension properties. Due to all of the above mentioned factors they have become a very interesting material for nanofabrication, but there are also some difficulties regarding the manipulation of this kind of nanomaterial.

One big issue is their poor solubility in most of the common solvents due to their high hamacker constant, they tend to aggregate and form bundles that afterwards precipitate. Another interesting point is post synthesis purification. The most common method to solve these two issues in one step is purification with strong oxidizing agents.[95,96] In this case, it is possible to not only eliminate impurities, but to oxidise the carbon nanotubes providing oxygen groups on their surface, it improves the solubility in polar solvents, facilitating the exfoliation of the bundles and also provide groups for further surface modifications.

Surface modification of CNTs can be performed covalently or non-covalently, e.g.: with polymers in a LbL fashion.[97,98] These modifications allow changes in the surface charge of the carbon nanotubes that can be integrated into PEMs; alternated with polymers, or assembled in a layer

by layer fashion themselves. Therefore, in this way well defined films and tunable surfaces of different materials can be produced using carbon nanotubes. [37,39–41]

Hybrid Polyelectrolyte / Carbon Nanomaterials

Carbon nanomaterials have been thoroughly used in the past combined with polymeric materials. Already during the 1990´s CNTs were presented as promising fillers in the field of polymer nanocomposites because of their remarkable electrical and mechanical properties. The first to present CNTs as fillers in polymer composites were Ajayan et al. in 1994.[102] Following this work, and during the next decades, extensive effort was expended in the development of this kind of application by improving the stiffness and strength of the original polymer.[103–105]

One of the main problems with the use of carbon nanomaterials as CNTs in composites is to have them in an isolated mode, minimising the formation of bundles or aggregates due to Van der Waals interactions between adjacent carbon sheets. Different strategies can be employed which depend on the solvent to be used for the suspension.

One of the most successful strategies is surface modification which can be done in different ways:

- Covalently attaching a molecule or grafting a polyelectrolyte to the side walls or to the edges.

- Non-covalent modification by wrapping a polymer around the walls of the nanotube or stabilisation with surfactants. It has the advantage of not disrupting the structure and electronic properties of the nanotubes.[106]

The first use of CNTs in LBL assembly with polyelectrolytes was done in order to avoid dispersion issues in polymer composite development. It was performed by Mamedov et al. in 2002, they assembled SWNTs with poly(ethyleneimine) (PEI) in a LBL fashion and reported the advantages of non-segregation between phases over the conventional mixing of the filler with the polymer matrix for the composite production.[107]

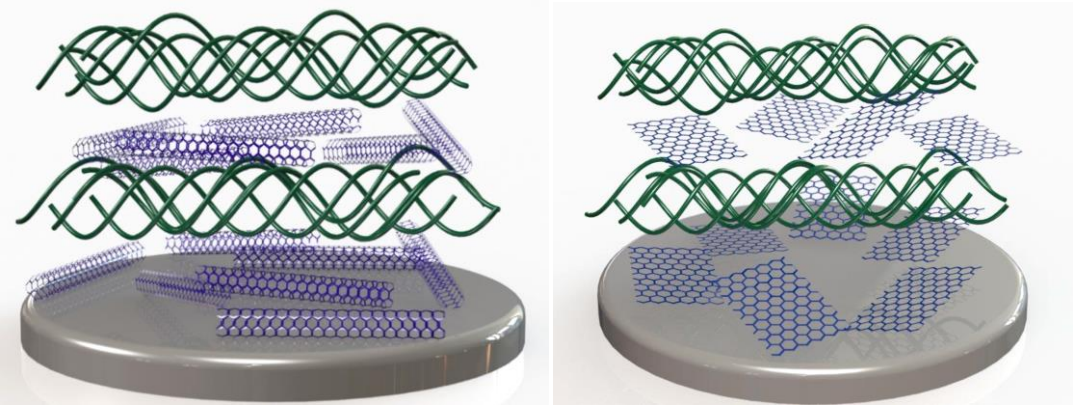

Figure 7. Representation of Layer by Layer assembly of polyelectrolytes and carbon nanomaterials; first sketch: carbon nanotubes/polyelectrolytes and second scketch: graphene sheets/ polyelectrolytes. *Image taken from (http://chem.ubbcluj.ro/~studiachemia/docs/Chemia32015.pdf).*

This was the start of several works that showed the huge potential of this technique for the development of a wide range of functional materials, such as:[108]

- Sensor applications: Sensors can be developed analyzing changes in the electrical properties of CNTs induced by chemical species, or in the electrochemical response of a polymeric co-partner in the case of nanocomposites, by structural deformation induced electrical resistance changes of the composite or specially designed micro/nano electrical mechanical systems (MEMS/NEMS).[108] For example Xue et al. in 2007 patterned LBL CNT nanocomposites as flexible cantilevers arrays.[109]
- Fuel Cell: These types of structures have been used in the construction of conductive and durable electrodes in fuel cell proton exchange membranes. For example Nafion and Pt wrapped in CNTs assembled to form a fuel cell proton exchange membrane showed unusual performances.[110]
- Optoelectronic applications: The layered nanostructure produced by the LBL technique together with the unique electrical properties of the CNTs offers an exceptional scenario from which to exploit these hybrid composite possibilities. These type of films were suggested for use as high performance transparent conducting films (TCF) like polymeric thin film transistors.[111,112]
- Biomedical applications: Hybrid composites with CNTs have been used to coat objects, for example, for protective purposes, Angelini et al. in 2007 reported the protection of liposomes with a composite of shortened CNTs.[113] Hollow capsules have also been produced by removing the core after the cover deposition.[114]

Another possibility is to wrap the carbon nanotube with a LBL assembly and produce systems for intracellular delivery, such as anti-cancer enzymes assembled in MWCNTs and afterwards injected into tumor cells.[115]

Graphene also has some drawbacks in order to use it as part of hybrid LBL structured composites. The main issue is to isolate the graphene platelets from the graphite. As previously explained, the most common method, especially if it is to be used in a aqueous environment, is to oxidise the graphene to produce graphene oxide.

The first reported case of the integration of GO in LBL multilayered films was by Fendler et al. in 1996, where they developed multilayered films of GO and polyelectrolyte that, post assembly, were reduced to graphene by chemical methods.[116,117] Similarly, with CNTs a lot of research has been done in this area in an effort to exploit its capabilities related to high opto-electrical and mechanical properties. Some applications are listed below:[118–120]

- Electrical conductor applications: graphene sheets present low intrinsic electrical resistivity making them suitable in transparent conducting films (TCF). Studies have been performed using graphene/polymer composites assembled by LBL, but it was found that they show worse performances compared to Indium Tin Oxide (ITO) unlike what it was observed with CNTs.[112,121]

TCFs based on graphene have been used as window electrodes in organic solar cells.[122]

- Batteries: graphene composites have been used in Lithium ion batteries as a replacement for commercial graphite. The capacity of the battery can be boosted due to the presence of more places available for lithiation by increasing the carbon based area where lithium ions penetrate. Casagneu et al. produced high reversible specific capacity lithium-ion batteries based on polyelectrolytes and GO nanosheets with a capacity of 1232 $mAhg^{-1}$ versus the 372 $mAhg^{-1}$ which is the theoretical limit of specific capacity for commercial graphite batteries.[117]
- Supercapacitors: materials with large specific surface area are suitable for use as supercapacitors where significant accumulation of electrical energy can be obtained at the electrode/electrolyte interface.[123] Supercapacitors with high capacitances as high as 263 Fg^{-1} have been produced using layered GO/polymer composites.[124,125]
- Sensors: they have attracted a lot of interest in electrochemical, electronic and optical sensors. Detection of gases is based on changes of conductance induced by charge transfer between adsorbates and graphene.[123] Single molecule detection sensors of NO_2 have been produced or other aggressive gases like HCN for example.[126,127] Also extensive research in biosensing has been reported as for example a cancer sensor with ultrahigh sensitivity based on LBL with graphene and PDADMAC multilayers reported from Zhang et al. in 2011.[128]

- Biomedical applications: the hybrid composites have been used to coat objects and create capsules for drug encapsulation. A dual drug encapsulation one inside the core and another one in the shell was reported by Kurapati et al. in 2012.[129]

References

(1) Borges, J.; Mano, J. F. *Chem. Rev.* **2014**, *114*, 8883–8942.

(2) Kuhn, H.; Möbius, D. *Angew. Chemie Int. Ed. English* **1971**, *10* (9), 620–637.

(3) Netzer, L.; Sagiv, J. *J. Am. Chem. Soc.* **1983**, *105* (3), 674–676.

(4) Decher, G. *Science (80-.).* **1997**, *277* (5330), 1232–1237.

(5) Decher, G.; Hong, J. D. *Berichte der Bunsengesellschaft für Phys. Chemie* **1991**, *95* (11), 1430–1434.

(6) Decher, G.; Hong, J. D.; Schmitt, J. *Thin Solid Films* **1992**, *210–211* (0), 831–835.

(7) Rydzek, G.; Schaaf, P.; Voegel, J.-C.; Jierry, L.; Boulmedais, F. *Soft Matter* **2012**, *8* (38), 9738.

(8) Quinn, J. F.; Caruso, F. *Langmuir* **2004**, *20* (1), 20–22.

(9) Kharlampieva, E.; Kozlovskaya, V.; Sukhishvili, S. A. *Adv. Mater.* **2009**, *21* (30), 3053–3065.

(10) Xiong, H.; Cheng, M.; Zhou, Z.; Zhang, X.; Shen, J. *Adv. Mater.* **1998**, *10* (7), 529–532.

(11) Zhang, Y.; Cao, W. *Langmuir* **2001**, *17* (16), 5021–5024.

(12) Dubacheva, G. V; Dumy, P.; Auzely, R.; Schaaf, P.; Boulmedais, F.; Jierry, L.; Coche-Guerente, L.; Labbe, P. *Soft Matter* **2010**, *6* (16), 3747–3750.

(13) Hatzor, A.; Moav, T.; Cohen, H.; Matlis, S.; Libman, J.; Vaskevich, A.; Shanzer, A.; Rubinstein, I. *J. Am. Chem. Soc.* **1998**, *120* (51), 13469–13477.

(14) Schlenoff, J. B.; Ly, H.; Li, M. *J. Am. Chem. Soc.* **1998**, *120* (30), 7626–7634.

(15) Schlenoff, J. B.; Dubas, S. T. *Macromolecules* **2001**, *34* (3), 592–598.

(16) Joseph, N.; Ahmadiannamini, P.; Hoogenboom, R.; Vankelecom, I. F. J. *Polym. Chem.* **2014**, *5* (6), 1817–1831.

(17) Dubas, S. T.; Schlenoff, J. B. *Macromolecules* **1999**, *32* (24), 8153–8160.

(18) Schlenoff, J. B.; Dubas, S. T.; Farhat, T. *Langmuir* **2000**, *16* (26), 9968–9969.

(19) Izquierdo, A.; Ono, S. S.; Voegel, J.-C.; Schaaf, P.; Decher, G. *Langmuir* **2005,** 21 (16), 7558–7567.

(20) Chiarelli, P. A.; Johal, M. S.; Holmes, D. J.; Casson, J. L.; Robinson, J. M.; Wang, H.-L. *Langmuir* **2002**, *18* (1), 168–173.

(21) Hong, J.; Han, J. Y.; Yoon, H.; Joo, P.; Lee, T.; Seo, E.; Char, K.; Kim, B.-S. *Nanoscale* **2011**, *3* (11), 4515–4531.

(22) Shiratori, S. S.; Rubner, M. F. *Macromolecules* **2000**, *33* (11), 4213–4219.

(23) Donath, E.; Sukhorukov, G. *Angew. Chemie Int. Ed.* **1998**, *37* (16), 2201–2205.

(24) Sukhorukov, G. B.; Donath, E.; Lichtenfeld, H.; Knippel, E.; Knippel, M.; Budde, A.; Möhwald, H. *Colloids Surfaces A Physicochem. Eng. Asp.* **1998**, *137* (1–3), 253–266.

(25) McAloney, R. A.; Sinyor, M.; Dudnik, V.; Goh, M. C. *Langmuir* **2001**, *17* (21), 6655–6663.

(26) Michel, M.; Toniazzo, V.; Ruch, D.; Ball, V. *ISRN Mater. Sci.* **2012**, *2012*, 1–13.

(27) Boudou, T.; Crouzier, T.; Ren, K.; Blin, G.; Picart, C. *Adv. Mater.* **2010**, *22* (4), 441–467.

(28) Delcea, M.; Möhwald, H.; Skirtach, A. G. *Adv. Drug Deliv. Rev.* **2011**, *63* (9), 730–747.

(29) Shao, Y.; Xu, S.; Zheng, X.; Wang, Y.; Xu, W. *Sensors* **2010**, *10* (4), 3585–3596.

(30) Manju, S.; Kunnatheeri, S. *Pharm. Dev. Technol.* **2010**, *15* (4), 379–385.

(31) Liu, G.; Dotzauer, D.; Bruening, M. *J. Memb. Sci.* **2010**, *354* (1-2), 198–205.

(32) Stanton, B. W.; Harris, J. J.; Miller, M. D.; Bruening, M. L. *Langmuir* **2003**, *19* (17), 7038–7042.

(33) Ouyang, L.; Malaisamy, R.; Bruening, M. L. *J. Memb. Sci.* **2008**, *310* (1-2), 76–84.

(34) Jin, W.; Toutianoush, A.; Tieke, B. *Langmuir* **2003**, *24* (16), 2550–2553.

(35) Eckle, M.; Decher, G. *Nano Lett.* **2001**, *1* (1), 45–49.

(36) Shimomura, H.; Gemici, Z.; Cohen, R. E.; Rubner, M. F. *ACS Appl. Mater. Interfaces* **2010**, *2* (3), 813–820.

(37) Miller, M. D.; Bruening, M. L. *Chem. Mater.* **2005**, *17* (21), 5375–5381.

(38) Harris, J. J.; Bruening, M. L. *Langmuir* **2000**, *16* (4), 2006–2013.

(39) v. Klitzing, R. *Phys. Chem. Chem. Phys.* **2006**, *8* (43), 5012–5033.

(40) Elzbieciak, M.; Zapotoczny, S.; Nowak, P.; Krastev, R.; Nowakowska, M.; Warszyński, P. *Langmuir* **2009**, *25* (5), 3255–3259.

(41) Salomäki, M.; Vinokurov, I. A.; Kankare, J. *Langmuir* **2005**, *21* (24), 11232–11240.

(42) Schmitt, J.; Gruenewald, T.; Decher, G.; Pershan, P. S.; Kjaer, K.; Loesche, M. *Macromolecules* **1993**, *26* (25), 7058–7063.

(43) Jaber, J. A.; Schlenoff, J. B. *J. Am. Chem. Soc.* **2006**, *128* (9), 2940–2947.

(44) Heuvingh, J.; Zappa, M.; Fery, A. *Langmuir* **2005**, *21* (7), 3165–3171.

(45) Hoda, N.; Larson, R. G. *J. Phys. Chem. B* **2009**, *113* (13), 4232–4241.

(46) Picart, C.; Mutterer, J.; Richert, L.; Luo, Y.; Prestwich, G. D.; Schaaf, P.; Voegel, J.-C.; Lavalle, P. *Proc. Natl. Acad. Sci. U. S. A.* **2002**, *99* (20), 12531–12535.

(47) Picart, C.; Lavalle, P.; Hubert, P.; Cuisinier, F. J. G.; Decher, G.; Schaaf, P.; Voegel, J.-C. *Langmuir* **2001**, *17* (23), 7414–7424.

(48) Collin, D.; Lavalle, P.; Garza, J. M.; Voegel, J.-C.; Schaaf, P.; Martinoty, P. *Macromolecules* **2004**, *37* (26), 10195–10198.

(49) Ghostine, R. A.; Jisr, R. M.; Lehaf, A.; Schlenoff, J. B. *Langmuir* **2013**, *29* (37), 11742–11750.

(50) Lavalle, P.; Gergely, C.; Cuisinier, F. J. G.; Decher, G.; Schaaf, P.; Voegel, J. C.; Picart, C. *Macromolecules* **2002**, *35* (11), 4458–4465.

(51) Picart, C. *Curr. Med. Chem.* **2008**, *15* (7), 685–697.

(52) Moya, S. *Macromol. Rapid Commun.* **2012**, *33* (12), 1022–1035.

(53) Irigoyen, J.; Han, L.; Llarena, I.; Mao, Z.; Gao, C.; Moya, S. E. *Macromol. Rapid Commun.* **2012**, *33* (22), 1964–1969.

(54) Sukhishvili, S. A. *Curr. Opin. Colloid Interface Sci.* **2005**, *10* (1-2), 37–44.

(55) Johansson, J. Å.; Halthur, T.; Herranen, M.; Söderberg, L.; Elofsson, U.; Hilborn, J. *Biomacromolecules* **2005**, *6* (3), 1353–1359.

(56) Gregurec, D.; Olszyna, M.; Politakos, N.; Yate, L.; Dahne, L.; Moya, S. E. *Colloid Polym. Sci.* **2015**, *293* (2), 381–388.

(57) Irigoyen, J.; Politakos, N.; Murray, R.; Moya, S. E. *Macromol. Chem. Phys.* **2014**, *215* (16), 1543–1550.

(58) Han, L.; Mao, Z.; Wuliyasu, H.; Wu, J.; Gong, X.; Yang, Y.; Gao, C. *Langmuir* **2012**, *28* (1), 193–199.

(59) Iturri Ramos, J. J.; Llarena, I.; Moya, S. E. *J. Mater. Sci.* **2010**, *45* (18), 4970–4976.

(60) Jaber, J. a.; Schlenoff, J. B. *Curr. Opin. Colloid Interface Sci.* **2006**, *11* (6), 324–329.

(61) Heuvingh, J.; Zappa, M.; Fery, A. *Langmuir* **2005**, *21* (7), 3165–3171.

(62) Mueller, R.; Köhler, K.; Weinkamer, R.; Sukhorukov, G.; Fery, A. *Macromolecules* **2005**, *38* (23), 9766–9771.

(63) Schneider, A.; Francius, G.; Obeid, R.; Schwinté, P.; Hemmerlé, J.; Frisch, B.; Schaaf, P.; Voegel, J. C.; Senger, B.; Picart, C. *Langmuir* **2006**, *22* (3), 1193–1200.

(64) Detzel, C. J.; Larkin, A. L.; Rajagopalan, P. *Tissue Eng. Part B. Rev.* **2011**, *17* (2), 101–113.

(65) Wang, Y.; Wang, S.; Xiao, M.; Han, D.; Hickner, M. A.; Meng, Y. *RSC Adv*. **2013**, *3* (35), 15467–15474.

(66) Lu, H.; Hu, N. *J. Phys. Chem. B* **2007**, *111* (8), 1984–1993.

(67) Chan, E. P. *Soft Matter* **2014**, *10* (17), 2949–2954.

(68) Liu, D. S.; Ashcraft, J. N.; Mannarino, M. M.; Silberstein, M. N.; Argun, A. A.; Rutledge, G. C.; Boyce, M. C.; Hammond, P. T. *Adv. Funct. Mater.* **2013**, *23* (24), 3087–3095.

(69) Yang, Y.-H.; Bolling, L.; Priolo, M. A.; Grunlan, J. C. *Adv. Mater.* **2013**, *25* (4), 503–508.

(70) Elżbieciak-Wodka, M.; Kolasińska-Sojka, M.; Nowak, P.; Warszyński, P. *J. Electroanal. Chem.* **2015**, *738*, 195–202.

(71) Miller, M. D.; Bruening, M. L. *Langmuir* **2004**, *20* (26), 11545–11551.

(72) Krasemann, L.; Tieke, B. *Langmuir* **2000**, *16*, 287–290.

(73) Tiwari, J. N.; Tiwari, R. N.; Kim, K. S. *Prog. Mater. Sci.* **2012**, *57* (4), 724–803.

(74) Khanna, V. K. In *Nanosensors: Physical, Chemical, and Biological*; CRC Press: Boca Raton, 2011; pp 85–142.

(75) Pokropivny, V. V.; Skorokhod, V. V. *Mater. Sci. Eng. C* **2007**, *27* (5-8), 990–993.

(76) Balaguru, R. J. B. Quantum size effect , electrical conductivity and Quantum transport School of Electrical & Electronics Engineering http://www.nptel.ac.in/courses/115106076/Module 6/Module 6.pdf.

(77) Balaguru, R. J. B. Introduction to Materials and Classification of Low Dimensional Materials School of Electrical & Electronics Engineering.

(78) Mani Naidu S. *Applied Physics*; Pearson, Ed.; Dorling Kindersley: Chennai, Delhi, Chandigarh, 2010.

(79) Kroto, H. W.; Heath, J. R.; O'Brien, S. C.; Curl, R. F.; Smalley, R. E. *Nature* **1985**, *318* (6042), 162–163.

(80) Oliveira, S. F.; Bisker, G.; Bakh, N. a.; Gibbs, S. L.; Landry, M. P.; Strano, M. S. *Carbon N. Y.* **2015**, *95*, 767–779.

(81) Iijima, S. *Nature* **1991**, *354* (6348), 56–58.

(82) Novoselov, K. S.; Geim, A. K.; Morozov, S. V; Jiang, D. *Science (80-.).* **2004**, *306*, 666–669.

(83) Liu, J.; Tang, J.; Gooding, J. J. *J. Mater. Chem.* **2012**, *22* (25), 12435.

(84) Schwierz, F. *Nat. Nanotechnol.* **2010**, *5* (7), 487–496.

(85) Blees, M. K.; Barnard, A. W.; Rose, P. A.; Roberts, S. P.; McGill, K. L.; Huang, P. Y.; Ruyack, A. R.; Kevek, J. W.; Kobrin, B.; Muller, D. A.; McEuen, P. L. *Nature* **2015**, *524* (7564), 204–207.

(86) Tasis, D.; Papagelis, K.; Spiliopoulos, P.; Galiotis, C. *Mater. Lett.* **2013**, *94*, 47–50.

(87) Nicolosi, V.; Chhowalla, M.; Kanatzidis, M. G.; Strano, M. S.; Coleman, J. *N. Science (80-.).* **2013**, *340* (6139), 1226419.

(88) Hernandez, Y.; Lotya, M.; Rickard, D.; Bergin, S. D.; Coleman, J. N. *Langmuir* **2010**, *26* (5), 3208–3213.

(89) Dreyer, D. R.; Park, S.; Bielawski, C. W.; Ruoff, R. S. *Chem. Soc. Rev.* **2010**, *39* (1), 228–240.

(90) Si, Y.; Samulski, E. T. *Nano Lett.* **2008**, *8* (6), 1679–1682.

(91) Hassouna, F.; Kashyap, S.; Laachachi, a; Ball, V.; Chapron, D.; Toniazzo, V.; Ruch, D. *J. Colloid Interface Sci.* **2012**, *377* (1), 489–496.

(92) Gao, X.; Jang, J.; Nagase, S. *J. Phys. Chem. C* **2010**, *114* (2), 832–842.

(93) Du, W.; Jiang, X.; Zhu, L. *J. Mater. Chem. A* **2013**, *1* (36), 10592.

(94) Popov, V. *Mater. Sci. Eng. R Reports* **2004**, *43* (3), 61–102.

(95) Balasubramanian, K.; Burghard, M. *Small* **2005**, *1* (2), 180–192.

(96) Banerjee, S.; Wong, S. S. *J. Phys. Chem. B* **2002**, *106* (47), 12144–12151.

(97) Lee, S. W.; Kim, B.-S.; Chen, S.; Shao-Horn, Y.; Hammond, P. T. *J. Am. Chem. Soc.* **2009**, *131* (2), 671–679.

(98) Iamsamai, C.; Soottitantawat, A.; Ruktanonchai, U.; Hannongbua, S.; Dubas, S. T. *Carbon N. Y.* **2011**, *49* (6), 2039–2045.

(99) Michel, M.; Taylor, A.; Sekol, R.; Podsiadlo, P.; Ho, P.; Kotov, N.; Thompson, L. *Adv. Mater.* **2007**, *19* (22), 3859–3864.

(100) Zhang, M.; Yan, Y.; Gong, K.; Mao, L.; Guo, Z.; Chen, Y. *Langmuir* **2004**, *20* (20), 8781–8785.

(101) Zhang, M.; Su, L.; Mao, L. *Carbon N. Y.* **2006**, *44* (2), 276–283.

(102) Ajayan, P. M.; Stephan, O.; Colliex, C.; Trauth, D. *Sci.* **1994**, *265* (5176), 1212–1214.

(103) Coleman, J. N.; Khan, U.; Blau, W. J.; Gun'ko, Y. K. *Carbon N. Y.* **2006**, *44* (9), 1624–1652.

(104) Moniruzzaman, M.; Winey, K. I. *Macromolecules* **2006**, *39* (16), 5194–5205.

(105) Wong, K. K.; Shi, S. Q.; Lau, A. K. T. *Key Eng. Mater.* **2007**, *334-335*, 705–708.

(106) Hao, J. *Self-assembled structures properties and applications in solution and on surfaces*; CRC Press: Boca Raton, 2011.

(107) Mamedov, A. A.; Kotov, N. A.; Prato, M.; Guldi, D. M.; Wicksted, J. P.; Hirsch, A. *Nat. Mater.* **2002**, *1* (3), 190–194.

(108) Shim, B. S. *Multifunctional carbon nanotube thin film composites by layer-by-layer assembly technique*, University of Michigan, 2009.

(109) Xue, W.; Cui, T. *Sensors Actuators A Phys.* **2007**, *136* (2), 510–517.

(110) Michel, M.; Taylor, A.; Sekol, R.; Podsiadlo, P.; Ho, P.; Kotov, N.; Thompson, L. *Adv. Mater.* **2007**, *19* (22), 3859–3864.

(111) Xue, W.; Liu, Y.; Cui, T. *Appl. Phys. Lett.* **2006**, *89* (16).

(112) Zhu, J.; Shim, B. S.; Di Prima, M.; Kotov, N. A. *J. Am. Chem. Soc.* **2011**, *133* (19), 7450–7460.

(113) Angelini, G.; Boncompagni, S.; De Maria, P.; De Nardi, M.; Fontana, A.; Gasbarri, C.; Menna, E. *Carbon N. Y.* **2007**, *45* (13), 2479–2485.

(114) Correa-Duarte, M. A.; Kosiorek, A.; Kandulski, W.; Giersig, M.; Liz-Marzán, L. M. *Chem. Mater.* **2005**, *17* (12), 3268–3272.

(115) Jia, N.; Lian, Q.; Shen, H.; Wang, C.; Li, X.; Yang, Z. *Nano Lett.* **2007**, *7* (10), 2976–2980.

(116) Kotov, N. A.; Dekany, I.; Fendler, J. H. *Adv. Mater.* **1996**, *8* (8), 637–641.

(117) Cassagneau, T.; Fendler, J. H. *Adv. Mater.* **1998**, *10* (11), 877–881.

(118) Chen, H.; Müller, M. B.; Gilmore, K. J.; Wallace, G. G.; Li, D. *Adv. Mater.* **2008**, *20* (18), 3557–3561.

(119) Park, S.; Dikin, D. A.; Nguyen, S. T.; Ruoff, R. S. *J. Phys. Chem. C* **2009**, *113* (36), 15801–15804.

(120) Rafiee, M. A.; Rafiee, J.; Wang, Z.; Song, H.; Yu, Z.-Z.; Koratkar, N. *ACS Nano* **2009**, **3** (12), 3884–3890.

(121) De, S.; Coleman, J. N. *ACS Nano* **2010**, *4* (5), 2713–2720.

(122) Park, H.; Brown, P. R.; Bulović, V.; Kong, *J. Nano Lett.* **2012**, *12* (1), 133–140.

(123) Yang, M.; Hou, Y.; Kotov, N. A. *Nano Today* **2012**, *7* (5), 430–447.

(124) Li, Z.; Wang, J.; Liu, X.; Liu, S.; Ou, J.; Yang, S. *J. Mater. Chem.* **2011**, *21* (10), 3397–3403.

(125) Yoo, J. J.; Balakrishnan, K.; Huang, J.; Meunier, V.; Sumpter, B. G.; Srivastava, A.; Conway, M.; Mohana Reddy, A. L.; Yu, J.; Vajtai, R.; Ajayan, P. M. *Nano Lett.* **2011**, *11* (4), 1423–1427.

(126) Schedin, F.; Geim, A. K.; Morozov, S. V; Hill, E. W.; Blake, P.; Katsnelson, M. I.; Novoselov, K. S. *Nat Mater* **2007**, *6* (9), 652–655.

(127) Robinson, J. T.; Perkins, F. K.; Snow, E. S.; Wei, Z.; Sheehan, P. E. *Nano Lett.* **2008**, *8* (10), 3137–3140.

(128) Zhang, B.; Cui, T. *Appl. Phys. Lett.* **2011**, *98* (7).

Chapter 1
Materials and Experimental Methods.

Experimental Methods

The main techniques used in this thesis are explained below.

1.1 Quartz Crystal Microbalance with Dissipation.

The QCM-D is a technique that utilizes acoustic waves generated by oscillating a piezoelectric crystal quartz plate in order to estimate adsorbed mass, with ng cm^{-2} sensitivity. These quartz plates nowadays are usually a circular piece of quartz sandwiched between two metal electrodes. When an alternating electric field is applied across the device, an oscillation that propagates through the crystal is induced. The frequency of such oscillation is determined by the thickness of the crystal and the speed of shear waves in quartz.[1]

In 1959, Sauerbrey demonstrated that there is a linear relationship between the frequency change (Δf) of the oscillating crystal and the mass adsorbed on the surface (Δm).[2] This relationship is given by:

$$\Delta m = -C\frac{\Delta f_i}{i} \qquad \text{(Eq. 1.1)}$$

Where *i* is the harmonic number and *C* is defined as:

$$C = \frac{t_q \rho_q}{f_0} \qquad \text{(Eq. 1.2)}$$

where t_q is the thickness of the quartz, ρ_q the density of the quartz, and f_0 is the resonant frequency of the particular crystal. Therefore, for a 4.95 ±0.02 MHz crystal the value of C=18.06 ± 0.15 ng (Hz cm^2). This theory is valid only if three assumptions are fulfilled:

- The adsorbed mass is small relative to the mass of the quartz crystal.
- The mass is adsorbed rigidly to the surface.
- The mass is distributed over the whole active area of the crystal.

Initially this theory was applied only in vacuum or gas phases. However, in 1980 it was proven to be applicable in liquid environments.[3] The drawback of these applications in liquid is that the liquid phase often incorporates viscous and elastic contributions to the frequency change therefore violating the assumption of the Sauerbrey condition of rigidity of the adsorbed film.

A film that is soft (viscoelastic) will not fully couple to the oscillation of the crystal; hence the Sauerbrey relation will underestimate the adsorbed mass. A soft film dampens the sensor oscillation. This damping or energy dissipation (D) reveals the viscoelasticity of the film.

$$D = \frac{E_{lost}}{2\pi E_{stored}} \qquad \text{(Eq 1.3)}$$

Where E_{lost} is the energy lost during one oscillation cycle and E_{stored} is the total energy stored in the oscillator.

The resolution of frequency and dissipation in liquids is on the order of ± 0.1 Hz and 10^{-7}, respectively, both are approximately one order of magnitude better in

air or vacuum. The QCM-D approach allows simultaneously recording the *f* and *D* values at multiple harmonics (n = 3, 5, 7,..) of a resonant frequency on a millisecond time scale. The recorded data allows the estimation of multiple parameters such as mass, thickness, density, viscosity, or storage modulus. Combined with complementary techniques, such as ellipsometry or surface plasmon resonance, the water content or associated solvent can also be estimated.[1]

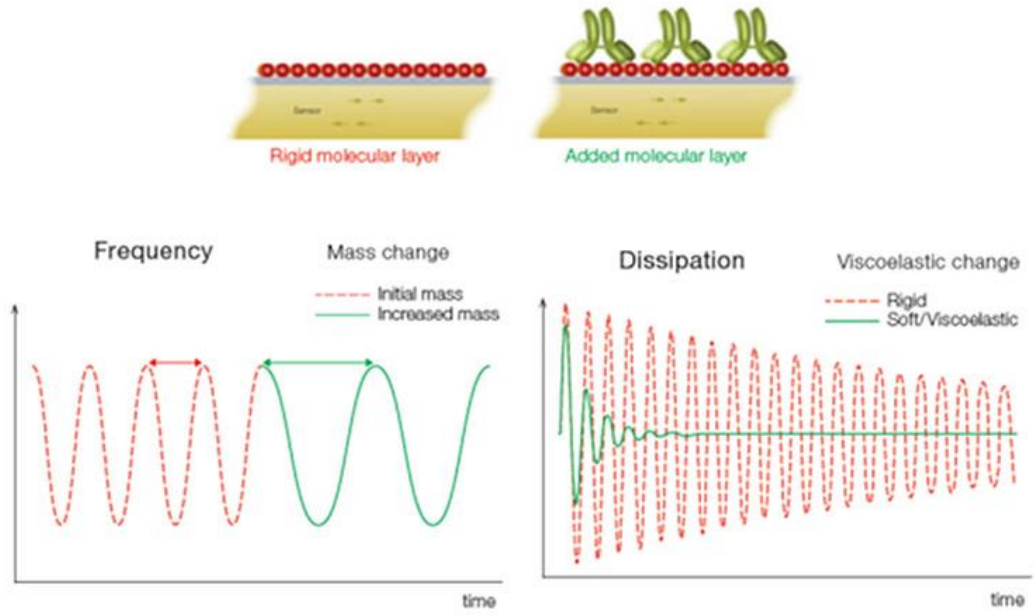

Figure 1.1. Frequency and dissipation changes in a quartz crystal resonator with a rigid layer or a viscolelastic layer. (Image taken from *http://www.egr.msu.edu*).

The QCM-D used in this thesis is an E4 quartz crystal microbalance with dissipation from Q-Sense, Goteborg, Sweden. The fundamental frequencies of the system are always found in water to establish a reference zero value. QCM-D data is acquired for the 3rd overtone (15 MHz) with subsecond time resolution. The silica crystals employed are always QSX 303 SiO_2 (50 nm)-

coated quartz crystals (5 MHz) from Q-Sense that are always treated using a UV-Ozone treatment of 20 minutes in a procleaner chamber from Bioforce nanoscience immediately before their use.

1.2 Ellipsometry.

Ellipsometry is a non-invasive, non-destructive optical characterisation technique which measures the change in polarisation that occurs after the reflection, or transmission, of a beam against a sample. The first ellipsometer was built buy P. Drude in 1945 but it was not until the 70s-80s that this technique started to be exploited.[4] Taking into account Maxwell´s theory light is a wave composed by two perpendicular vectors, E related to the electric field strength and B the magnetic field, both vectors are also perpendicular to the direction of propagation. Polarization is the change in orientation with time of E along the propagation direction. If light pass through a polarizer linearly polarized light is transmitted, when linearly polarised light at an acute angle of incidence is reflected on a film there is a change in the polarisation to elliptically polarised light. The two components of E which were in phase for linearly polarized light emerge out of phase for elliptically polarized light.[4]

The collected data in an ellipsometric measurement allows obtaining this phase difference, Δ, and the change in the ratio of their amplitudes given by $\tan\Psi$. These parameters are function of the complex refractive index of the material. If the refractive index of a certain film and the substrate on which is deposited are known then the thickness of this film can be calculated by ellipsometry. For

this kind of calculations usually a model must be applied and by iterative methods the parameters that fit the model better are obtained.[5]

The spectroscopic rotating ellipsometer used in this thesis is a M2000, Woollam, NE, USA.

1.3 Atomic Force Microscopy.

In 1982 Binning and Roher invented the scanning tunnelling microscope, where a conducting tip is brought close to the surface to be examined, the voltage difference applied between the two can allow electrons to tunnel through the vacuum between them.[6] Information is acquired by monitoring the current as the tip scans across the surface, and is usually displayed in image form. Following this, a new family of microscopes, scanning probe microscopes, emerged based on the distance dependence interaction between a tip (sharp probe) and a sample. One of these was the atomic force microscope.[7]

AFM uses the force existing between a probe and the sample to create an image. In Fig. 1.2 a) a scheme of the components of one of the most common models is shown.

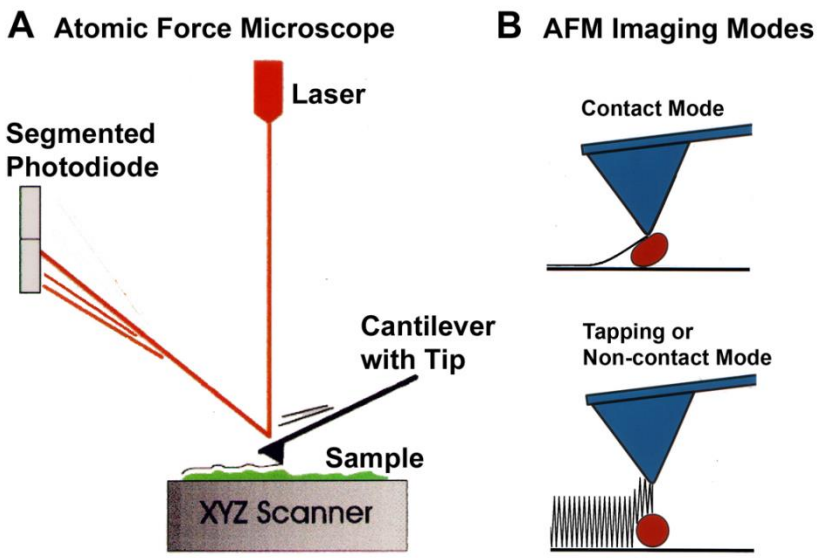

Figure 1.2. a) Components of a standard AFM. b) Scanning modes in AFM.

(Image taken from *http://web.physics.ucsb.edu*).

A nanometer sharp tip is grown at the free end of a flexible cantilever, the reflection of a beam focused at the back of the cantilever is collected in a photodiode, amplifying and measuring the movement of this cantilever while it scans the sample. The sample is placed onto a piezoelectric scanner that can move with subnanometer precision. In this configuration the sample moves over the tip while in others is the tip which moves over the sample.[8]

There are different operating modes of AFM available, with the most commonly used being:

- Contact mode: also called static mode. The tip scans the sample in close contact with the surface. The deflection of the cantilever is sensed and compared in a direct-coupled feedback amplifier to some desired deflection value.

- Tapping mode: also called intermittent contact mode, or a type of dynamic mode. The cantilever oscillates near its resonant frequency gently touching the surface in an intermittent fashion. The oscillation is reduced and this reduction in the oscillation amplitude is used to identify and measure surface features. This oscillation amplitude is maintained at a constant value by a feedback loop.
- Non-contact mode: also a dynamic mode. The tip hovers 50-150 Å above the sample surface where attractive Van der Waals forces acting between the tip and the sample are detected. The tip is given a small oscillation so that detection methods can be used to detect small forces by measuring changes in the amplitude, phase or frequency of the oscillating cantilever in response to force gradients from the sample.

There are other non-topographic modes such as Magnetic Force microscopy, force spectroscopy, nanoindentation, thermal modes and Kelvin probe microscopy.[9]

The great advantage of this technique over other microscopy techniques is the possibility to analyse samples in any kind of environment, i.e.: air, gas, vacuum, or liquid.

All the atomic force microscopy analysis performed during this thesis has been done with a Veeco Multimode atomic force microscope attached to a Nanoscope V controller.

1.4 Ion Cromathography.

Ion chromatography is an analytical technique for the separation and determination of ionic compounds. The first reported use of this technique was made by Thompson in 1850 in a study about the adsorption of ammonium ions to soils. In its modern form it was introduced by Small, Stevens and Bauman in 1975, it has been used for many years and still continues to be used for the separation of various ionic compounds.[10]

Essentially, it consists of a mobile phase or eluent with the mixture to be resolved. It is injected and pumped into a separation column, stationary phase, where the ions interact with fixed ions of opposite charge. The stationary phase typically consists of an inert organic matrix chemically derivative with ionizable functional groups (fixed ions) which carry displaceable oppositely charged ion.[11] Analytes are slowed down to an extent characteristic of each ion and arrived separate to the detector, where they are analyzed.

There are three important factors to take into consideration:

- Efficiency: mainly controlled by the column choice and flow system, in order to have high and narrow chromatographic peaks.
- Capacity: related to the ability of the column to attract ions and the eluent strength.
- Selectivity: capability of separation between analytes.

Ion chromatography measurements were taken with a Thermo Scientific Dionex ICS-1100 ion chromatography system equipped with a Dionex IonPac

CS12A cation-exchange column and a CSRS Ultra II cation self-regenerating suppressor.

1.5 Conductometry.

A conductometer measures the electrical conductivity of ionic solutions by applying an alternating electrical current to two electrodes immersed in a solution and measuring the resulting voltage. Under the effect of the potential difference cations migrate to the cathode and anions to the anode while the solution acts as an electrical insulator. Most conductive solutions are aqueous solutions and have the ability to stabilise the ions formed by solvation.

Conductivity measurements can only be performed after determination of the cell constant by calibration in a solution with a known specific conductivity.

Conductometry is used for direct measurements and in titration. The theory is identical for both methods. Whereas in direct measurements it is the absolute value that is of interest, in titrations it is the change in the measured value.[12]

Conductometry measurements were performed with a Knick Konduktometer 703.

1.6 Scanning Electron Microscopy.

The Scanning Electron Microscope (SEM) was developed in 1937 by Manfred von Ardenne due principally to two limitations of the optical microscope:[13]

- The rather long wavelength of visible light, 400-700 nm, resulting in a theoretical limit of resolution of 200-500 nm, which could be enhanced until a maximum of 100 nm using shorter wavelength light as blue or ultraviolet or immersing the lenses in a high refractive index medium as oil for example. In electron microscopy, electrons have a much shorter wavelength allowing higher resolution.[14]
- A poor depth of field, which means the area of the specimen which can be on focus at the same time. High power objective lens has a short focal length, increasing the aperture angle and decreasing the depth of field. In electron microscopy the working distance is long and has a small aperture making a shallow aperture angle and hence a good depth of field.[15]

Nonetheless, SEM has its limitations. Electrons cannot travel freely through air, they may be absorbed easily if they strike any molecules present, as such they need to be in high vacuum. Another limitation is that sample needs to be conductive enough to dissipate charge.

The electron beam is generated in the electron gun at the top of the column; see Fig. 1.3, and travels along the electron column which is composed by a series of lenses and apertures until hitting the sample at the bottom of it, all the column needs to be at high vacuum.

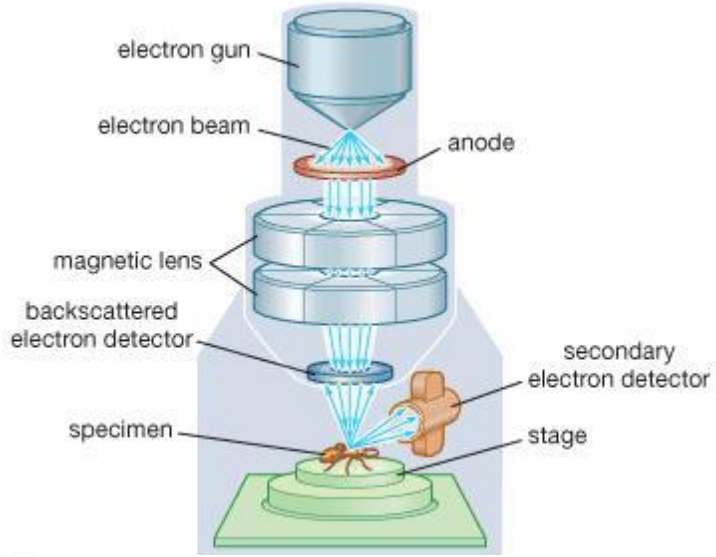

Figure 1.3. Components of a Scanning Electron Microscope. (Image taken from *http://www.britannica.com*).

Electrons are generated by a filament or catode and accelerated toward an anode with an adjustable voltage. Afterwards the condenser lenses merge the beam and focus it down to be 1000 times smaller than its original size. Finally the electron beam passes through different apertures which reduce extraneous electrons and determine the spot size of the beam when it reaches the specimen.

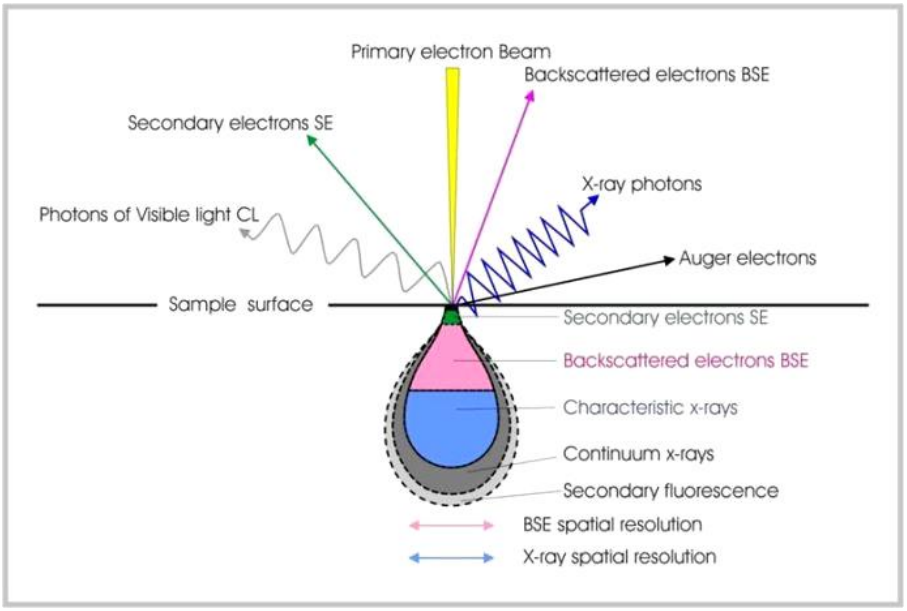

Figure 1.4. Resulting components of the interaction between the electron beam and the sample. (Image taken from *http://www.gla.ac.uk*)

Electrons interact with the atoms of the sample to produce shattered electrons, X-rays and visible light. In electron microscopy two types of signals are used for the visual inspection of the sample, secondary and backscattered electrons.

Secondary electrons are the result of inelastic collisions and scattering of the incident electrons by the specimen electrons. They are used to reveal the surface structure with a resolution of 10 nm or better.

Backscattered electrons are the result of elastic collisions and scattering between the incident electrons and specimen nuclei or electrons. They are used to resolve topographical contrast and atomic number contrast.

The X-ray signal generated allows for the determination of the elemental composition through energy dispersive x-ray spectroscopy (EDS).

SEM has up to 2 million times magnification and a resolution of 0.4 nanometers.[16]

Scanning electron micrographs were obtained using a Jeol JSM-5800 electron microscope.

1.7 Transmission Electron Microscopy.

The first Transmission Electron Microscopy (TEM) was created in 1938 by Prebus and Hillier at the University of Toronto using the concepts exposed by Knoll and Ruska some years before.[17] A TEM operates on the same principle as SEM, nevertheless, in this method the image of the sample is based on transmitted electrons, the electron beam is pointed toward the sample and the electrons that pass through sample illuminate a fluorescent screen where the image is recorded. In order to achieve it the configuration of the instrument is different to that of SEM.

In this case the sample or specimen is placed after the condenser lens which is responsible for concentrating the electron beam produced in the electron gun, see Fig. 1.5.

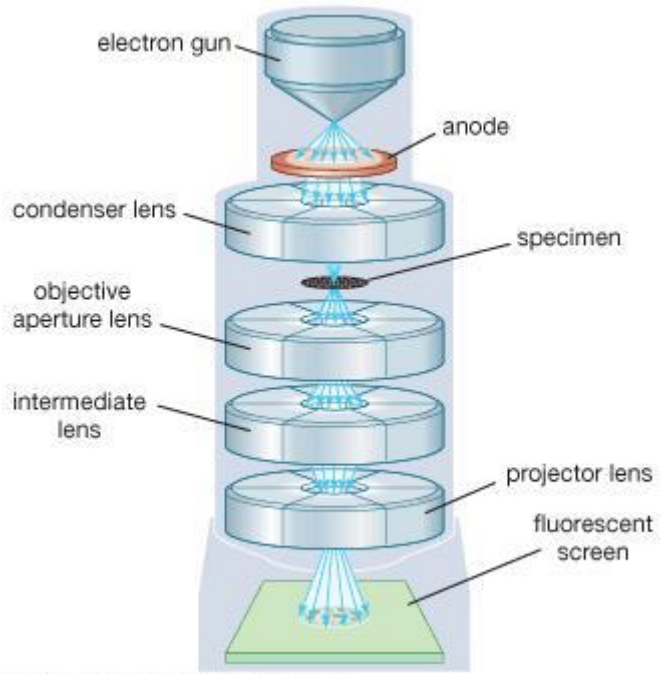

Figure 1.5. Components of a Transmission Electron Microscope. (Image taken from *http://www.britannica.com*).

Afterwards the transmitted electrons encounter the objective lens that produces a real intermediate image that is further magnified by the projector lens and imaged onto the fluorescent screen. TEM has up to 50 million times magnification and a resolution of 0.5Å.[18]

TEM imaging of the GO in this particular case was done using an FEI Titan 80e300 kV field emission gun microscope, which has a symmetrical condenser-objective lens type S-TWIN (with an spherical aberration Cs ¼ 1.25 mm).

In the case of the capsules a JEOL JEM-1400PLUS (40–120 kV) equipped with a GATAN US1000 CCD camera was used.

1.8 X-ray Difraction.

Solid matter can be described as; amorphous where atoms are arranged in a random way or crystalline where atoms are arranged in a regular pattern, called crystals. Approximately 95% of all solid materials can be described as crystalline and when x-rays interact with a crystalline substance they produce a diffraction pattern. This diffraction pattern is like a fingerprint of the substance. The same substance always gives the same pattern and even in a mixture each of the components gives its pattern independently of the others.

When an x-ray beam hits an atom the electrons around the atom begin to oscillate at the same frequency as the incoming beam. In almost all directions there will be destructive interference, while in some specific directions there is constructive interference. These directions are regulated by Bragg´s law:

$$2dsin\theta = n\lambda \qquad \text{(Eq. 1.4)}$$

Where d is the space between diffraction planes, θ is the incident angle, n is an integer, and λ is the wavelength of the beam. These specific directions appear as spots on the diffraction pattern.[19,20]

XRD data for was obtained using a Siemens D-5000 x-ray diffraction system.

1.9 Raman Spectroscopy and Confocal Raman Microscopy.

The Raman effect was first published in 1928 by C.V. Raman.[21] It was first observed by L. Mandelstman and G. Landsberg but their results were published

months later.[22] Nevertheless, the effect was theoretically described in 1923 by A. Smekal.[23]

The Raman effect can be described as changes in the wavelength of light that occur when a light beam is deflected by molecules. When photons interact with a media they can be absorbed or scattered and these scatterings can be either elastic or inelastic. See Fig. 1.6.

- Elastic scattering: there is no energy transfer between the photons and the media. There are two types depending in the size of the scattering particle. Mie scattering occurs when the wavelength of the light is smaller than the size of the particle size, while Rayleigh scattering occurs when the wavelength of the light is larger than the particle.
- Inelastic scattering: there is an energy transfer between photons and the media. If the energy of the photon is high enough it excites a molecule to higher electronic states. Relaxation to the lower level occurs via radiant emission.

  If the energy is not high enough it is excited to a virtual state, which is a quantum mechanically forbidden state, with immediate relaxation to the lowest level via emission a photon.

  If the initial and final states are at the same energy level Rayleigh scattering has occurred. If it relaxes to a higher energy level state than the initial one it has gained energy and the emitted photon has been Stokes shifted. If it relaxes to a lower energy state than the initial one it has lost energy and has been anti-Stokes shifted.

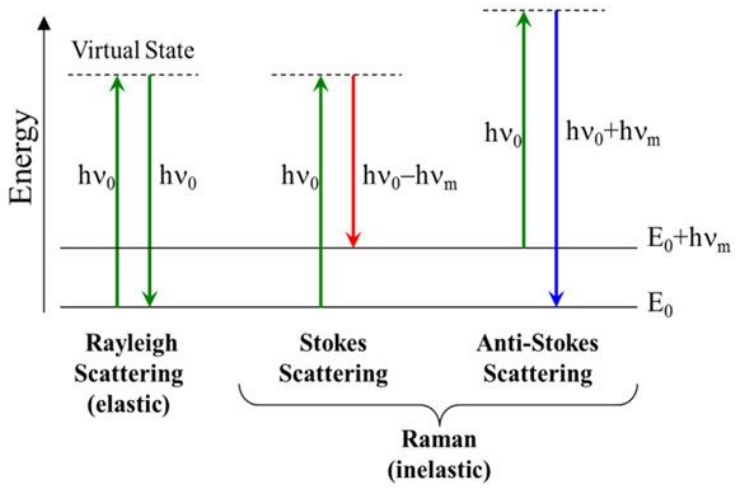

Figure 1.6. Energy translations for elastic and inelastic scattering. (Image taken from *http://bwtek.com*)

Raman spectroscopy is a convenient probe of the energy levels within a molecule providing a molecular fingerprint of it. Therefore collecting the Raman frequencies we can determine the composition of a material. Analysing the polarisation of a Raman peak we can determine the crystal symmetry and orientation. The width of a peak gives an indication of the quality of a crystal; the intensity reflects the amount of a particular molecule while changes in the frequency of the Raman peak reveal the stress/strain state.

Raman analysis was performed using a Renishaw inVia Raman microscope.

1.10 Zeta Potential.

The Z-potential is a property related to the surface charge of a material when suspended in a fluid. A particle dispersed in water is solvated, the boundary between this solvated layer and the bulk solution is called the shear plane, see Fig. 1.7.

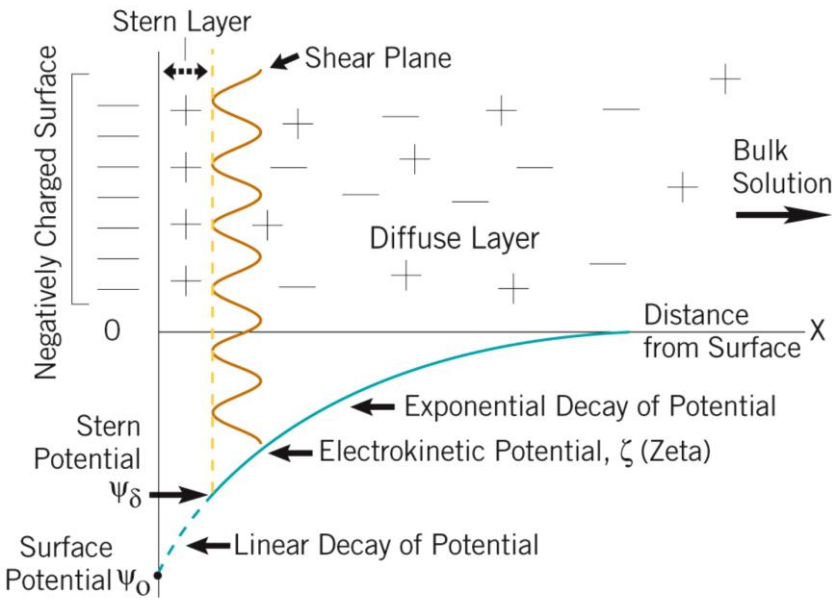

Figure 1.7. Scheme of a simplified model of the electric double-layer at a charged interface in aqueous solution. (Image taken from *http://www.particlesciences.com)*

The distribution of charges at the interface is different to that in the bulk phase. A structure called a double-layer is developed in which ions of opposite charge to that of the surface create an adjacent layer counterbalancing the surface charge, these ions are called counterions. The ions with the same charge as the surface are called coions.

The double layer, as its name suggests, is composed of two regions:

- Stern layer: region closest to the surface with immobile adsorbed ions.
- Diffuse layer: outer region with mobile ions distributed according to influence of electrical forces and thermal motion.

Z-potential is an electrokinetic potential defined as the potential at the shear plane, in order to measure it electrophoresis is used. It is determined by applying an electric field to the suspension and recording the particle transit time. The particles move faster if their charge is greater. The electric field pulls the particle in one direction and the counterions in the opposite direction. Ions in the immobile phase move together with the particle, therefore the shear plane marks the separation limit in which the ions move with the particle or not.[24]

The velocity (m s^{-1}) for unit field strength (1 Volt per meter) is called the electrophoretic mobility and is related to the Z-potential by Henry´s equation:[25]

$$\mu_e = \frac{\varepsilon\zeta}{6\pi\eta} f(k_a) \qquad \text{(Eq. 1.5)}$$

Where ε is the dielectric constant of the media, η is the viscosity, $f(K_a)$ is Henry´s factor and ζ is the Z-potential. Henry´s factor depends on the ratio between the particle radius and the thickness of the double layer. If the radius is much smaller that the double layer $f(K_a)=1$, if it is larger $f(K_a)= 1.5$.

If the Z-potential is large enough there is repulsion between particles when they approach one another keeping them in a state of dispersion. In general, it is accepted that Z-potentials greater than 30 mV, positive or negative, will result in relatively stable dispersions.

The z-potential was measured with a NanoSizer MALVERN Nano-ZS, U.K. All the z-potential measurements were performed at 25°C.

1.11 Electrochemical Impedance Spectroscopy.

Electrochemical impedance spectroscopy (EIS) is a perturbative characterisation of the dynamics of an electrochemical process. It is commonly used in the characterisation of electrode processes and complex interfaces. EIS involves the study of the variation of the impedance of an electrochemical system with the frequency of a small amplitude alternating current perturbation.

Impedance is a measure of the ability of a circuit to resist the flow of electrical current. It is similar to the resistance concept but for more complex systems. As the applied potential is alternating current (AC) the applied excitation is sinusoidal. The response to a sinusoidal potential will be a sinusoid at the same frequency but shifted in phase and it is expressed as a complex number:

$$Z(\omega) = \frac{E}{I} = Z_0 \exp(j\Phi) = Z_0(cos\emptyset + jsin\Phi) \qquad \text{Eq. 1.5}$$

where Z_0 is a magnitude and Φ is the phase.

Impedance data are usually expressed in the form of a Nyquist plot in which the real part of the equation is plotted on the X-axis and the imaginary part on the Y-axis, see Fig. 1.8. Each point corresponds to the value of impedance at a specific frequency; low frequency data are on the right side of the plot and higher frequency data are to the left.

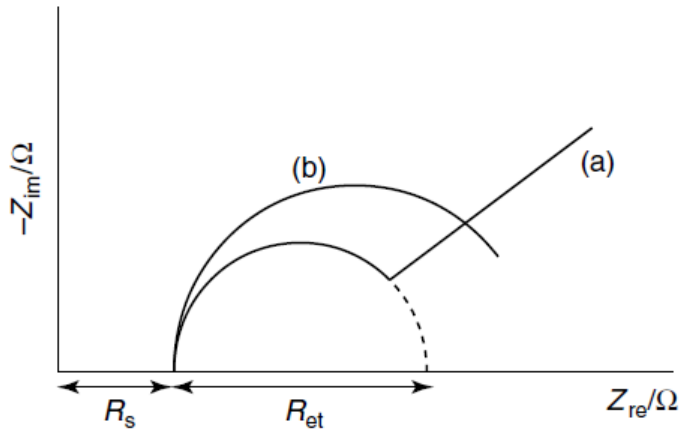

Figure 1.8. Nyquist plot of a modified electrode in which a) impedance is governed by the diffusion of the redox probe and b) impedance is dominated by electron transfer process.[26]

A typical response shows a semicircle at high frequencies corresponding to electron transfer processes, followed by a straight line at low frequencies representing linear diffusion or the so called Warburg diffusion. The diameter of the semicircle reveals the electro transfer resistance (R_{et}) and the intercept with the x-axis corresponds to the solution resistance (R_s).[26]

The electrochemical measurements in this thesis were performed in a typical glass electrochemical cell with a Pt counter-electrode, a saturated calomel electrode (SCE) 0,242V vs normal hydrogen electrode (NHE) was used as a reference electrode, with solutions of 1mM tripotassium hexacyanoferrate (III) ($K_3Fe(CN)_6$) and 1mM Potassium hexacyanoferrate (II) trihydrate ($K_4Fe(CN)_6$) as a probe in a 0.1M potassium chloride as a support electrolyte, see Fig 1.9. All the glass material was precleaned in a warm sulfonitric solution sulfuric acid:nitric acid 2:1 and rinsed with water.

The solution must be degassed with nitrogen for approximately thirty minutes prior to making a measurement.

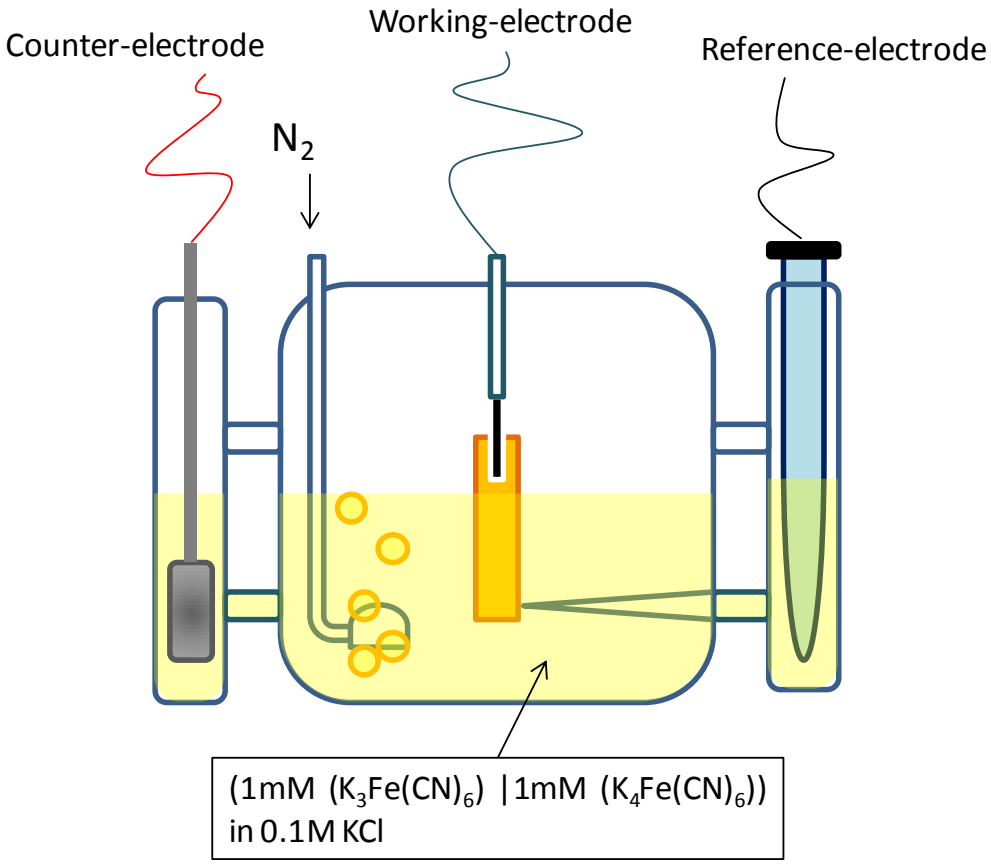

Figure 1.9. Scheme of electrochemical cell set-up.

1.12 Cyclic voltammetry.

Cyclic Voltammetry is a potentiometric method, meaning that the potential that develops between two electrodes is measured. A typical procedure is to control the potential of a working electrode with respect to a reference electrode and measure the resulting current. The magnitude of the resulting current, and its dependence on the applied potential, provides the analytical information. In cyclic voltammetry the potential is swept and reversed at a fixed potential at a

specific rate (in volts s^{-1}) and the current versus time is measured.[27] Time is then converted to potential and recorded as current versus potential, see Fig. 1.10.

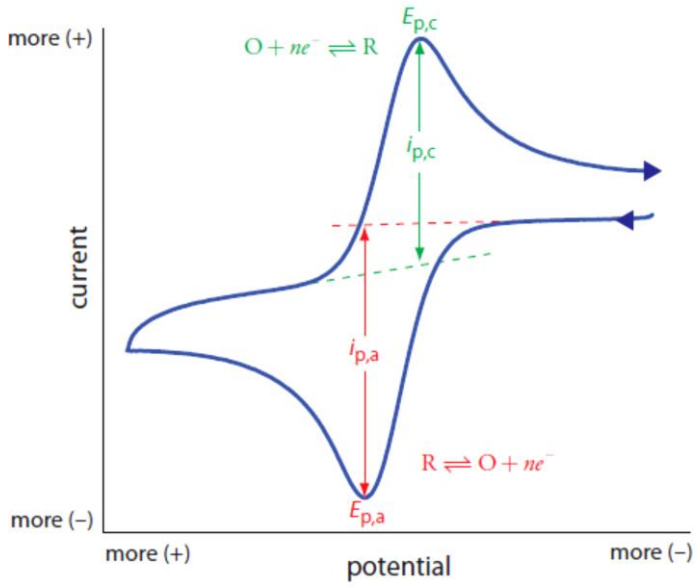

Figure 1.10. Typical cyclic voltammogram showing the measurement of the peak currents and peak potentials.[27]

It is a technique to acquire qualitative information about electrochemical reactions, offering a rapid determination of redox potentials. The cyclic voltammetry measurements can be performed in the same cell as that shown above for EIS.

1.13 Contact Angle

Contac angle or wettability studies is a technique that involves the measurement of the angle formed by the intersection of the solid-liquid interface and the liquid-vapor interface when a drop is resting on a flat,

horizontal solid surface. This angle is acquired by applying a tangent line from the contact point along the liquid-vapor interface in the droplet profile. This interface where solid, liquid and vapor coexist is called the three phase contact line.[28]

The contact angle is defined by the mechanical equilibrium of the drop under three interfacial tensions and it is determine by Young's equation:[29]

$$\gamma_{sv} - \gamma_{sl} - \gamma_{lv} cos\theta_{\gamma} = 0 \qquad \text{(Eq. 1.6)}$$

where γ_{lv}, γ_{sv} and γ_{sl} are the liquid-vapor, solid-vapor and solid-liquid interfacial tensions, and θ_{γ} is the contact angle.

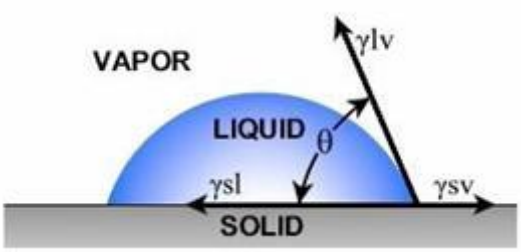

Figure 1.11. Illustration of the contact angle measurement with the sessile drop method. (Image taken from *http://petroleum.mst.edu/*).

This angle is a proof of the wetting properties of the surface, angles of less than 90° indicates that the wetting is favourable and therefore the surface is considered more hydrophilic. Contact angles of more than 90° mean unfavourable wetting, the droplet minimizes its contact with the surface and it is considered a more hydrophobic surface. If contact angles are greater than

150° the surface is considered superhydrophobic, such as the lotus flower effect.[30]

Contact angle measurements were performed with a DSA 100 contact angle measurement device from Kruss Company using the technique of direct image analysis of shape of sessile drops.

1.14 X-ray photoelectron spectroscopy

X-ray photoelectron spectroscopy also known as electron spectroscopy for chemical analysis (ESCA) is a technique used for obtaining information about the composition and chemical state of materials. It is based on the photoelectric effect discovered by Albert Einstein in 1905.[31] The test specimen is irradiated by X-rays of a fixed wavelength (hv) and photoelectrons are excited from the specimen and collected in a detector where the electron kinetic energies ($E_{kinetic}$) of these photoelectrons are measured. See Fig. 1.12.

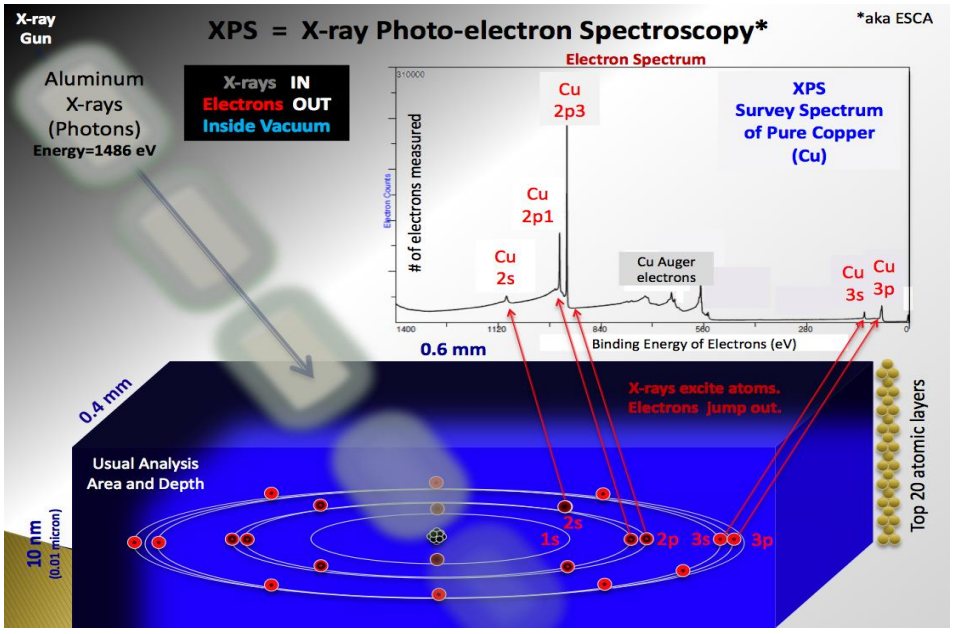

Figure 1.12. Illustration of an XPS measurement. (Image taken from *https://en.wikipedia.org/*).

As the x-ray energy is known (E_{photon}), using the following conservation of energy equation the electron binding energy ($E_{binding}$) of each of the emitted photoelectrons can be determined:

$$E_{binding} = E_{photon} - (E_{kinetic} + \emptyset) \qquad \text{(Eq. 1.7)}$$

where $\emptyset$ is the work function of the detector.

The electron binding energy is an energy associated to the excited electron in a particular orbital and it is unique and depends on the bonding environment, therefore it can act as a fingerprint for identifying elements, measuring the elemental composition, empirical formula, chemical state and electronic state of the elements within a material.[32] These measurements must be conducted in a high vacuum due to the fact that photoelectrons have low kinetic energies.

Surface analysis by XPS during this thesis was performed in a SPECS SAGE HR 100 system spectrometer in an ultra high vacuum (UHV) chamber.

Materials

Chapter 2		
Materials	Acronym	Distributor
3-mercapto-1-propanesulfonic acid	MPS	Sigma Aldrich
Ethanol		Scharlau
Nitric acid		Sigma Adrich
Poly (allylamine hydrochloride)	PAH	Sigma Adrich
Poly (diallylmethylammonium chloride)	PDADMAC	Sigma Adrich
Poly (vinylbenzyltrimethylammonium chloride)	PVBTMAC	Scientific Polymer
Poly(sodium 4-styrene sulfonate)	PSS	Sigma Adrich
Potassium chloride		Sigma Adrich
Potassium hexacyanoferrate (II) trihydrate		Sigma Adrich
Sodium chloride		Sigma Adrich
Sulfuric acid		Sigma Adrich
Tripotassium hexacyanoferrate (III)		Sigma Adrich

Chapter 3		
Materials	Acronym	Distributor
Poly(diallyldimethyl ammonium chloride)	PDADMAC	Sigma Adrich
Poly(sodium 4-styrene sulfonate)	PSS	Sigma Adrich
Sodium chloride		Sigma Adrich

Chapter 4		
Materials	Acronym	Distributor
(1-tetradecyl) trimethylammonium bromide	TTAB	Alfa Aesar
Acetic acid		Sigma Adrich
Bovine serum albumine	BSA	Sigma Adrich
Hydrochloric acid		Sigma Adrich
Poly (acrylic acid)	PAA	Acros
Poly (allylamine hydrochloride)	PAH	Sigma Adrich

Poly (diallylmethylammonium chloride)	PDADMAC	Sigma Adrich
Poly(sodium 4-styrene sulfonate)	PSS	Sigma Adrich
Polyethyleneimine	PEI	Sigma Adrich
Sodium acetate trihydrate		Sigma Adrich
Sodium chloride		Sigma Adrich
Sodium dodecyl sulfate	SDS	Sigma Adrich
Sodium hydroxide		Scharlau

Chapter 5

Materials	Acronym	Distributor
Multi walled carbon nanotubes	MWCNT	Nano-lab
Magnesium Chloride hexahydrate		VWR International
Magnesium sulfate heptahydrate		Fluka
Nitric acid fuming		Fluka
Poly (allylamine hydrochloride)	PAH	Sigma Adrich
Poly (diallylmethylammonium chloride)	PDADMAC	Sigma Adrich
Poly(sodium 4-styrene sulfonate)	PSS	Sigma Adrich
Sodium chloride		Merck KGaA
Sodium hydroxide		Fluka
Sulfuric acid		Fluka

Chapter 6

Materials	Acronym	Distributor
Full blood chicken collected in Alsever's anticoagulant solution		Harlan Laboratories Models S.L
Glutaraldehyde solution grade II		Sigma Adrich
Graphite powder		Sigma Adrich
Hank´s balanced salt solution 10x		Sigma Adrich
Lymphocytes isolation solution (Ficoll)		Rafer
Phosphate buffered saline 10x	PBS	Sigma Adrich
Poly(sodium 4-styrene sulfonate)	PSS	Sigma Adrich
Polyallylamine hydrochloride	PAH	Sigma Adrich
Sodium chloride		Sigma Adrich
Sodium hypochlorite with active chlorine		Sigma Adrich

References

(1) Dixon, M. C. *J. Biomol. Tech.* **2008**, *19*, 151–158.

(2) Sauerbrey, G. *Zeitschrift für Phys.* **1959**, *155*, 206–222.

(3) Cernosek, R. W.; Martin, S. J.; Hillman, A. R.; Bandey, H. L. *Ultrason. Ferroelectr. Freq. Control. IEEE Trans.* **1998**, *45*, 1399–1407.

(4) Gonçalves, D.; Irene, E. A. *Quim. Nova* **2002**, *25*, 794–800.

(5) Xifré Pérez, E. Design, fabrication and characterization of porous silicon multilayer optical devices, Universitat Rovira i Virgili, 2008.

(6) Binnig, G.; Rohrer, H.; Gerber, C.; Weibel, E. *Phys. Rev. Lett.* **1982**, *49*, 57–61.

(7) Moreno-Herrero, F.; Gomez-Herrero, J. In *Atomic Force Microscopy in Liquid: Biological Applications.*; M. Baró, A., G. Reiifenberg, R., Eds.; Wiley-VCH Verlag GmbH & Co. KGaA, 2012; pp 1–34.

(8) Binnig, G.; Quate, F.; Gerber, C. *Phys. Rev. Lett.* **1986**, *56*, 930–933.

(9) Eaton, P.; West, P. *Atomic Force Microscopy*; Oxford University Press, 2010.

(10) Acikara, Ö. B. In *Column Chromathography*; Martin, D. F., Martin, B. B., Eds.; InTech, 2013; p 31.

(11) Cummins, P.; Dowling, O.; O'Connor, B. In *Protein Chromatography SE - 12*; Walls, D., Loughran, S. T., Eds.; Methods in Molecular Biology; Humana Press, 2011; Vol. 681, pp 215–228.

(12) Khopkar, S. . *Basic Concepts of Analytical Chemistry*, 3rd Editio.; New Age Science Ltd, 2008.

(13) Von Ardenne, M. *Zeitschrift für Phys.* **1938**, *109*, 553–572.

(14) Stadtländer, C. … *Res. Educ. Top. Microsc.* **2007**, *1*, 122–131.

(15) Flegler, S. L.; Heckman, J. W.; Klomparens, K. L. *Scanning and Transmission Electron Microscopy: An Introduction*; Oxford University Press, 1993.

(16) Dunlap, M.; Adaskaveg, J. E. *Introduction to the Scanning Electron Microscope: Theory, Practice, & Procedures*; 1997.

(17) Ma, H.; Shieh, K.-J.; Qiao, T. X. *Nat. Sci.* **2006**, *4*, 14–22.

(18) Williams, D. B.; Barry Carter, C. *Transmission Electron Microscopy*, 2nd ed.; Springer US, 2009.

(19) Birkholz, M. In *Thin Film Analysis by X-Ray Scattering*; Wiley-VCH Verlag GmbH & Co. KGaA, 2005; pp 1–40.

(20) Fultz, B.; Howe, J. In *Transmission Electron Microscopy and Diffractometry of Materials*; Springer Berlin Heidelberg: Berlin, Heidelberg, 2013; pp 1–57.

(21) Raman, C. V. *Indian J. Phys.* **1928**, *2*, 387–398.

(22) Landsberg, G.; Mandelstam, L. *Naturwissenschaften* **1928**, *16*, 557–558.

(23) Smekal, A. *Naturwissenschaften* **1923**, *11*, 873–875.

(24) Particle sciences. *Technical briefs; An Overview of the Zeta Potential*; 2012; Vol. 2.

(25) Smoluchowski M. *Bull. Int. Acad. Sci. Cracovie.* **1904**, 182–199.

(26) Azzaroni, O.; Gervasi, C. In *Functional Polymer Films*; Wiley-VCH Verlag GmbH & Co. KGaA, 2011; pp 809–830.

(27) Harvey, D. In *Modern Analytic Chemistry*; Kane, K. T., Ed.; James M. Smith, 2000; pp 461–542.

(28) Yuehua, Y.; Randall Lee, T. In *Springer Series in Surface Sciences*; Bracco, G., Holst, B., Eds.; Springer-Verlag Berlin Heidelberg, 2013; Vol. 51, pp 3–34.

(29) Young, T. *Philos. Trans. R. Soc. London* **1805**, *95*, 65–87.

(30) Lafuma, A.; Quere, D. *Nat. Mater.* **2003**, *2*, 457–460.

(31) Einstein, A. *Ann. Phys.* **1905**, *322*, 132–148.

(32) Hüfner, S. *Photoelectron Spectroscopy- Principles and Applications*, 3rd ed.; Springer-Verlag, Berlin Heidelberg), 2003.

POLYELECTROLYTE MULTILAYERS

Chapter 2- A Comparison of the Transport Properties of Supralinearly and Linearly Growing Polyelectrolyte Multilayers: A Cyclovoltametry and Impedance Study

2.1 Introduction

In recent years there has been continuously growing interest in the use of polyelectrolyte multilayers (PEMs) for nanofiltration and reverse osmosis applications.[1–8] Since PEMs thicknesses vary normally from 10 to 50 nm and possess a high density of charged functional groups PEMs are very attractive for nanofiltration. Several articles have explored the possibilities of PEMs as filtration membranes using different combinations of polyelectrolytes with very high retention for specific ions.[9–11]

A key aspect related to the use of PEMs for nanofiltration/reverse osmosis is their permeability, and in particular their ionic permeability. PEM permeability is also of fundamental importance for applications in drug delivery[12] and as anticorrosive coatings.[13]

There are several studies dealing with the ionic permeability of PEMs. Some articles have focused on understanding the permeability of polyelectrolyte capsules with respect to drug delivery applications as already mentioned. For

capsules, ionic permeability was studied with confocal microscopy and also by means of electrorotation.[14] It was found that the process of capsule templation generated pores responsible for permeability and transport of molecules in the capsules

On planar PEMs ionic transport was studied by means of electrochemical techniques: cyclic voltammetry and electrochemical impedance. Electrochemical techniques have been thoroughly used in the past to study the interaction between films and an analyte and/or the kinetics of charge and mass transport through polyelectrolyte multilayers.[15] One of the first studies on multilayers was performed by Liu et al., where they analysed the pH-switchable behaviour of a polyelectrolyte membrane by cyclic voltammetry.[16] Multiple combinations of polyelectrolytes have been studied. One of the most common pairs in PEMs is PAH/PSS, which display a linear growth regime. Ionic permeability for these films has been studied as a function of layer number, temperature, nature of salt solutions, amongst others.[15,17]

A theoretical model for understanding the permeability of these films, taking into account their layered structure and the progressive coating of the electroactive surface with increasing number of polyelectrolyte layers, has been reported by Silva et al.[15] This model, named Capillary Membrane Model (CMM), describes the polyelectrolyte membrane as a porous film with circular uncovered spots. By increasing the number of deposited polyelectrolyte layers, the holes on the surface decrease in number and size.[18] Indeed, PEMs of PAH/PSS display high permeability with small electron charge resistance for

the first assembled layers. As the number of layers increases the charge resistance increases and transport in the films decreases, which can be understood as the films becoming denser and holes on the conductive substrate become covered. In linear growth regimes the amount of polyelectrolyte deposited per pair is mostly constant with a low degree of interpenetration, meaning that the newly adsorbed layer neutralizes the majority of the charges of the previous layer. However, not all multilayers grow in a linear regime. Some polyelectrolyte combinations display exponential or supralinear growth regimes. In an exponential or supralinear regime the amount of polymer assembled increases as the number of layers deposited increases, the interaction between polyelectrolyte layers is not so strong and there is diffusion of polyelectrolyte molecules between layers, it leads to thicker highly hydrated films.

The chemistry of the polyelectrolytes, spatial arrangement, and the nature of the interactions between the polyelectrolyte pairs has an influence on determining one or the other regime. In a recent study run by the group of Piotr Warszynsky they analysed, using electrochemical methods, the difference in permeability between pairs of polyelectrolyte showing linear and exponential growth.[19] They compared PAH/PSS versus PDADMAC/PSS and concluded that linearly grown polyelectrolyte multilayers form denser films and perform better as a diffusion barrier for electroactive species compared to the pair that grows exponentially, which forms a highly hydrated spongy like structure with high viscosity and high permeability. The different growth

regimes for both films results in two well defined structures but it is not clear why one or other regimes occurs. The reason for the different growth regimes in these two polyelectrolyte pairs lies probably in the different interactions between primary amines of PAH and the sulfonate of PSS , and between the quaternary amines of PDADMAC and the sulfonate groups of PSS.[20] The different interaction between the two types of amines with the sulfonate may also influence the transport of a redox probe as the strength of the interaction between polyanion and polycation may affect the interaction of the probe with the charged groups of the PEM. It is also the case that primary or quaternary amines interact differently with the redox probe. The probes are normally complexes formed by a cation or an anion surrounded by small charged organic molecules. The complexes have several charges and can interact with the charged polyelectrolytes of the multilayer. In order to compare the transport properties of supralinearly and linearly growing PEMs formed by a pair of polyelectrolytes with similar chemistry but different growing regime we have decided to work with PEMs with polystyrene sulfonate (PSS) as the polyanion and two polycations bearing quaternary amines:; poly(diallydimethylammonium chloride) (PDADMAC) in one case and poly(vinylbenzyltrimethylammonium chloride) (PVBTMAC) in the other. Both polycations have quaternary amines but when assembled with PSS the first results in a film with a supralinear growth while the second is linear. Despite both polycations have a similar chemistry, both entail quaternary amines, they differ significantly in their stereochemistry and the chemistry of the backbone

chain. The similitude in the chemistry between PDADMAC/PSS and PVBTMAC/PSS films make them suitable to compare the transport properties between the two films in relation to the growth regime, without a difference in the chemistry of the charged groups in polymer and differences in the interaction between charged functional groups play a role. In addition we will study the properties ofthe two films to try to understand why they display different tendencies of growth.

2.2 Materials and methods

Poly (allylamine hydrochloride) (PAH) [Mw= 15 $kgmol^{-1}$], poly (diallylmethylammonium chloride) (PDADMAC) [Mw = 200-350 $kgmol^{-1}$] 20 % wt. in water, polyestyrene sulfonate (PSS) [Mw= 70 $Kgmol^{-1}$], Poly (vinylbenzyltrimethylammonium chloride) [Mw =100 Kgmol-1] 26.81 % wt in water, sodium chloride, Tripotassium hexacyanoferrate (III) ($K_3Fe(CN)_6$), Potassium hexacyanoferrate (II) trihydrate ($K_4Fe(CN)_6$), 3-mercapto-1-propanesulfonic acid (MPS), Ethanol, Sulfuric acid, and Nitric acid.

Gold films with a thickness of around 100 nm were deposited on glass substrates with non-reactive magnetron sputtering using an AJA-ATC 1800 system with a base pressure of 10^{-7} Pa. Prior to deposition, the substrates were sputter cleaned with a negative bias of 180 V (25 W) in a 4 Pa Ar atmosphere for 10 min. In order to improve the adhesion of the films to the substrates, a pure Ti layer of around 50 nm was deposited on the substrates at a Ti target d.c. power of 270 W. The deposition of the films was done with a 2 inch target, with

a purity of 99.999% at a pressure of 0.25 Pa of pure Ar and a direct current (d.c.) target power of 150 W. The distance between target and substrates was about 15 cm.

2.2.1 Quartz Crystal Microbalance with Dissipation (QCM-D)

Polyelectrolyte membrane assembly was monitored in a quartz crystal microbalance with dissipation. The substrates, gold (100 nm)-coated quartz crystals were previously cleaned in a UV-Ozone procleaner. Prior to polyelectrolyte assembly the sensors were incubated overnight in a MPS 10^{-2} M in ethanol solution.

All polyelectrolyte solutions were prepared to a concentration of 1 $mgml^{-1}$ in 0.5 M NaCl. The deposition of each layer is followed by a decrease in the resonance frequency of the 3rd overtone (15 MHz) with subsecond time resolution.

The mass of the PEM was calculated using the Sauerbrey equation, $\Delta m=-C(\Delta f)$ where C = 18.06±0.15 $ngcm^{-2}Hz^{-1}$.

2.2.2 Atomic Force Microscopy (AFM)

The PEMs were previously assembled and monitored in the QCM-D. All the measurements were analysed in a fluid cell with 10 mM NaCl. For the PVBTMAC/PSS PEM a DNP cantilever with K=0.35 Nm^{-1} in contact mode was used. In the case of PDADMAC/PSS two different cantilevers were used a DNP of K=0.35 Nm^{-1} for contact mode and a K=0.06 Nm^{-1} for tapping mode.

2.2.3 Cyclic Voltammetry and Impedance Spectroscopy

Electrochemical measurements were performed in a glass electrochemical cell with a Pt counter-electrode, saturated calomel electrode (SCE) 0,242 V VS ENH as reference electrode, and as probe a solution of 1 mM ($K_3Fe(CN)_6$) and 1 mM ($K_4Fe(CN)_6$) in a 0.1 M KCl solution support electrolyte. The solution must be degassed with N_2 for approximately half an hour before measurement. All glass material was precleaned in a warm sulfonitric solution H_2SO_4:HNO_3 2:1 and rinsed with water.

Gold substrates were precleaned prior to the assembly by a 2 minute immersion in a cleaning solution of ½ H_2O+½ H_2O_2 + 1/15 H_2SO_4, rinsed with water, rinsed with Acetone and finally rinsed with Ethanol.

Samples were incubated overnight in a solution 10^{-2} M MPS in Ethanol in order to give a negative charge to the surface, we rinsed with ethanol, and finally rinsed with water.[21]

The assembly of the polyelectrolytes was performed by consecutive immersion of the substrate for 15 minutes in a 1 $mgml^{-1}$ of the polyelectrolyte in 0.5 M NaCl solution followed by rinsing in water three times before the next polyelectrolyte with opposite charge was assembled. This procedure was repeated until the desired number of layers was assembled. Every set of membranes were assembled simultaneously.

2.2.4 Contact Angle

A 5 μl drop of nanopure water was placed onto a glass substrate previously functionalised with a thiol and the corresponding PEM on top. The same procedure as for the electrochemistry experiments explained before.

2.2.5 XPS

The X-ray source employed for this analysis was a non-monochromatic Mg Kα (1253.6 eV) operated at 250 W, calibrated using the $3d_{5/2}$ line of Ag with a full width at half maximum (FWHM) of 1.1 eV. The take- off angle was fixed at 90^{o} and the analysis was conducted at a pressure of ~10^{-6} Pa.

A multilayer of $(PDADMAC/PSS)_{6.5}$ at 0.5 M NaCl was assembled on top of a gold substrate coated with MPS and incubated for 2.5 hours in a ferro/ferri 1 mM at 0.1 M KCl solution. The substrate was rinsed several times and left in nanopure water for one hour prior to XPS measurements.

Surfaces were brought into the XPS chamber within 5 min after cleaning/preparation. The selected resolution for the spectra was 30 eV of Pass Energy and 0.5 eV/step for the general survey spectra and 15 eV of Pass Energy and 0.15 eV/step for the detailed spectra of N1s, Fe3p, Fe 2p, O 1s and C 1s.

The resulting atomic percentages of Fe(CN) oxidation states are calculated from the fitting of the Fe 2p region. Spectra were analysed with the Casa XPS 2.3.15dev87 software. The analysis consisted of satellite removal, Shirley background subtraction, calibration of the binding energies related to the C 1s C-C peak at 285 eV, and symmetric peak fitting with Gaussian-Lorentzian line

shapes where the FWHM of all the peaks were constrained while the peak positions and areas were set free.

2.3 Results and discussion

In this work we intend to compare the assembly and transport properties of two different PEMs with the same polyanion, PSS, and polycations bearing quaternary amines but with different stereochemistry and backbone chemistry, PDADMAC and PVBTMAC. In PDADMAC the quaternary amine is located inside a cyclopentyl group in the chain, while in PVBTMAC the quaternary amine is pendant of a benzyl group, as it can be seen in Fig. 2.1.

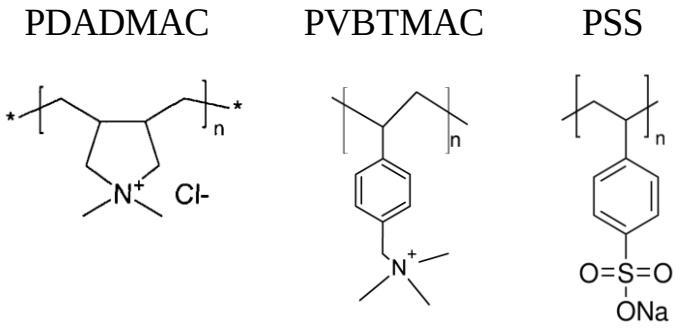

Figure 2.1. Chemical structure of the polyelectrolytes involved in the different assemblies.

The assembly of both PEMs was monitored by QCM-D as can be seen in Fig. 2.1a and 2.1b. Frequency decreases stepwise after each polyelectrolyte deposition with a constant value for PVBTMAC, Fig. 2.1a, while in the case of PDADMAC/PSS films the value for the frequency steps resulting from polyelectrolyte deposition increase with the increasing of the number of layers. In both cases after each deposition step the excess of polyelectrolyte is rinsed

with 0.5 M NaCl, the same salt concentration as the polyelectrolyte solution. In the last step both PEMs are rinsed with water, it can then be observed that in the case of PVBTMAC there is not a large change in frequency when we replace the salt for pure water. However, in the case of PDADMAC there is a large uptake of water resulting in a doubling of its hydrated mass. Also the dissipation increases dramatically showing a more loose and swollen structure, while the PVBTMAC is more rigid and compact as illustrated in Fig. 2.2d. The hydrated mass for both PEMs have been calculated for each layer and it is plotted in Fig. 2.2c.

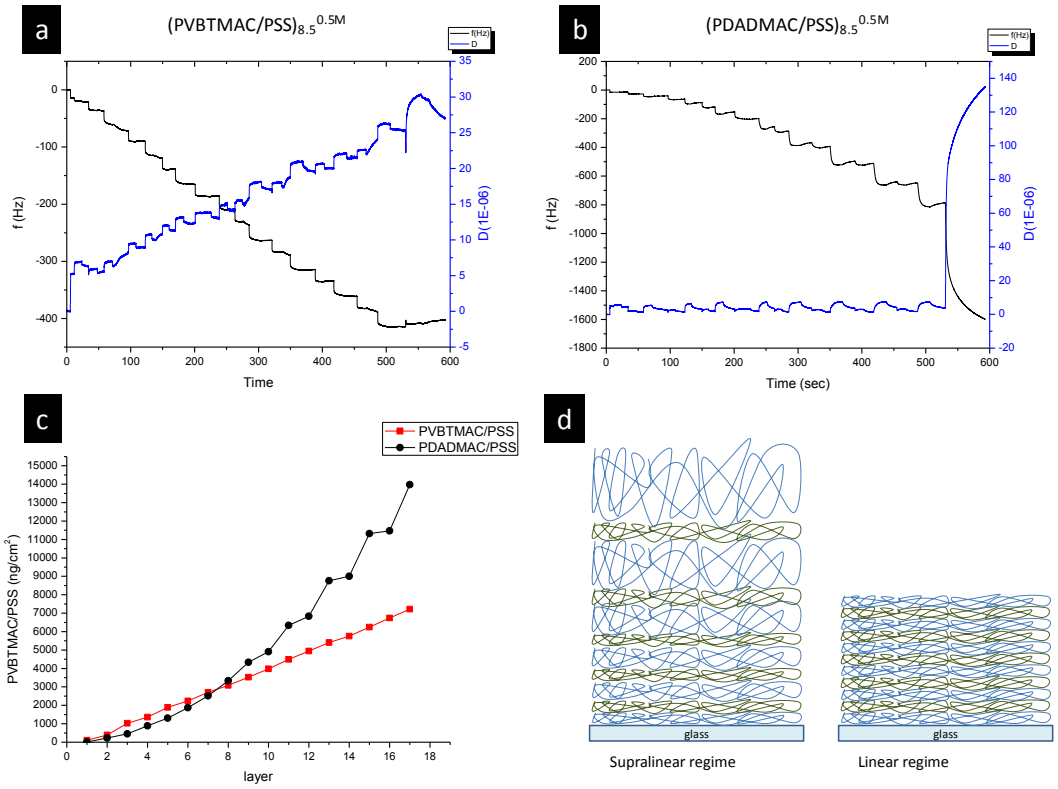

Figure 2.2. a) Deposition of 17 layers of PVBTMAC and PSS at 0.5 M NaCl by QCM-D. b) Deposition of 17 layers of PDADMAC and PSS at 0.5 M NaCl by QCM-D. c) Representation of mass vs layer for 17 layers of PDADMAC/PSS

and PVBTMAC/PSS assembled by QCM-D. d) Sketch of supralinear and linear assemblies.

The plotts reveal a linear growth tendency for PVBTMAC/PSS and supralinear growth in the case of PDADMAC/PSS. It can also be observed that in the case of PDADMAC/PSS the increase in hydrated mass of PDADMAC is larger than the amount of PSS. After 17 layers of PVBTMAC/PSS the hydrated mass deposited is approximately the same as 12 layers in the case of PDADMAC/PSS. The capacity of PDADMAC/PSS to hydrate upon changing from a NaCl solution, 100-500 mM, to water has already been reported.[22] This sponge like behaviour is pronounced when the film has over 10 or 11 layers of polyelectrolyte. Making an analogy with PE brushes the PDADMAC/PSS PEMs must have uncompensated charges and a certain capacity for chain reorganization. In a supralinear regime there are more uncompensated charges, than in a linear regime, as PVBTMAC/PSS does not have similar hydration behaviour. The nature of the pending group does not seem to play a role here. In both cases the amines are quaternary and when we look at the molecular structure of PDADMAC the amines in this polymer are likely to be imbibed in a more hydrophobic environment. This is because for PDADMAC the amine groups are located in the back bone chain while the quaternary amines in PVBTMAC are pending groups. The responsiveness of the film is, however, lost when PSS is the top layer.[22] This could be due to the PSS providing less uncompensated charges or that being a glassy polymer, it has a limited capacity to reorganize once in the layer and for that reason the PEM does not hydrate as

in the case with PDADMAC as the top layer. This also hints that most of the uncompensated charges are in the top layer of PDADMAC. An explanation for the different growth behaviour for the two pairs and the absence of a response with changes in ionic strength for PVBTMAC/PSS PEMs could indeed lie in the nature of PVBTMAC which is also a polymer with aromatic rings in the structure. PVBTMAC once deposited probably cannot rearrange or reorganize like PDADMAC. It may also not easily interdifuse in the layers or interdigitate with previous layers, which seems to be fundamental for supralinear or exponential growth.

The sponge like nature of the PDADMAC/PSS film should result in a very soft material. This can be observed by AFM. First, the topology of both samples has been analysed by AFM as can be seen in the height images shown in Fig. 2.3. In both cases the analysis was performed in a liquid cell filled with 10 mM NaCl, and using a cantilever of k = 0.35 Nm^{-1} in contact mode, Fig. 2.3b and c. In the case of PDADMAC/PSS, Fig. 2.3c, the PEM is by the cantilever and the surface is distorted, with polymer being dragged during the scanning, this is evidence of the difference in the stiffness of both PEMs. Therefore, for the analysis of the PDADMAC/PSS PEM we used a softer cantilever of k = 0.06 Nm^{-1} in tapping mode. Even in these conditions there is some unavoidable drift due to the spongy swelled structure of the PDADMAC/PSS.

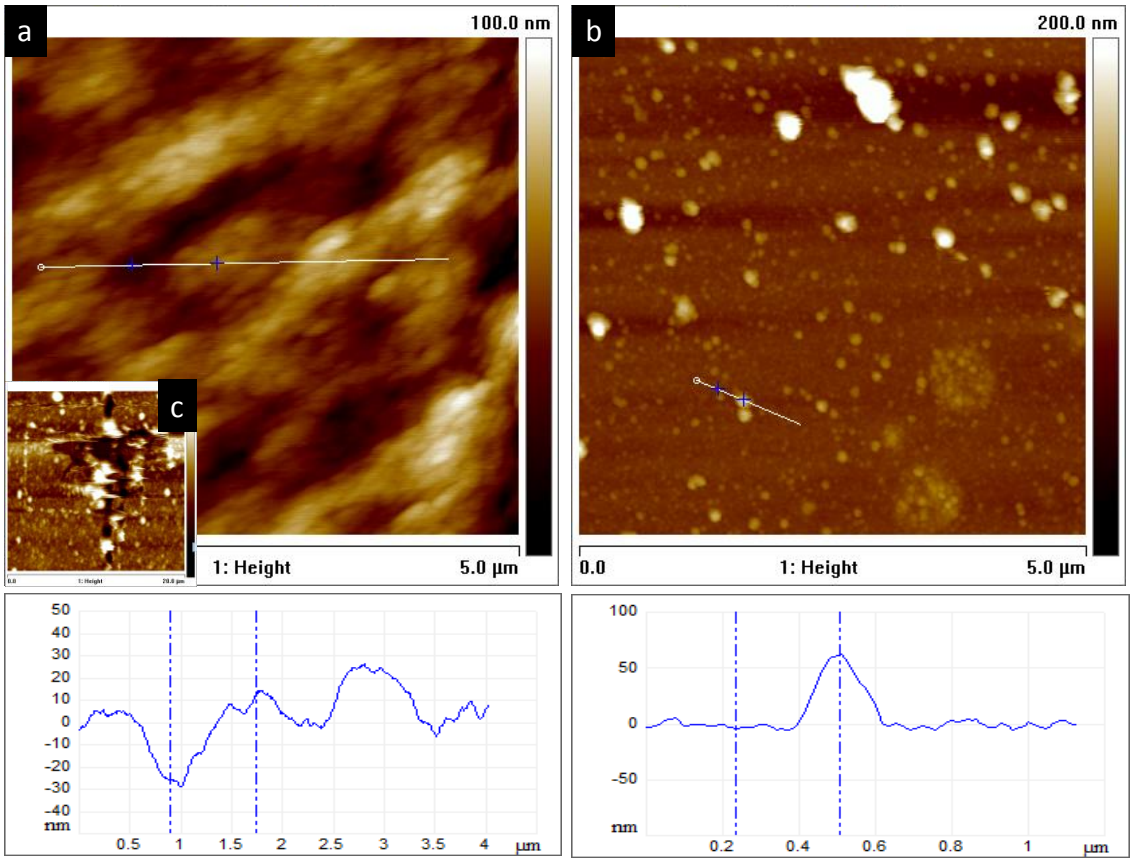

Figure 2.3. AFM images of a) 17 layers of PDADMAC and PSS assembled at 0.5 M NaCl, analysed in 10 mM NaCl in tapping mode with a DNP cantilever of 0.06 Nm^{-1}. b) 17 layers of PVBTMAC and PSS assembled at 0.5 M NaCl, analysed in 10 mM NaCl in contact mode with a DNP cantilever of 0.35 Nm^{-1}. c) 17 layers of PDADMAC and PSS assembled at 0.5 M NaCl, analysed in 10 mM NaCl in contact mode with a DNP cantilever of 0.35 Nm^{-1}.

Comparing Fig. 2.3a for PDADMAC/PSS and Fig. 2.3b for PVBTMAC and their profiles, we can clearly see the difference not only in topology but also in stiffness. In the case of PVBTMAC the PEM is stiff and flat with some grains of a considerable height of around 50 nm and sometimes bigger, popping out from the surface probably due to aggregates or defects in the compression of the layers. For PDADMAC/PSS, the structure is clearly less compact, very soft, resulting in a less flat profile as a consequence of the water swelled membrane.

Analysing the evolution of the contact angle as the PEMs grow provides additional information on the assembly mechanism between the two polyelectrolyte pairs. In Table 2.1 the difference in the contact angle for both systems at a different number of assembled layers can be observed. Interestingly the contact angle for PBVTMAC/PSS measured always with PVBTMAC as top layer at the 5th, 11th and 17th layers is almost constant with values between 24 and 29 degrees indicating a hydrophilic film. A very different situation is encountered for PDADMAC/PSS films. At an initial stage the PDADMAC/PSS film is quite hydrophobic with a value at the 5th layer of 73 degree. At the 11th and 17th layers the contact angle becomes smaller but still much more hydrophobic than the PVBTMAC/PSS PEM, remaining between 42 and 49 degrees.

Table 2.1 Contact angle measurements at different number of layers for PDADMAC/PSS and PVBTMAC assemblies.

	5 layers	11 layers	17 layers
PDADMAC/PSS	73	42	49
PBVTMAC/PSS	27	29	24

The consistency of the contact angle of PVBTMAC/PSS with increasing layer number reflects the linearity of the growth. The density of the functional groups in the PBVTMAC/PSS PEM is always the same. The film is quite hydrophilic meaning that the charge density is high. For PDADMAC/PSS the situation is different. The initial value of the contact angle is high, indicative of more hydrophobic behaviour. This can be because the quaternary amines are not pendant but part of the backbone chain. Despite this the PDADMAC/PSS

films are always more hydrated and there is much more mass of PDADMAC in the top layer compared to PBVTMAC, which also would mean a larger number of charged amines for PDADMAC. The high contact angle would however be a consequence of a lower surface density of amines. This could be because the layers of PDADMAC are thicker meaning that the charges are distributed over a larger volume than for PBVTMAC. The decrease in the contact angle with increasing layer number for PDADMAC/PSS can be explained by the increase in charged amines per layer as a consequence of the supralinear growth of the film.

Transport studies were carried out by analysing the electrochemical behaviour of two probes ($K_3Fe(CN)_6$) and ($K_4Fe(CN)_6$) when the solution is in contact with a gold electrode covered with a monolayer of MPS thiols covered with either a PDADMAC/PSS or PBVTMAC/PSS PEM. At the surface of the gold the probes can undergo oxidation or reduction, depending on their oxidation state, by exchanging electrons with the substrate. Initial experiments were performed with cyclic voltametry. Both cathodic and anodic currents were measured with increasing numbers of layers for both PDADMAC/PSS and PBVTMAC/PSS as shown in Fig. 2.4a and b. For clarity the maximum of the cathodic and anodic peaks have been plotted as a function of the layer number in Fig. 2.4c.

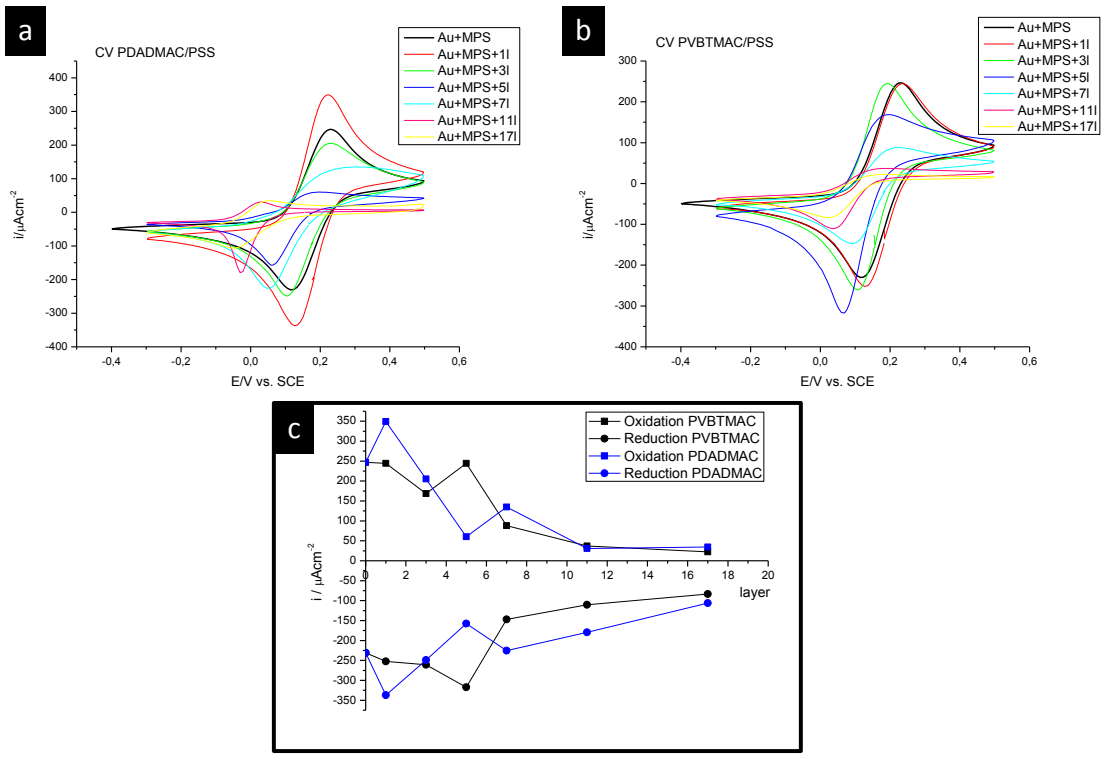

Figure 2.4. Cyclic voltammograms for a) PDADMAC/PSS and c) PVBTMAC/PSS PEMs onto MPS functionalised gold substrates. C) Maximum current in oxidation and reduction steps for each PEM.

We have plotted only the voltammograms for the odd layers, which correspond to the polycation as the top layer in the PEM for two reasons. Firstly, because in both assemblies in our study the samples differ in the choice of polycation, and their different behaviour is what we want to analyse; and secondly because as we are using negative redox probes, if a polyanion is the top layer there will be electrostatic repulsion, affecting diffusion.

It has been reported in literature that although PEMs are very permeable to monovalent and divalent ions used as supporting electrolytes, permeability decreases rapidly with increasing the number of layers in the PEM for heavily charged electroactive probes.[18] This effect has been explained in different ways.

It has been postulated that it is caused by a reduction of the active area of the electrode as the number of deposited layers increases, the so called Capillary Membrane Model (CMM).[23] Another explanation is that the diffusion of the probe in the film is due to the hopping between exchange sites created within the film by the supporting electrolyte. The decrease in permeability with the number of layers is attributed to a decrease in the concentration gradient of the probe inside the film as the thickness increases,[24,25] this model is called the Homogeneous Membrane Model (HMM).[18]

As can be seen in Fig. 2.4c, in both cases there is a strong decay in the current for the initial layers as well as some irregularities in the current until the 5th layer. It is well known in LbL technique the assembly of the first layers are quite irregular and the amount of polymer and charge distribution per layer is not homogeneous. For the first layers it is likely that the coverage of the surface is partial, with areas remaining free of polymer. The reduction of the current intensity can be interpreted as a reduction in the active area as the number of layers increase and the polymer free areas are covered with polymer.

After the fifth layer for both PEMs the current decreases only slightly until reaching a state after the 17th layer of nearly blocked current. This is observed for both PEMs at approximately the same number of layers despite having different thicknesses. Also the shape of the voltammogram plateaus with the decrease of the peak current as has previously been reported as a consequence of the reduction of the diffusion coefficient in the film and the nonlinear diffusion of the probe.[18] In both cases the anodic current is less favoured than

the cathodic current. In the case of PDADMAC this difference is more evident. Therefore, reduction is less affected compared to oxidation by the number of assembled layers. It can also be observed that in the case of PDADMAC, Fig. 2.4a, there is a shift of the apparent redox potential to values close to zero, meaning that there is complex formation between the probe and the polyelectrolyte, and that this complex is formed after the assembly of the 11th layer.

Impedance studies were also performed on the PEMs. In Fig. 2.5 we can see the Nyquist diagrams of both assemblies. In both cases PDADMAC/PSS, Fig. 2.5a, and PVBTMAC/PSS, Fig. 2.5b, after the assembly of the first and third layers the impedance does not appear to differ from the bare gold electrode. Only a straight line of approximate unit slope at low frequencies can be seen, resulting from the mass transport by linear diffusion. In these cases the coverage is so poor that the electrode is behaving as if it is not coated.

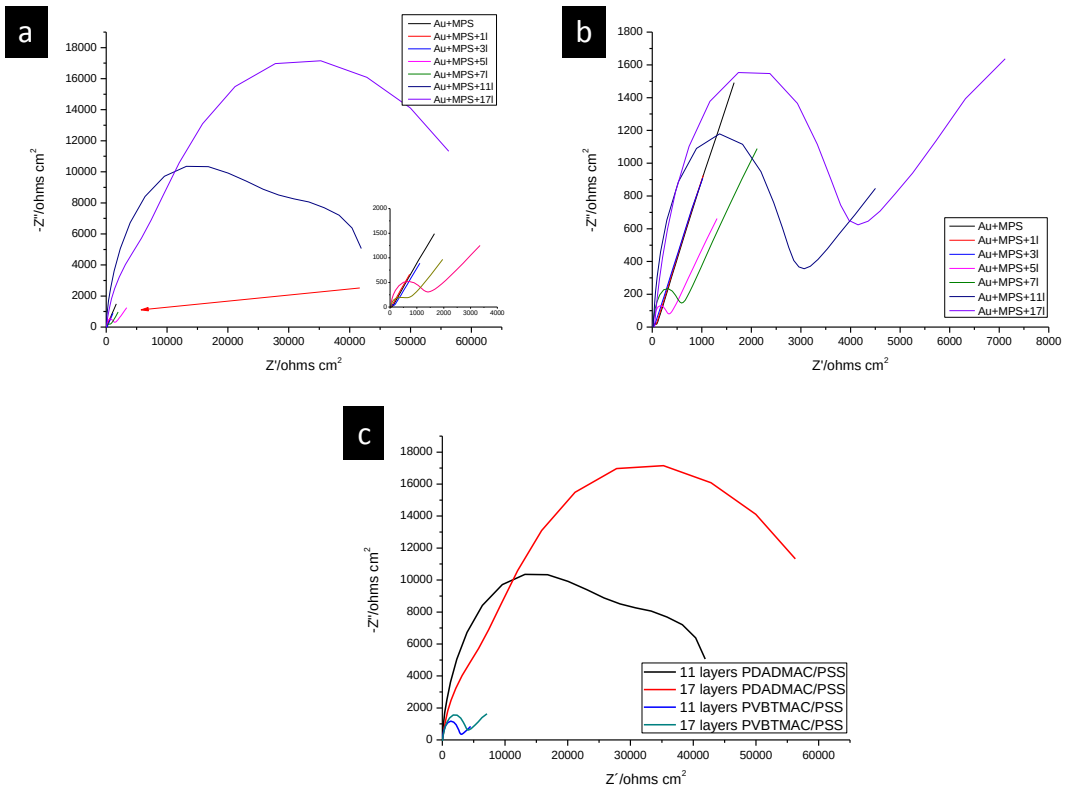

Figure 2.5. Nyquist diagrams for PDADMAC/PSS assembly, b) Nyquist diagrams for PBVTMAC/PSS assembly and c) Nyquist for 11 and 17 layers of PDADMAC/PSS and PVBTMAC/PSS PEMs.

After assembly of the fifth and seventh layers we see a change in the shape of the Nyquist diagrams in both cases, the typical semicircle at high frequencies associated with the impedance due to charge transfer appears, related to capacitance and resistance elements. With increasing numbers of layers we can see that this semicircle of the impedance response increases, the polymer free areas of the electrode start getting covered with layers of PE on top. However, at low frequencies we can still observe the straight line of the linear diffusion of the probes through these layers until they reach the surface of the electrode.

After the assembly of the 11th layer a difference in behaviour between both assemblies can be observed. In the case of PVBTMAC/PSS, Fig. 2.5b, the

changes in impedance show a linear behaviour following the law of the growth of a linear film. Increasing the number of layers leads to an increase in the impedance to the charge transfer and a linear diffusion of the species through the membrane. On the other hand, PDADMAC/PSS PEMs show a dramatic change in behaviour. We can observe that for the 11th layer the impedance to the charge transfer increases dramatically and there is a deviation from the straight line at lower frequencies indicating an alteration in the way mass transport is carried out. For the 17th layer we can observe that there are two semicircles superimposed and the second semicircle is even bigger than the first one at higher frequencies. This effect can be related to the formation of a complex between the electroactive species and PDADMAC, because it appears after the 11th layer at which the shift of the apparent redox potential in the CV of this assembly was observed. Also, this complex formation seems to happen after the 11th layer, where we have seen in the QCM data for PDADMAC/PSS the exponential growing regime becomes more evident and a more hydrated mass of PDADMAC assembles. The increase in the amount of assembled polyelectrolyte in the 11th layer can be fundamental for the complex formation. As can be seen in Fig. 2.5c, a complete change in behaviour is observed between the two assemblies after the 11th layer. The linear diffusion of the redox species through the PEMs is still visible in the case of PVBTMAC/PSS, but not in the case of PDADMAC/PSS where the mechanism of mass transport seems to have changed. Also the impedance values are dramatically larger in the case of PDADMAC/PSS compared to PVBTMAC/PSS. We have observed that,

according to cyclic voltammograms, PVBTMAC/PSS acts as a better insulator than PDADMAC/PSS reducing the current in a more effective way. This peculiar behaviour in PDADMAC seems to affect how mass transport through the PEM occurs but somehow it does not affect so much the electron transfer necessary to carry out the redox reaction between both species because there is not such a big difference in the current reduction observed by cyclic voltammetry.

Complex Formation Between PDADMAC and ferro/ferri

As we have already mentioned during this chapter the apparent redox potential shifts when the assembly of PDADMAC/PSS reaches the 11^{th}. In Fig. 2.6 the cyclic voltammograms after the first layer and the 11^{th} layer have been deposited onto the gold substrate are shown. It can be clearly seen how the redox potential has shifted to lower values, from $E^{1/2}$ (1 layer) = 0.164 V to $E^{1/2}$ (11 layer) = 0 V.

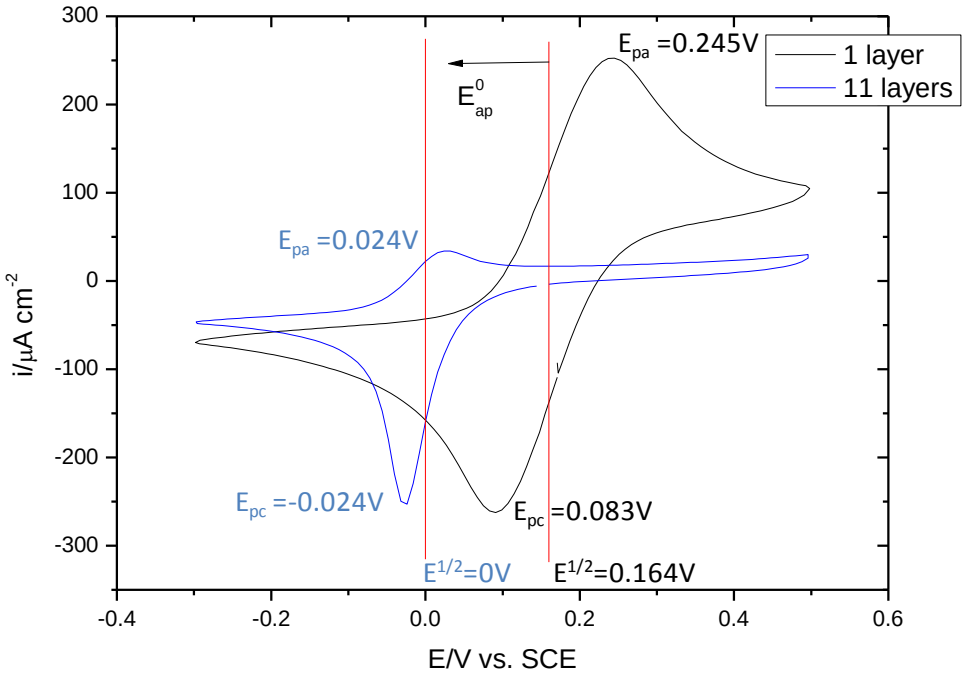

Figure 2.6. Cyclic voltammograms for PDADMAC/PSS assemblies after the first and the 11th layer have been deposited.

In this case we will consider the formal redox potential ($E^{1/2}$) in order to simplify the explanation. The formal redox potential for a reversible couple is centred between the anodic potential and the catodic potential.

As we have seen it seems that the shift in the formal redox potential occurs once assembly takes place after the 10th layer, as the PDADMAC/PSS system grows supralinearly and the amount of mass deposited increases with each layer. In order to create a complex with cyanoferrate molecules a certain amount of free quaternary amines from PDADMAC are needed. This amount seems to be reached at the 11th layer when the assembly is performed at these conditions of ionic strength.

In order to analyse the complex formation a bare gold substrate was placed as a contact inside the electrochemical cell filled with a solution of ferro/ferri-cyanate couple at 1 mM in 0.1 M KCl. A 10 $mgml^{-1}$ solution of PDADMAC in 0.1 M KCl was added drop by drop (100 µl each) into the electrochemical cell and cyclic voltammograms were recorded time to time. The concentration of PDADMAC in the cell was recalculated each time.

In Fig. 2.7 we can see that when the concentration of PDADMAC is below 0.03 $mgml^{-1}$ the shape of the voltammogram is that related to the diffusion of the ferro/ferri species from the solution to the substrate where the redox reaction occurs. Once the concentration is greater than 0.03 $mgml^{-1}$ an elbow related to the complex formation appears at potentials close to zero. When more PDADMAC is added this elbow related to the complex starts growing meaning that more cyanoferrate molecules are complexing with the PDADMAC until all of them are in complex form This phenomena of the shifting of the potential is related to the entrapment of ferrocyanide ions inside the PEMs with PDADMAC and has already been reported.[26]

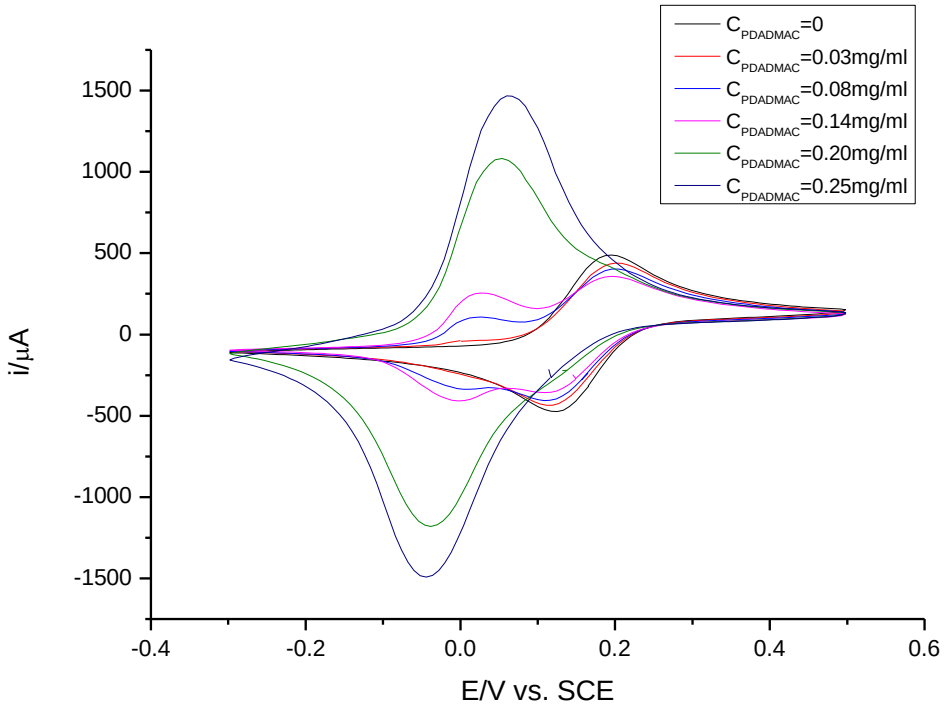

Figure 2.7. Cyclic voltammograms at different concentrations of PDADMAC in the electrochemical cell.

It is not until the total concentration of the cell reaches ~0.25 $mgml^{-1}$ that there are no free cyanoferrate molecules in the cell as seen by the absence of the typical peak related to the free ferro/ferri reaction.

In order to know if there is any preference for any of them to create the complex we prepared solutions in which the amount of ferro- and ferri- cyanate are present in the same proportions.. A multilayer of $(PDADMAC/PSS)_{6.5}$ at 0.5 M NaCl was previously incubated with ferro/ferri solution, rinsed and analysed by XPS afterwards, see Fig. 2.8.

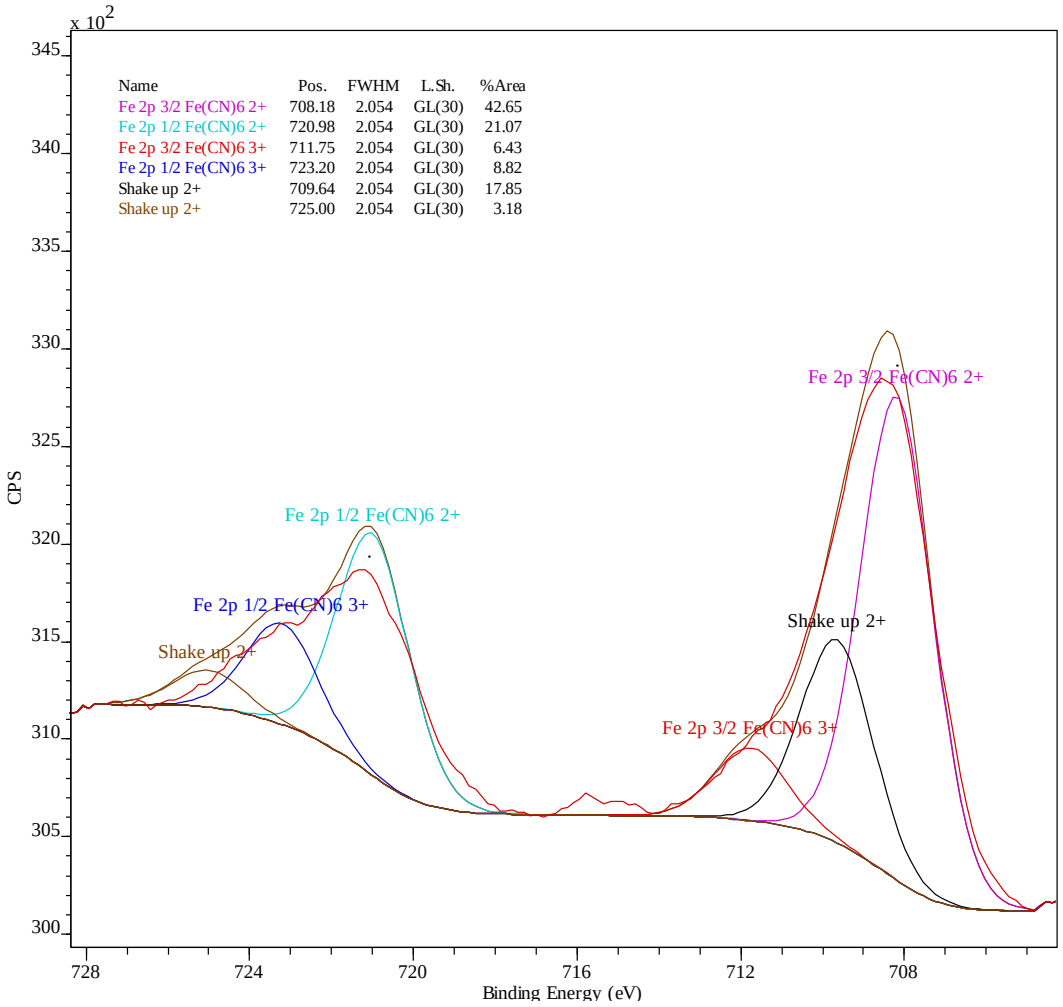

Figure 2.8. XPS analysis of Au+MPS+(PDADMAC/PSS)$_{6.5}$ incubated in ferro/ferri 1 mM 0.1 M KCl.

It can be observed in Fig. 2.8 that most of the signal after rinsing is related to potassium hexacyanoferrate (II) trihydrate ($K_4Fe(CN)_6$) indicating that there seems to be a preference to form a complex with the ferro rather than with the ferri molecule. In a paper published by Bekturov et al. in 1985, they confirmed the complex formation between ferro-/ferri- species with PDADMAC, and explained that the ratio in the complex formation between them is 5:1 for PDADMAC: Fe^{2+} and 3:1 for PDADMAC: Fe^{3+}.[27] They also reported that about 25 % of the Fe^{2+} ions are oxidised to Fe^{3+} once the complex is formed; a deficit of

electrons created by the attraction of the electrons of the CN groups from the nitrogen on the PDADMAC attracts the electrons of Fe^{2+} causing the oxidation of Fe^{3+}. These could explain the amount of ferro-/ferri- species observed by XPS, it seems that in the PEM we need to reach to a point in which the supralinear growth of the multilayer creates a sponge like structure with enough free amines of different PDADMAC monomers to create the complex, in a proportion of 5:1 with $K_4Fe(CN)_6$. The smaller amount of $K_3Fe(CN)_6$ found could be due to less favoured complex formation or the self-oxidation of part of the Fe^{2+} when the complex is created.

Taking into account the shape of the voltammograms and the accumulation of -$Fe(CN)_6^{2+}$ it can be postulated that after the 11th layer all the redox reaction is carried out through electron transfer among the cyanoferrate molecules attached to the complex and there is no diffusion of the free cyanoferrate molecules through the multilayer as the voltammogram is fully centred at 0 V, there are not elbows centred at 0.164 V related to the free cyano ferrate species. Therefore, the molecules entrapped in the film forming the complex with the PDADMAC are responsible for regulating the electron transfer between the gold electrode and the free cyanoferrate molecules in solution.

2.4 Conclusions

We have discussed the differences in assembly between PSS and two different polycations with quaternary amines, PDADMAC showing a supralinear growth and PVBTMAC which displays a linear growth pattern. The assembly of

PVBTMAC/PSS creates denser and less hydrated PEMs than PDADMAC/PSS assembly. PBVTMAC/PSS PEMs are also more hydrophilic and they act as better insulators. Their permeability seems not to vary with the number of layers after a certain number of layers have been assembled and their insulating behaviour increases in a regular manner with the number of layers assembled. The PDADMAC/PSS PEMs on the other hand grow in a supralinear fashion, creating sponge-like membranes especially when more than 11 layers have been assembled. The nature of the membranes is more hydrophobic than the PVBTMAC/PSS. It also acts as an insulator and becomes a more efficient insulator with increasing numbers of layers. A particular phenomenon has been observed during the electrochemical experiments performed, once the membrane has more than 11 layers, there is complex formation between the quaternary amines of the PDADMAC and the ferro specie used as the electrochemical probe, affecting how mass transport along the membrane is produced and its capacity as insulator. Even if the PDADMAC/PSS membrane is thicker than the PVBTMAC/PSS membrane, the current reduction is more effective in the latter.

2.5 References

(1) Geise, G. M.; Lee, H.-S.; Miller, D. J.; Freeman, B. D.; McGrath, J. E.; Paul, D. R. *J. Polym. Sci. Part B Polym. Phys.* **2010**, *48* (15), 1685–1718.

(2) Ali, M.; Yameen, B.; Cervera, J.; Ramírez, P.; Neumann, R.; Ensinger, W.; Knoll, W.; Azzaroni, O. *J. Am. Chem. Soc.* **2010**, *132* (24), 8338–8348.

(3) Stanton, B. W.; Harris, J. J.; Miller, M. D.; Bruening, M. L. *Langmuir* **2003**, *19* (17), 7038–7042.

(4) Jin, W.; Toutianoush, A.; Tieke, B. *Langmuir* **2003**, *19* (7), 2550–2553.

(5) Shan, W.; Bacchin, P.; Aimar, P.; Bruening, M. L.; Tarabara, V. V. *J. Memb. Sci.* **2010**, *349* (1-2), 268–278.

(6) Miller, M. D.; Bruening, M. L. *Langmuir* **2004**, *20* (26), 11545–11551.

(7) Ouyang, L.; Malaisamy, R.; Bruening, M. L. *J. Memb. Sci.* **2008**, *310* (1-2), 76–84.

(8) Tripathi, B. P.; Dubey, N. C.; Stamm, M. *J. Hazard. Mater.* **2013**, *252-253*, 401–412.

(9) Cheng, C.; Yaroshchuk, A.; Bruening, M. L. *Langmuir* **2013**, *29* (6), 1885–1892.

(10) Armstrong, J. A.; Bernal, E. E. L.; Yaroshchuk, A.; Bruening, M. L. *Langmuir* **2013**, *29* (32), 10287–10296.

(11) Bruening, M. In *Multilayer Thin Films*; Wiley-VCH Verlag GmbH & Co. KGaA, 2002; pp 487–510.

(12) Mansouri, S.; Winnik, F. M.; Tabrizian, M. *Expert Opin. Drug Deliv.* **2009**, *6* (6), 585–597.

(13) Jiang, C.; Luo, C.; Liu, X.; Shao, L.; Dong, Y.; Zhang, Y.; Shi, F. *ACS Appl. Mater. Interfaces* **2015**, *7* (20), 10920–10927.

(14) Georgieva, R.; Moya, S.; Donath, E.; Bäumler, H. *Langmuir* **2004**, *20* (5), 1895–1900.

(15) Silva, T. H.; Garcia-Morales, V.; Moura, C.; Manzanares, J. A.; Silva, F.

Langmuir **2005**, *21* (16), 7461–7467.

(16) Liu, Y.; Zhao, M.; Bergbreiter, D. E.; Crooks, R. M. *J. Am. Chem. Soc.* **1997**, *119* (37), 8720–8721.

(17) Han, S.; Lindholm-Sethson, B. *Electrochim. Acta* **1999**, *45* (6), 845–853.

(18) Barreira, S. V. P.; García-Morales, V.; Pereira, C. M.; Manzanares, J. a.; Silva, F. *J. Phys. Chem. B* **2004**, *108* (46), 17973–17982.

(19) Elżbieciak-Wodka, M.; Kolasińska-Sojka, M.; Nowak, P.; Warszyński, P. *J. Electroanal. Chem.* **2015**, *738*, 195–202.

(20) Estrela-Lopis, I.; Iturri Ramos, J. J.; Donath, E.; Moya, S. E. *J. Phys. Chem. B* **2010**, *114* (1), 84–91.

(21) Goss, C. A.; Charych, D. H.; Majda, M. *Anal. Chem.* **1991**, *63* (1), 85–88.

(22) Moya, S. *Macromol. Rapid Commun.* **2012**, *33* (12), 1022–1035.

(23) Harris, J. J.; Bruening, M. L. *Langmuir* **2000**, *16* (4), 2006–2013.

(24) Farhat, T. R.; Schlenoff, J. B. *Langmuir* **2001**, *17* (4), 1184–1192.

(25) Rmaile, H. H.; Farhat, T. R.; Schlenoff, J. B. *J. Phys. Chem. B* **2003**, *107* (51), 14401–14406.

(26) Wang, B.; Anzai, J. *Langmuir* **2007**, *23* (13), 7378–7384.

(27) Bekturov, E. A.; Kudaibergenov, S. E.; Ushanov, V. Z.; Saltybaeva, S. S. *Die Makromol. Chemie* **1985**, *186* (1), 71–75.

Chapter 3
Regenerable Polyelectrolyte Multilayers for Applications in Foulant Removal.

3.1 Introduction.

Conceptually LbL is simple and easy to apply. It only requires the alternating exposition of a charged surface to solutions of oppositely charged polyelectrolytes and washings in between deposition steps to remove excess polymer.[1,2] PEMs are very stable and in most cases are not easy to disassemble once fabricated. There are practical situations, however, where it would be desirable to remove PEMs fully or partially after the assembly as a means of surface exposure or to liberate an encapsulated material. Another reason for the removal of a PEM could be that PEMs are no longer capable of fulfilling their functions, i.e.: as filtration membranes. This is often the case when PEMs are covered with foulants. Devices and coatings fabricated with PEMs retain charges from the last assembled polyelectrolyte layer. These charges can be used to build up additional polyelectrolyte layers but can also attract other charged molecules that could be present in the environment in contact with the PEM.[3,4] For example, in the case of polyelectrolyte capsules for drug delivery the charge of the PEM can lead to the coating of the capsules with proteins present in biological fluids. The formation of protein coronas on top of the capsules will impact on their interaction with cells.[5,6] For PEMs used for

membrane fabrication with applications in water reuse or desalination, the charges in the PEMs can lead to the deposition of foulants present in aqueous media like small charged organic molecules, proteins, and other biomolecules. The deposition of foulants on top of the PEM can significantly hinder their use as membranes as pores will be covered by the foulant and their filtering capacity will be diminished.

One way to avoid the deposition of proteins or foulants on top of the PEMs is their chemical modification with molecules like polyethylene glycol (PEG) known for its low protein binding.[7-9] In some cases the multilayer can also be crosslinked reducing the charge density on the surface.[10] The chemical modification or the crosslinking can be effective in preventing foulant deposition but at the same time they can also interfere with the functionality of the PEMs.

The removal of foulants deposited on top of the PEM is not simple since the electrostatic interactions of the foulant with the PEM can be strong and the surfactant treatment may also lead to the degradation of the layer.

In this chapter we want to explore the possibility of foulant removal from the surface of PEMs by using sacrificial polyelectrolyte layers on top of non-removable PEMs. Since the foulants will be located mostly on the surface of the multilayers we will show that it is possible to develop multilayers where only the top polyelectrolyte layers can be removed. The idea beyond this is that with the removal of the top sacrificial layers, foulants present on the surface of the

PEM will also be removed with the sacrificial layers leaving the non-removable layers unaltered. This strategy would be most suitable in situations where it is necessary to rebuild the PEM after foulant removal. By having a PEM with only a removable top block it is not necessary to rebuild the whole multilayer but only the top layers.

An example for the potential application of regenerable membranes is the cleaning of PEM membranes used for water filtration.[11] Then, it will be possible to regenerate the PEMs as "foulant free". If the process can be repeated many times the operating life of the membrane will be enhanced.

We will show here that depending on the particular combination of polycations and polyanions employed for multilayer fabrication, different strategies for the removal of the polyelectrolyte have to be applied[11,12] e.g.: variation of pH,[13] or the use of cationic or anionic surfactants.[14]

As a proof of concept it will be demonstrated that the top layers of a polyelectrolyte multilayer coated with proteins can be removed together with the protein layer and then a few polyelectrolyte layers can be assembled and that the whole procedure can be repeated.

The quartz crystal microbalance and atomic force microscopy will be applied to study PEM removal and regeneration.

3.2 Materials and Methods

Poly acrylic acid (PAH) [Mw = 15 $kgmol^{-1}$], PDADMAC Mw = 20 % wt. in water [Mw = 200-350 $kgmol^{-1}$], PSS [Mw = 70 $kgmol^{-1}$], poly ethylene imine (PEI) 50 % wt. in water [Mw = 2 $kgmol^{-1}$], poly (acrylic acid) (PAA) 50 % wt. in water [Mw = 5 $kgmol^{-1}$], sodium dodecyl sulfate (SDS) 99.9 %, BSA, tetramethyl rhodamine labelled bovine serum albumine (BSA), acetic acid 99.80 %, hydrochloric acid 1N, sodium acetate trihydrate, sodium chloride, (1-tetradecyl) trimethylammonium bromide (TTAB) 98 % and sodium hydroxide.

3.2.1 Quartz Crystal Microbalance

PEM formation, deconstruction and regeneration were monitored by QCM-D using silica crystals as substrates. All the polyelectrolyte solutions were at 1 $mgml^{-1}$ in the corresponding salt concentration and pH for each of the following; blocks of PAH/PSS and PDADMAC/PSS at 0.5 M NaCl, blocks of PDADMAC/ PAA and PEI/PAA, at 0.3 M NaCl at pH 3. Blocks of PEI/ PSS in 50 mM acetate buffer pH 5.6, 0.2 M NaCl. The deposition of each layer is followed by a decrease in the resonance frequency of the 3rd overtone (15 MHz) with subsecond time resolution.

3.2.2 Atomic Force Microscopy

The PEMs were deposited on top of a glass substrate, and analysed in tapping mode in a fluid cell with a solution of 10 mM NaCl and a DNP cantilever with a k = 0.24 Nm^{-1}.

3.3 Results and Discussion

The strategy followed in this work is illustrated in Fig. 3.1, where a PEM consisting of two blocks, one removable block on top of a second non-removable block is shown. The top block is removed by means of pH or surfactant treatment and then rebuilt.

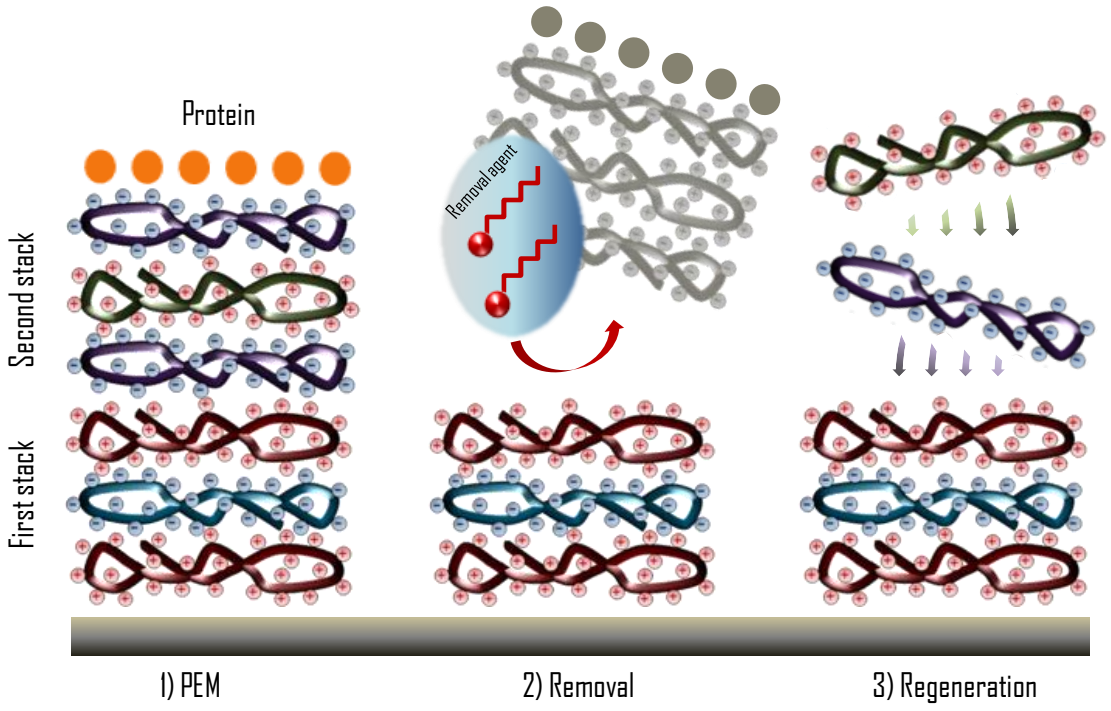

Figure 3.1. Schematic of the removal and regeneration of a di-block polyelectrolyte membrane.

3.3.1 Ph Changes

Weak polyelectrolytes are sensitive to changes in the pH by varying the number of charged functional groups as the pH increases or decreases. PAA is a typical anionic weak polyelectrolyte. As the pH increases the dissociation of the carboxylic acid of the PAA monomers increase and PAA becomes more

charged. In a recent study we have reported that the assembly of PAA/PDADMAC is very sensitive to pH at which the assembly is performed. As PDADMAC is a strong polymer the pH is only affecting PAA. In 2013, Alonso et al. showed that there is a supralinear growth for PAA/PDADMAC at low pH, approximately pH 3, and as the pH increases the amount of polymer deposited in the assembly decreases.[15] At high pH, 12-13, almost no polymer is assembled compared to the assembly at pH 3. Intuitively, one would think that the opposite situation should be taking place. At higher pH since PAA is more charged the assembly should proceed more effectively due to electrostatic interactions than at lower pH, like 3, where the degree of charging of the PAA is lower. The reason for this behaviour is that at high pH PAA is significantly hydrated and the interaction with the more hydrophobic PDADMAC would decrease this hydration and the PAA assembly becomes less favourable thermodynamically.

Taking advantage of this pH dependence for PAA/PDADMAC we fabricated the films at pH 3 and then exposed them to pH 13. Film growth and the treatment with NaOH at pH 13 were followed with the QCM-D. As can be observed in Fig. 3.2 a) and d) the PAA/PDADMAC display a supralinear growth at pH 3, and increasing to pH 13 results in a frequency decrease of 186 Hz from an initial value of 320 Hz, approximately 58 % of the PEM has been removed.

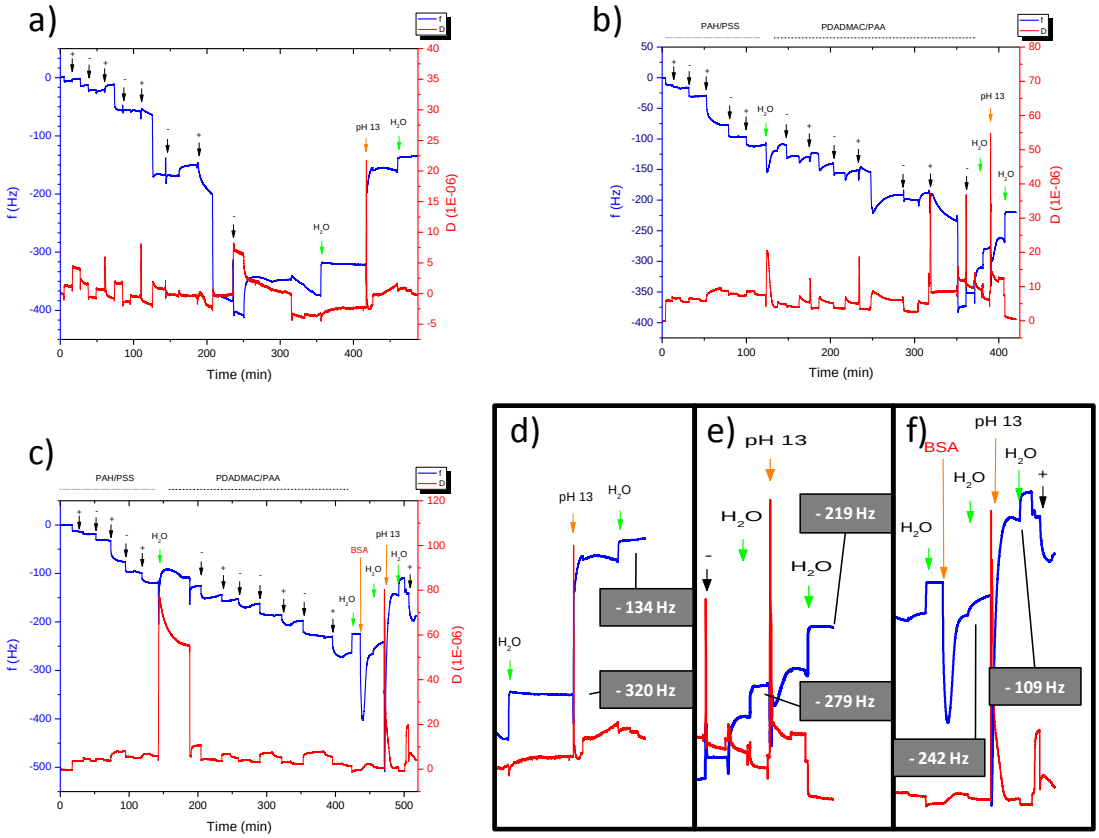

Figure 3.2. a) 4 bilayers of PDADMAC/PAA at 0.3 M naCl and pH 3 treated with water at pH 13, b) 2.5 bilayers of PAH/PSS at 0.5 M NaCl and 3.5 bilayers of PDADMAC/PAA at 0.3 M NaCl and PH 3 treated with water at pH 13, c) 2.5 bilayers of PAH/PSS at 0.5 M NaCl, 3.5 bilayers of PDADMAC/PAA at pH3 and BSA on top treated with water at PH 13, d), e), f) zoom ins of the PEM removal from figures a, b and c respectively.

Frequency and mass values for the first and second blocks and including BSA, before and after pH or surfactant treatment as well as the percentages of mass removal are shown in Table 3.1.

Table 3.1. Frequency and mass for the 1st and 2nd stacks before and after removal of the second block. Mass removal is also given in percentages.

Figure	Nº Layers	Polyelectrolytes 1st Stack	$\|f_1\|$ (Hz)	Mass of 1st stack (ng/cm^2)	Polyelectrolytes 2nd Stack	$\|f_2\|$ (Hz)	Mass of 2nd stack (ng/cm^2)	Treatment	% removed from total	% removed from 2nd
3a	8	$(PDADMAC/PAA)_4$	320	5779				H_2O pH 13	58	
3b	12	$(PAH/PSS)_{2.5}$	119	2149	$(PDADMAC/PAA)_{3.5}$	279	2890	H_2O pH 13	22	38
3c	12	$(PAH/PSS)_{2.5}$	108	1950	$(PDADMAC/PAA)_{3.5}$ + BSA	242	2420	H_2O pH 13	55	99
4a	9	$(PAH/PSS)_2$	53	950	$(PDADMAC/PSS)_{2.5}$	236	3307	TTAB 50mM	29	37
4b	10	$(PAH/PSS)_2$	79	1423	$(PDADMAC/PSS)_3$ + BSA	324	4427	TTAB 50mM	56	74
6a	9	$(PEI/PSS)_2$	28	511	$(PEI/PAA)_{2.5}$	140	2018	SDS 2%	44	55
6b	8	$(PEI/PSS)_2$	38	678	$(PEI/PAA)_2$ + BSA	176	2501	SDS 2%	98	125

Then, we fabricated a di-block PEM with an initial block of PAH/PSS on top of which we assembled the PAA/PDADMAC film. The film growth was followed by QCM-D and is shown in Fig. 3.2 b). Then we exposed the PEM to pH 13 and as it can be seen in the same Fig. 3.2 b) and e) that there is a decrease in the frequency of 38 % of the second block. Since the idea behind this work is to create a surface that can be removed and regenerated to eliminate foulants attached to the surfaces we decided to expose the di-block PEM to BSA. The protein deposits on top of the PEMs, see Fig. 3.2 c) and f). When the PEM with BSA on top is exposed to pH 13 solution we can see from the change in frequency that the protein, together with the top layers of the PEMs, are being removed, 99 % of the mass of the second block including the protein on top is removed The PAA/PDADMAC film could be rebuilt.

3.3.2 Surfactants

It has been shown in previous work by Iturri et al. 2010, that PDADMAC/PSS PEMs can be easily removed in the presence of the TTAB surfactant while PAH/PSS PEMs remain stable and even bind surfactant to the PEMs.[14] The TTAB surfactant is positively charged and binds therefore to PSS in both cases. The stability of the PAH/PSS can be attributed to stronger binding of the

primary amines of PAH to the sulfonate groups of PSS than that of the quaternary amines of PDADMAC to the sulfonate groups of PSS.

We combined PDADMAC/PSS with PAH/PSS in a di-block structure and followed the assembly in the QCM-D Fig. 3.3 a) and c). The top layers of the PDADMAC/PSS block could be removed in the presence of TTAB as measured by QCM-D.

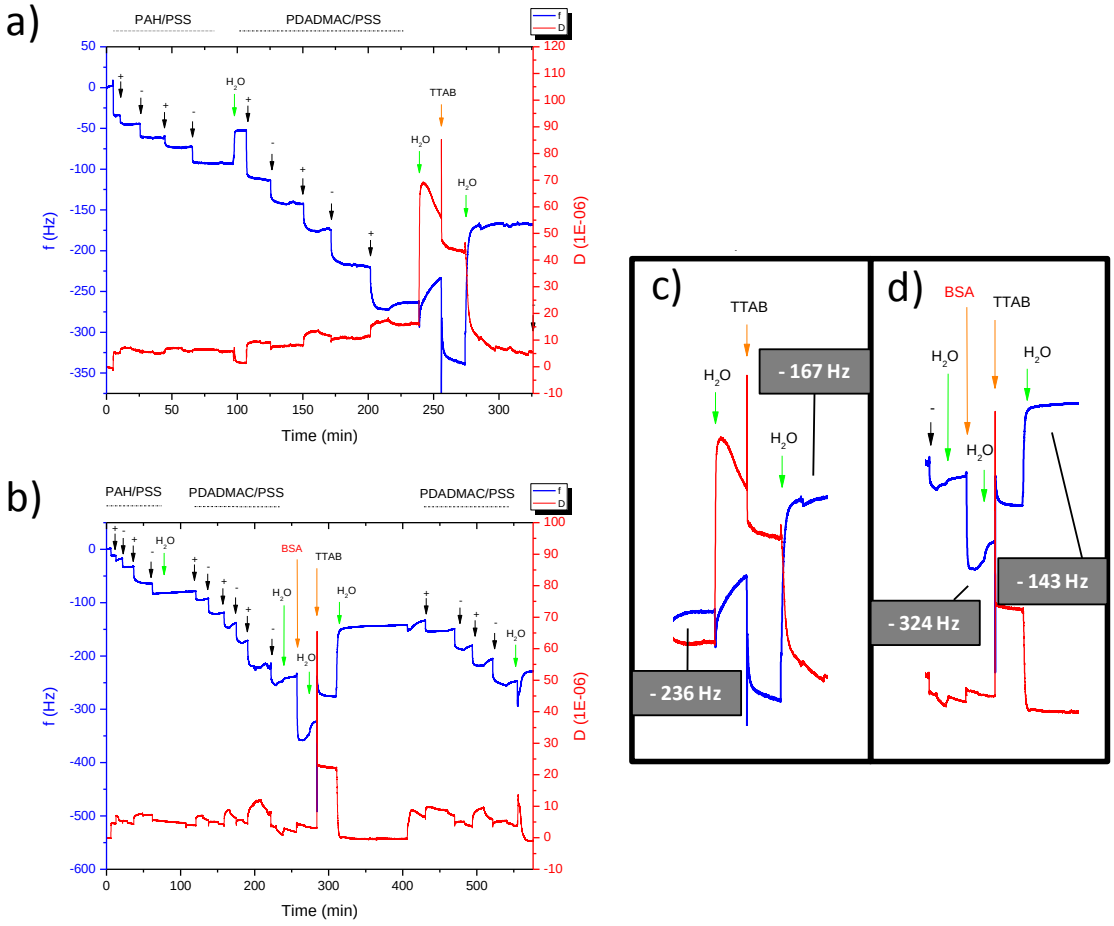

Figure 3.3. a) 2 bilayers of PAH/PSS and 2.5 bilayers of PDADMAC/PSS treated with 50 mM TTAB, b) 2 bilayers of PAH/PSS at 0.5 M NaCl, 3 bilayers of PDADMAC/PSS at 0.5 M NaCl and BSA on top, treated with TTAB and reconstructed with 2 bilayers of PDADMAC/PSS at 0.5 M NaCl afterwards, c), d) zoom ins of the PEMs removal from figures a, and b respectively.

The change in frequency after treatment with TTAB proved the removal of 37 % of the second block as shown in Table 3.1. After removal the PDADMAC/PSS bilayers could be easily reassembled up to the frequency values before TTAB treatment. The di-block PEM was also coated with BSA, Fig. 3.3 b) and d). The coating increased the mass of the PEM by 35 %. The treatment with TTAB after BSA deposition removed the protein together with the bilayers of PDADMAC/PSS, which could be easily regenerated. In principle, the strategy of removal could be applied several times. The removal of BSA and the top layers in a di-block PEMs of PAH/PSS and PDADMAC/PSS was also studied by AFM. In Fig. 3.4 a) we can observe the AFM micrograph of the di-block PEM of 2 bilayers of PAH/PSS and 3 bilayers of PDADMAC/PSS on top, the roughness and the structure are characteristics of the PDADMAC/PSS film.[16]

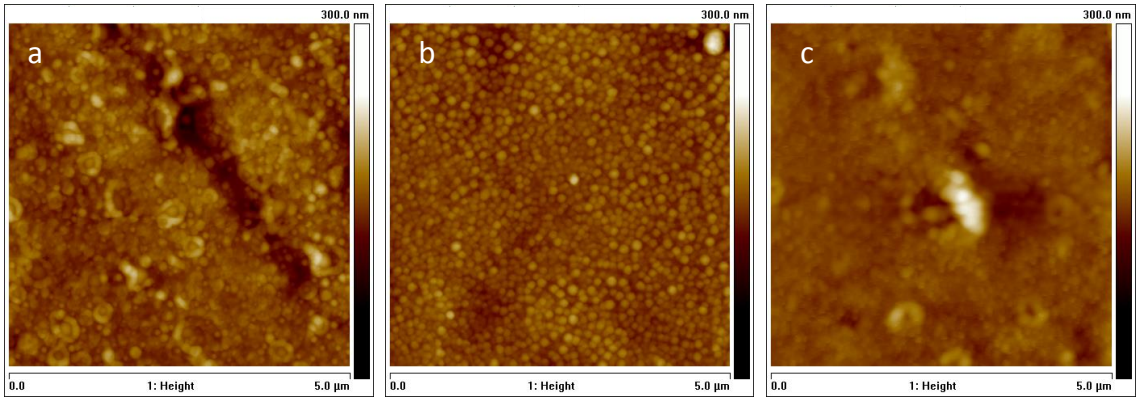

Figure. 3.4. a) AFM micrograph of a PEM di-block of 2 bilayers of PAH/PSS at 0.5 M NaCl and 3 bilayers of PDADMAC/PSS at 0.5 M NaCl on top, b) PEM with BSA deposited on top, c) PEM with BSA after 50 mM TTAB treatment.

In Fig. 3.4 b) the film has been exposed to BSA. The change in the topology of the film is complete after deposition of the protein. BSA covers the whole

surface and has a clear rounded structure. The treatment with TTAB shown in Fig. 3.4 c) results in a surface with a topography that is clearly not that of the BSA but it is also not that of the PDADMAC/PSS film. Most likely this is due to remnants of the PDADMAC/PSS PEM on top of the PAH/PSS. Finally, PDADMAC/PSS bilayers are assembled again on top and the original topology and roughness of the PDADMAC/PSS film is restored.

In order to confirm that there is no remaining foulant on the film we labelled BSA fluorescently and measured the fluorescence of the film after BSA deposition and after PEM removal. QCM-D is not capable of differentiating between the mass of the PEM and the mass of BSA. In Fig. 3.5 a) a PEM composed of a di-block assembly of (PAH/PSS)+(PDADMAC/PSS)$_{1.5}$ does not show any fluorescence. When BSA labelled with tetramethyl rhodamine was assembled on top of the PEM, the typical emission fluorescence signal from rhodamine at 572 nm can be observed in Fig. 3.5 b).

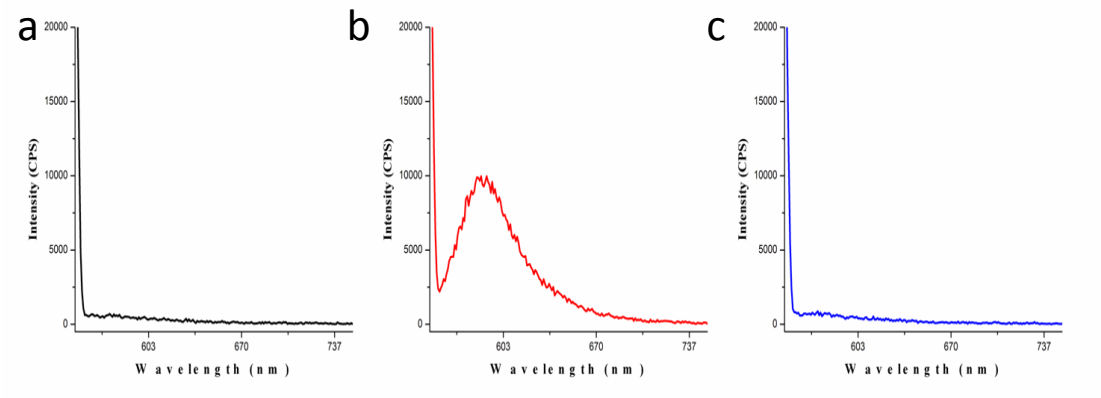

Figure 3.5. Fluorescence Intensity of a) 1 bilayer of PAH/PSS at 0.5 M NaCl and 1.5 bilayers of PDADMAC/PSS at 0.5 M NaCl, b) with rhodamine labelled BSA on top, c) after 50 mM TTAB treatment.

After treatment with 50 mM TTAB no fluorescence can be detected from the surface (Fig. 3.5 c), meaning that all labelled BSA has been removed.

Alternatively to the use of the cationic TTAB, and taking into account industrial applications of the removal and regeneration strategy, we looked at PEM combinations that could be removed with the negatively charged Sodium Dodecyl Sulfate (SDS), which is a standard surfactant used for cleaning in multiple industrial applications. SDS, as a negatively charged molecule, must bind to a positively charged polyelectrolyte. We tried several polyelectrolyte combinations as in the previous cases but all proved to be resistant to the SDS treatment with the exception of PDADMAC/PAA and PEI/PAA. The first PEM showed 60 % removal in the presence of SDS and the second almost 100 %. We decided to work with PEI/PAA on top of PEI/PSS. PEI/PSS was not affected by SDS.

When BSA was deposited on top of a di-block membrane of PEI/PSS and PEI/PAA, and afterwards treated with 2 % SDS in water, we observed (Fig. 3.6 b) and d)) that the top block with BSA was removed but also part of the first stack.

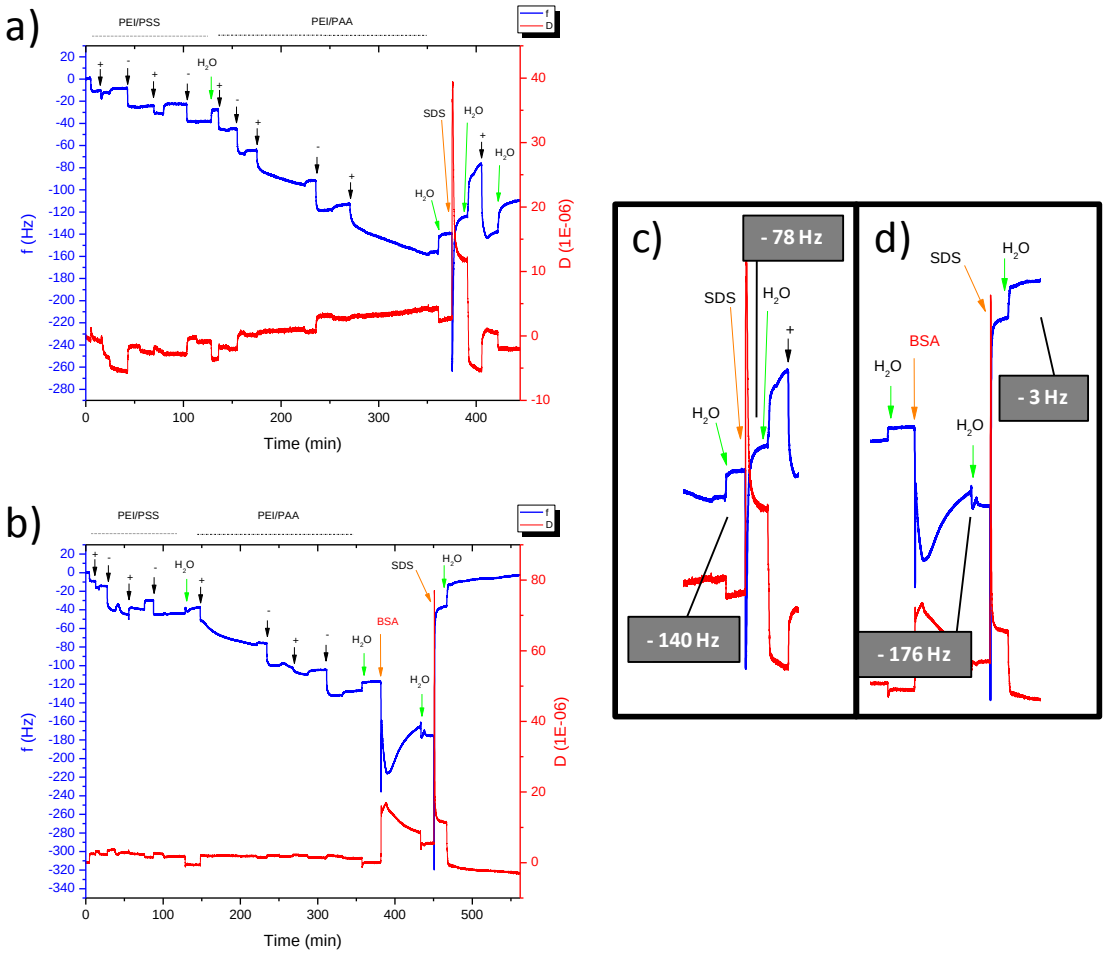

Figure 3.6. a) 2 bilayers of PEI/PSS in acetate buffer and 2.5 bilayers of PEI/PAA at 0.3 M NaCl and pH 3 on top treated with 2 % SDS in water, b) 2 bilayers of PEI/PSS in acetate buffer and 2 bilayers of PEI/PAA at 0.3 M NaCl and pH 3 with BSA on top and treated with 2 % SDS in water, c), d) zoom ins of the PEMs removal from figures a and b respectively.

The only explanation for this that we can give at the moment, is that the BSA layer interdigitates with the top PEM and this also affects the 1st stack that can be removed then. We have seen that the removal of the 2nd stack for the PDADMAC/PAA with basic pH is more significant when BSA is on top of the film than when it is not and the same for PDADMAC/PSS in the presence of

TTAB. It is reasonable to think that the protein alters the PEM structure to a certain extent.

3.4 Conclusions

Di-block PEMs with a top removable block have been fabricated. We have prepared different polyelectrolyte combinations and we have shown that depending on the particular combination of polyelectrolyte chosen different procedures can be applied to remove the top layers: pH variations, and treatment with SDS and TTAB surfactants, see Fig. 3.7.

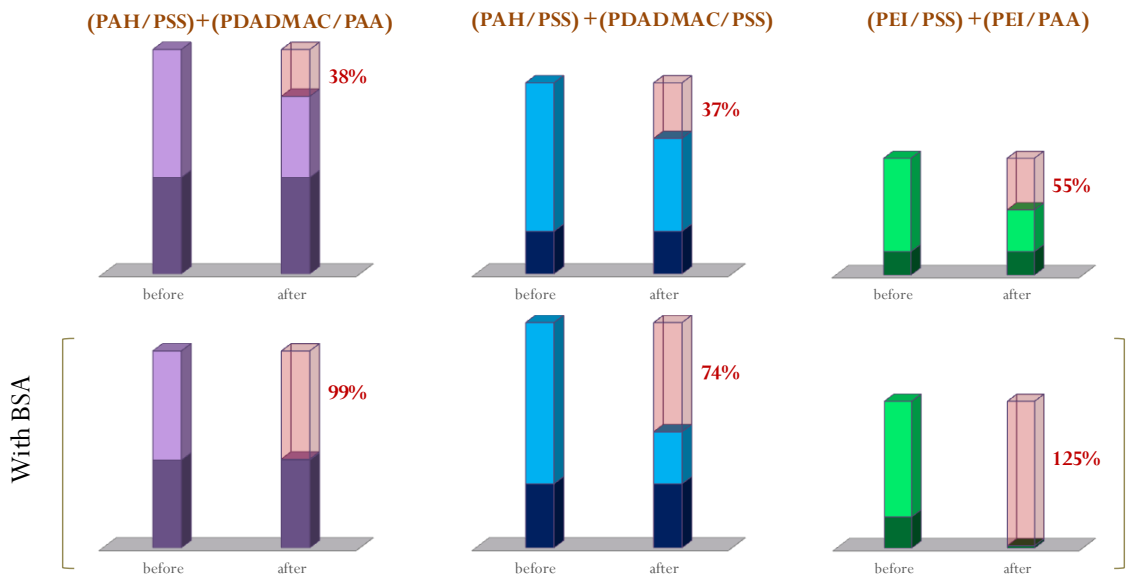

Figure 3.7. Schematic sketch of all the different combinations tested.

The removal of the top layers does not affect, in most cases, the 1st block of the PEM, which is fabricated upon polyelectrolytes that are resistant to the stimuli that leads to the removal of the top block. There is a certain interdigitation between the stacks, making the removal of the top blocks less than the removal if this top block were standing alone without the supporting stack. Foulant

present on top of the PEM, as shown for BSA in this chapter, can be removed together with the top layers applying the corresponding stimuli. Surprisingly the removal of the top block is enhanced in the presence of BSA and for the case of the di-block PEI/PSS with PEI/PAA on top the presence of BSA leads to complete removal of the PEMs after SDS treatment.

Once the layers have been removed they can be rebuilt free from foulants. The whole procedure from the regeneration to the removal can be repeated several times.

If applied to a filtration membrane the removal and reassembly could extend the operating life of the membrane.

The work presented in this chapter resulted in the following publication:

Irigoyen, J.; Politakos, N.; Murray, R. A.; Moya, S. E. *Macromol. Chem. Phys.* **2014**, *215* (16), 1543–1550.

3.5 References

(1) Decher, G.; Hong, J. D.; Schmitt, J. *Thin Solid Films* **1992**, *210–211* (0), 831–835.

(2) Decher, G.; Hong, J. D. *Berichte der Bunsengesellschaft für Phys. Chemie* **1991**, *95* (11), 1430–1434.

(3) Caruso, F.; Donath, E.; Möhwald, H. *J. Phys. Chem. B* **1998**, *102* (11), 2011–2016.

(4) Ladam, G.; Gergely, C.; Senger, B.; Decher, G.; Voegel, J.-C.; Schaaf, P.;

Cuisinier, F. J. G. *Biomacromolecules* **2000**, *1* (4), 674–687.

(5) Saptarshi, S. R.; Duschl, A.; Lopata, A. L. *J. Nanobiotechnology* **2013**, *11* (1), 26.

(6) Mahmoudi, M.; Monopoli, M. P.; Rezaei, M.; Lynch, I.; Bertoli, F.; McManus, J. J.; Dawson, K. A. *ChemBioChem* **2013**, *14* (5), 568–572.

(7) Leung, M. K. M.; Such, G. K.; Johnston, A. P. R.; Biswas, D. P.; Zhu, Z.; Yan, Y.; Lutz, J.-F.; Caruso, F. *Small* **2011**, *7* (8), 1075–1085.

(8) Banerjee, I.; Pangule, R. C.; Kane, R. S. *Adv. Mater.* **2011**, *23* (6), 690–718.

(9) Yang, W. J.; Pranantyo, D.; Neoh, K.-G.; Kang, E.-T.; Teo, S. L.-M.; Rittschof, D. *Biomacromolecules* **2012**, *13* (9), 2769–2780.

(10) Zhu, X.; Jańczewski, D.; Lee, S. S. C.; Teo, S. L.-M.; Vancso, G. J. *Appl. Mater. Interfaces* **2013**, *5* (13), 5961–5968.

(11) Shan, W.; Bacchin, P.; Aimar, P.; Bruening, M. L.; Tarabara, V. V. *J. Memb. Sci.* **2010**, *349* (1-2), 268–278.

(12) Han, L.; Mao, Z.; Wuliyasu, H.; Wu, J.; Gong, X.; Yang, Y.; Gao, C. *Langmuir* **2012**, *28* (1), 193–199.

(13) Dubas, S. T.; Schlenoff, J. B. *Macromolecules* **2001**, *34* (11), 3736–3740.

(14) Iturri Ramos, J. J.; Llarena, I.; Moya, S. E. *J. Mater. Sci.* **2010**, *45* (18), 4970–4976.

(15) Alonso, T.; Irigoyen, J.; Iturri, J. J.; Larena, I. L.; Moya, S. E. *Soft Matter* **2013**, *9* (6), 1920–1928.

(16) Gao, C.; Leporatti, S.; Moya, S.; Donath, E.; Möhwald, H. *Langmuir* **2001**, *17* (11), 3491–3495.

Chapter 4
Responsive Polyelectrolyte Multilayers Assembled at High Ionic Strength.

4.1 Introduction

PEM assembly is principally driven by electrostatic interactions between oppositely charged polyelectrolytes. From a practical point of view, Layer by Layer assembly only requires the dipping of a charged substrate in a solution of a polyelectrolyte with a charge opposite to that of the substrate. The procedure is repeated a number of times alternating between polycations and polyanions, including water or salt washings in between layers, until a film of the desired thickness is obtained.[1-3] The practical procedure applied by the different groups working in LbL assembly varies, regarding the number of washings between the deposition of layers, the use of NaCl or water for the washings, assembly time, pH and the ionic strength of the polyelectrolyte solution.[4-7] For some of these parameters, variations in the conditions of assembly can have a strong impact on the quality of the assembled PEMs.

For instance, since polyelectrolyte conformation is determined by the ionic strength in bulk solution, the thickness of a LbL film will be notably influenced by the ionic strength at which the assembly has been performed. If polyelectrolyte assembly takes place at low ionic strength the polymer chains are normally extended and the resulting film will be thin. Increasing the ionic

strength results in the coiling of the chains, which become less extended but increase in volume.[7] This in turn results in an increase in layer thickness. Standard values of ionic strength for PEM fabrication range between 0.5 and 1 M NaCl due to considerations of layer thickness and packing of polyelectrolyte chains.[3, 8, 9]

Polyelectrolyte assembly can, nevertheless, be performed at higher ionic strengths even though the electrostatic interaction between subsequent layers is reduced due to charge screening. There are examples in literature of PEM assembly and studies of PEM stability at salt concentrations higher than 1 M NaCl. It has been reported that PDADMAC/PSS remains stable at 3 M NaCl but post-treatment of these multilayers with 4 and 5 M NaCl leads to the destruction of the layered structure.[10]

In this study we explore the LbL assembly of PDADMAC and PSS at 3 M NaCl. Working at this salt concentration, polyelectrolyte assembly takes place and results in highly hydrated thick PEMs. These films release water and experience a reduction in thickness of more than 200 nm when they are exposed to pure water as we have proven employing both the QCM-D and AFM. Changes in thickness and water content are fully reversible and comparable with those observed in polyelectrolyte brushes following changes in the ionic strength. However, contrary to polyelectrolyte brushes, PDADMAC/PSS PEMs assembled at 3 M remain in a collapsed state at low ionic strength but are fully extended at 3 M NaCl.[11] The observed phenomena can be interpreted as a consequence of high water uptake during assembly at 3 M NaCl and a

reversible conformational change in the polyelectrolytes in the PEM. At low ionic strength the chains expand, occupying more lateral space and displacing solvent, while at high ionic strength the PEM coils, absorbing water into the film.

PDADMAC/PSS PEMs combining ease of preparation with the capability of reversible changes in thickness of more than 200 nm can have interesting applications in the fabrication of smart surfaces and nanoactuators.

4.2 Materials and Methods

PSS [Mw ~ 70 $kgmol^{-1}$], PDADMAC 20 % in water [Mw = 200-350 $kgmol^{-1}$] and sodium chloride.

4.2.1 Quartz Crystal Microbalance with Dissipation

The LbL technique was performed in situ in the QCM-D chamber onto silica crystals by passing, with a peristaltic pump, a 1 mg ml^{-1} polyelectrolyte solution in 3 M NaCl through the water-filled QCM-D chamber. Polyelectrolyte deposition was followed by the decrease of the resonance frequency of the quartz crystal. When the frequency levels stabilised, the polyelectrolyte solution was replaced by a 3 M NaCl solution until a plateau in the frequency response was reached. This procedure was repeated until the deposition of the desired number of layers was achieved.

4.2.2 In Situ Combination of QCM-D and Ellipsometry

Wet mass and dry mass of the PEM were measured simultaneously using an in situ combination of QCM-D and ellipsometry assembly. Spectroscopic

ellipsometry gives information about solvent-free mass of polymer adsorbed as a thin film onto a planar surface due to calculations of differences in the optical density between the adsorbate and free solution. QCM-D gives information about hydrated mass deposited onto a planar surface due to changes in the resonance frequency of a quartz crystal. Both systems combined allow calculating film hydration, which is calculated from the difference between the dry and wet mass. A Q-Sense E-1 setup with a specific cell with two windows was mounted on a spectroscopic rotating ellipsometer.

Ellipsometric data was obtained at 65º incident angle for a wavelength range from 380 to 1000 nm with a time resolution of 5 seconds.

The QCM data was acquired as explained previously in parallel to the ellipsometric data. The working temperature was maintained constant at 23 ºC. The quartz crystal used was a QSX 335 specific sensor from Q-sense for the ellipsometric mode. It is made of a 100 nm titanium layer on top of 50 nm of silicon dioxide.

The quantitative evaluation of the ellipsometric data was performed using a three layer model. The first layer is the titanium layer deposited on top of the quartz crystal, the second layer the polyelectrolyte membrane and the third layer is the bulk solution.

4.2.3 Atomic Force Microscopy

PEMs films previously deposited by QCM-D were manually, softly cut with a razor blade, making stripes, and imaged in tapping mode in a closed fluid cell

allowing the "in situ" exchange of salt to water. The particular silicon nitride cantilever used was a DNP available from Bruker with a K = 0.32 Nm^{-1}.

4.3 Results and Discussion

PDADMAC/ PSS PEMs were grown at 3 M NaCl in the QCM-D chamber. Changes in frequency response and dissipation were measured for each layer deposited (Fig. 4.1).

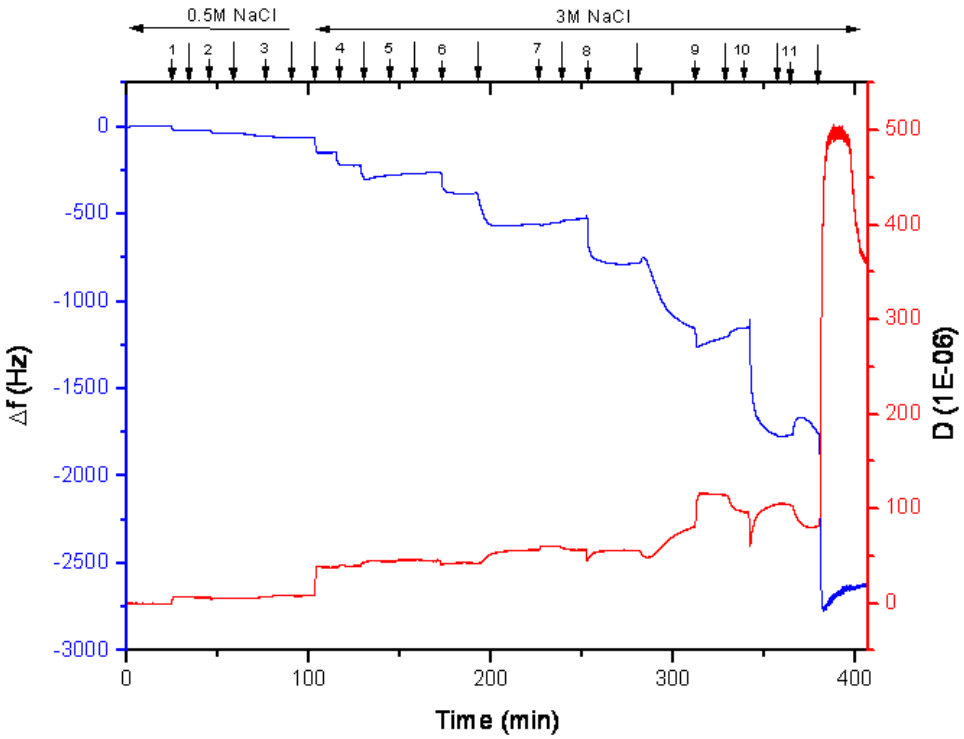

Figure 4.1. Frequency response and dissipation curves measured with QCM-D showing the variation of the 3rd overtone during the assembly of 11th layers PDADMAC/PSS system in 3 M NaCl.

The initial three polyelectrolyte layers were assembled in 0.5 M NaCl to facilitate the polyelectrolyte deposition on top of the silica surface. After the 3rd layer, polyelectrolytes were assembled at a salt concentration of 3 M NaCl. A

total change in the frequency response of 2600 Hz was measured after the 11th polyelectrolyte layer was deposited. This frequency variation is significantly higher than for the same polyelectrolyte combination assembled at 0.5 M NaCl, around 300 Hz after 11 layers and 800 Hz after 17 layer deposition.[12] A total mass of 47.28 μgcm^{-2} can be calculated according to the Sauerbrey equation (Eq. 4.1), where C = 18.06 ± 0.15 ngcm^{-2}Hz^{-1}.

$$m_{QCM} = -C.(\frac{\Delta f_i}{i}) \quad \textbf{(4.1)}$$

The mass measured with QCM-D corresponds to the mass of the assembled polyelectrolytes and that of the entrapped water in the film. The higher values of mass obtained, in relation to the deposition at 0.5 M NaCl may therefore be due to more polymer being assembled per layer or more water being entrapped in the film, or a combination of both situations. In Fig. 4.2 the difference between dry mass and wet mass per layer during the assembly can be seen.

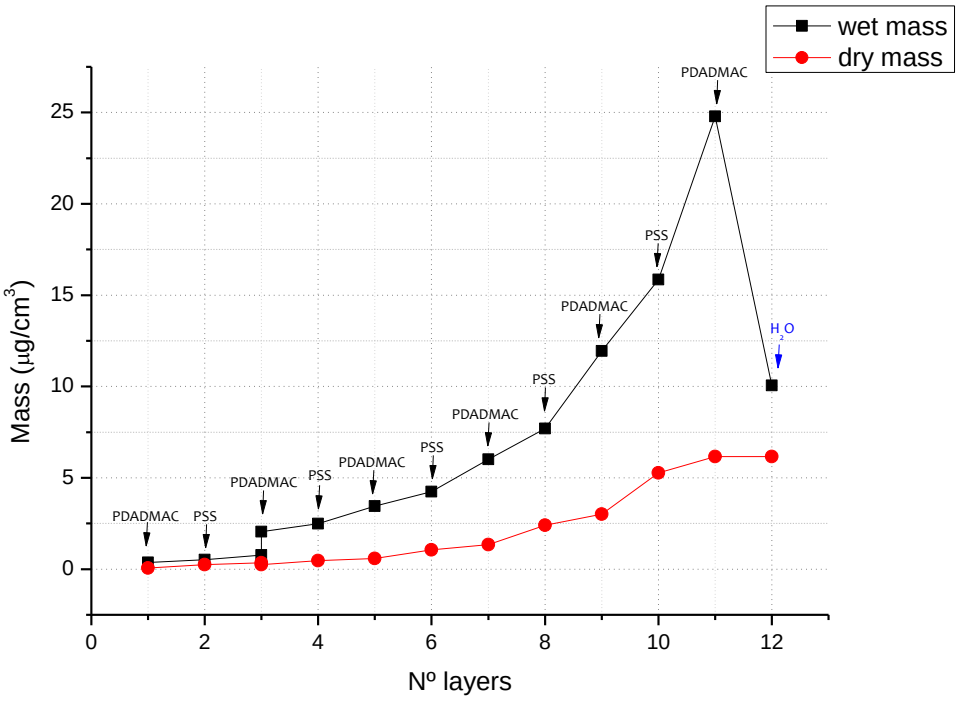

Figure 4.2. Wet mass and dry mass per layer during the assembly of $(PDADMAC/PSS)_{1.5}^{0.5M\ NaCl}+(PDADMAC/PSS)_4^{3M\ NaCl}$.

Wet mass calculations were performed as explained before. In the case of dry mass or optical mass calculations as we have already explained a three layer model was used. The first layer of titanium was calibrated prior to the assembly. The PEM was considered as a single, transparent and homogeneous layer, Cauchy medium, same as the last layer the bulk solution layer. In this case for the calculation of mass the Feitjer´s equation (Eq. 4.2) was used:[13]

$$m_{opt} = \frac{d_{opt}(n_{PEM} - n_{sol})}{\frac{dn}{dc}} \qquad (4.2)$$

where *(dn/dc)* was considered to be *0.150* cm^3g^{-1}.[14]

n_{PEM}, n_{H2O}, $n_{0.5M}$ and n_{3M} were calculated using Eq. 3:

$$n_x(\lambda) = A_x + B_x(\lambda\mu m^{-1})^{-2} \quad (4.3)$$

For the calculations λ=*632.5 nm*, the values of A and B for H_2O were taken from the literature A = *1.323* and B = *0.0032*.[15] In the case of 0.5 M NaCl A = *1.328* and B = *0.0032* and in the case of 3 M NaCl A = *1.351* and B = *0.0032*.[16]

Values of d_{opt} and A_{PEM} were obtained by fitting of this model using the software CompleteEase (Woolam) for each particular layer, and afterwards hydration was calculated following Eq. 4.4:

$$Hydration(\%) = \frac{m_{QCM} - m_{opt}}{m_{QCM}} * 100 \quad (4.4)$$

As can be seen most of the mass assembled per layer in these conditions is solvated water. After the 11th layer the solvent is changed from 3 M NaCl to pure water, there is a 60% loss of mass, but only water is lost because dry mass remains the same. Taking each polyelectrolyte individually it can also be observed, Fig. 4.3 a) and b), that comparing the wet and dry mass per polyelectrolyte, PDADMAC is the mainly responsible for the large amount of water incorporated in the resulting PEM. The difference between dry and wet mass is always bigger in the case of PDADMAC compared to PSS.

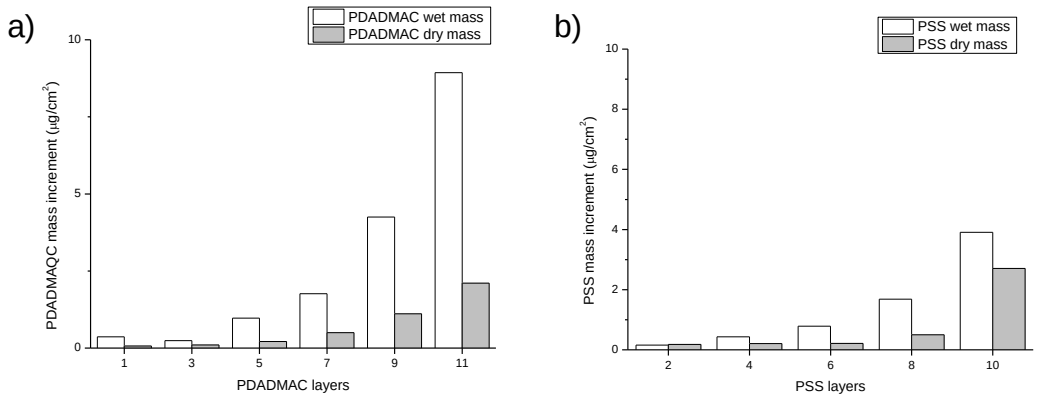

Figure 4.3. a) Comparison between dry and wet mass per layer for the PDADMAC layers in the PEM, b) Comparison between dry and wet mass per layer for the PSS layers in the PEM.

When the 3 M NaCl solution is replaced by water in the QCM-D chamber, the frequency response increases and dissipation decreases. The response of the QCM-D to the changes in ionic strength is shown in Fig. 4.4.

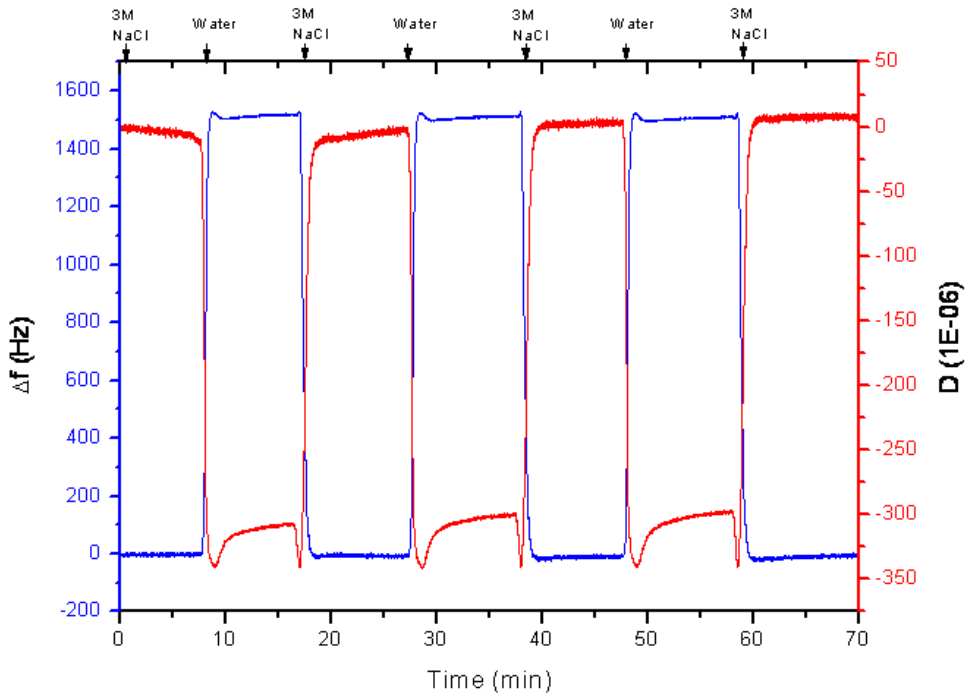

Figure 4.4. Frequency response and dissipation curves measured with QCM-D (3rd overtone) for the alternating rinsing of 11 layers of PDADMAC/PSS with water and 3 M NaCl.

In Fig. 4.4, the PEM is subsequently exposed to water and 3 M NaCl up to 6 times. As can be observed the changes are fully reversible. The exchange of the 3 M NaCl bulk solution with water results in a change of frequency of approximately 1500 Hz and a reduction in dissipation of 3E-08. The frequency change corresponds to a mass variation of 27.30 μgcm^{-2}, or approximately 42 % of the total mass. This change in frequency would mean, in terms of acoustic thickness, a variation of approximately 273 nm of the total thickness of the film. A reversible decrease in the frequency response of the PEM can only be explained by the system losing water when exposed to water and regaining the lost water when exposed to 3 M NaCl. The change in dissipation is also indicative of a system becoming more rigid when the ionic strength is reduced. Such behaviour resembles that of a polyelectrolyte brush but with an opposite trend. Brushes are extended in water and reduce thickness, losing water and become more rigid as the ionic strength increases. Recently, we have shown that PDADMAC/PSS multilayers assembled at 0.5 M NaCl display similar behaviour to a polyelectrolyte brush and also show pronounced thickness variations with reversible loss of water when exposed to water and solutions of higher ionic strengths.[14] Assembling PEMs at 3 M NaCl, results in thicker PEMs at 11 layers with a mass significantly larger than that obtained after assembling 17 layers at 0.5 M NaCl. The opposite behaviour in response to the ionic strength variation highlights a different arrangement of the polymer

chains in the PEM and hints that the chains have different conformational freedom.

We employed AFM to verify the changes observed by QCM-D measurements. AFM allows us to visualise thickness variations in the film. A stripe of PEM was removed from the film as explained in the experimental method. By doing this a profile of the film was created that allows changes in film thickness to be measured from the naked substrate to the top of film.

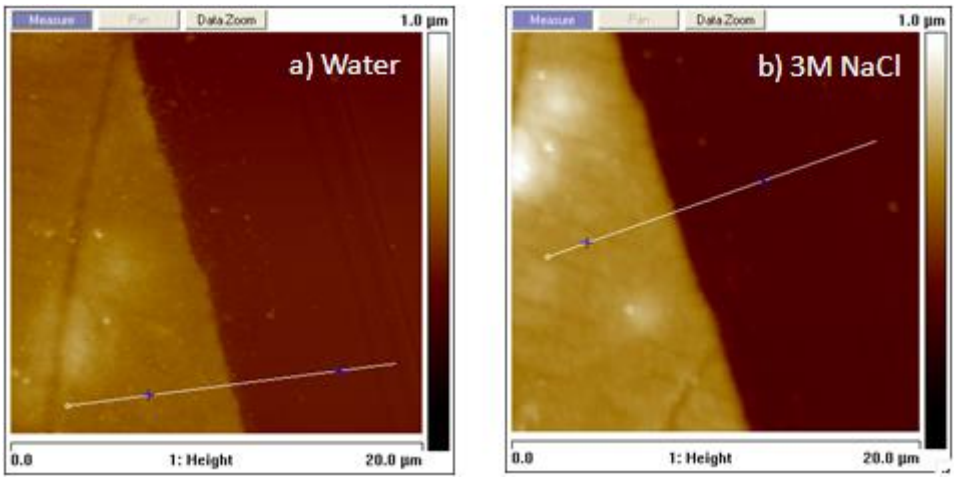

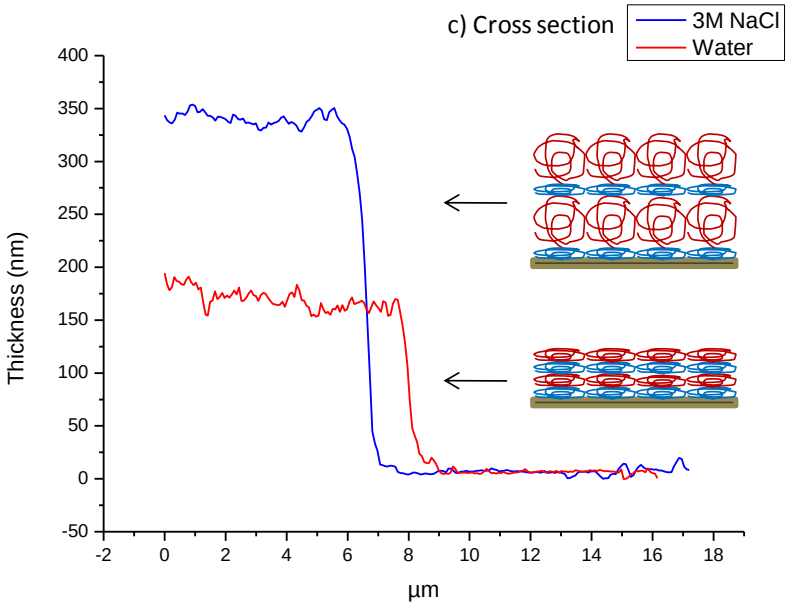

Figure 4.5. AFM images of an 11 layer PDADMAC/PSS PEMs in a) water and in b) 3 M NaCl, and cross sectional analysis c).

AFM images in Fig. 4.5 a) and b) have been taken in water and at 3 M NaCl respectively. The thickness profile of the PEM, from the removed area to the top of the PEM, is shown in Fig. 4.5 c) for both water and 3 M NaCl. The profiles clearly illustrate that there is a decrease in thickness of the film of approximately 185 nm, approximately 46 % of the total thickness, when going from 3 M NaCl to water. The AFM measurements confirmed that the change was reversible and the multilayer regained its original thickness when going back to 3 M NaCl.

However, the roughness of the films increased as the ionic strength decreased. An average roughness (Ra) of 1.03 was calculated in 3 M NaCl, while in water the values of Ra increased to 18.03. This can be understood as the chains grow laterally; the packing of the grains is altered creating defects between grains.

Both QCM-D and AFM measurements prove the reversible collapse of the PEM when decreasing the ionic strength by means of water loss and thickness reduction. The changes in thickness correspond to approximately 200 nm, and the water loss represents approximately 42-46 % of the total mass. Such variations in thickness and water content are more significant than those usually observed with polyelectrolyte brushes.[11] Taking brushes as a reference for responsive polyelectrolyte films with varying ionic strength, PDADMAC/PSS PEM prepared at 3 M NaCl shows an opposing behaviour to

the expected ionic strength response. Due to a decrease in the ionic strength, the thickness of the film decreases. This can be explained by the change in conformation of the polyelectrolyte molecules that results in a thickness reduction and a lateral growth of the chains that, in turn causes the water entrapped in the layers to be expelled. The collapse of brushes can be explained by the screening of the charges of the chains which diminish the internal repulsion of the charged monomers, allowing the chains to acquire a more coiled conformation. For the PDADMAC/PSS PEMs prepared at 3 M NaCl, decreasing the ionic strength also varies the polymer chain conformation. The chains can now extend themselves but they do so by occupying lateral space in the film that was filled with water instead of pumping out as brushes do. This results in uncompensated charges in the film that allow reorganisation in the PEM.[17] The lateral displacement results in the reduction of the water content of the film. It is not fully clear why the chains tend to preferentially extend laterally but it is likely due to the presence of oppositely charged layers below or above. When the ionic strength is reduced the attractive electrostatic interaction among subsequent layers must increase. This interaction may indeed trigger a lateral displacement of the chains in a layer trying to maximise the contact with the layers below and above. Nevertheless, the reversibility of the collapse indicates that the reorganisation of the chains in the PEM does not lead to a strong interaction between layers that would indeed prevent the chains from going back to their original conformations.

4.4 Conclusions

PEMs with the ability to collapse, displaying a variation in thickness of 200 nm, approximately a 46 % reduction in its thickness, has been fabricated by assembling PDADPMAC/PSS at 3 M NaCl. PEM assembly at 3 M NaCl with the chains highly coiled results in a high content of water entrapped between polyelectrolyte chains. PDADMAC assembles at these conditions with a higher content in water with respect to PSS as has been measured by combined ellipsometry-qcm. When reducing the ionic strength to that of pure water the chains expand and flatten, thus occupying lateral space and removing the water between chains. As a consequence, the thickness of the PEM is reduced. An increase in the ionic strength to 3 M NaCl reverses the process and the film stands up and regains the lost water. Such a PEM film could have interesting applications, such as nanoactuators or controllable barrier applications where polyelectrolyte brushes are frequently applied, with the advantage that the response of the PEMs to varying ionic strength would be opposite to that observed by a brush. Additionally, the thickness of the film can be easily controlled over a few hundred nanometres by controlling the number of polyelectrolyte layers assembled.

The work presented in this chapter resulted in the following publication:

Irigoyen, J.; Han, L.; Llarena, I.; Mao, Z.; Gao, C.; Moya, S. E. *Macromol. Rapid Commun.* **2012**, *33* (22), 1964–1969.

4.5 References

(1) G. Decher, J. D. Hong, J. Schmitt, *Thin Solid Films* **1992**, *210-211, Part 2*, 831.

(2) G. Decher, *Science* **1997**, *277*, 1232.

(3) S. T. Dubas, J. B. Schlenoff, *Macromolecules* **1999**, *32*, 8153.

(4) S. S. Shiratori, M. F. Rubner, *Macromolecules* **2000**, *33*, 4213.

(5) E. Donath, G. B. Sukhorukov, F. Caruso, S. A. Davis, H. Möhwald, *Angewandte Chemie - International Edition* **1998**, *37*, 2202.

(6) G. B. Sukhorukov, E. Donath, H. Lichtenfeld, E. Knippel, M. Knippel, A. Budde, H. Möhwald, *Colloids and Surfaces A: Physicochemical and Engineering Aspects* **1998**, *137*, 253.

(7) J. B. Schlenoff, S. T. Dubas, *Macromolecules* **2001**, *34*, 592.

(8) R. v. Klitzing, J. E. Wong, W. Jaeger, R. Steitz, *Current Opinion in Colloid & Interface Science* **2004**, *9*, 158.

(9) L. Han, Z. Mao, H. Wuliyasu, J. Wu, X. Gong, Y. Yang, C. Gao, *Langmuir* **2012**, *28*, 193.

(10) R. Zhang, K. Köhler, O. Kreft, A. Skirtach, H. Möhwald, G. Sukhorukov, *Soft Matter* **2010**, *6*, 4742.

(11) J. J. I. Ramos, S. E. Moya, *Macromolecular Rapid Communications* **2011,** *32*, 1972.

(12) J. J. I. Ramos, I. Llarena, S. E. Moya, *Journal of Polymer Science Part A: Polymer Chemistry* **2011**, *49*, 2346.

(13) J. A. De Feijter, J. Benjamins, F. A. Veer, *Biopolymers* **1978**, 17, 1759–1772.

(14) J. J. Iturri Ramos, S. Stahl, R. P. Richter, S. E. Moya, *Macromolecules* **2011,** *43*, 9063.

(15) M. Daimon, A. Masumura, *Appl. Opt.* **2007**, 46, 3811.

(16) Lide, D. R. *Handbook of chemistry and physics*, 85th ed.; CRC Press: Boca Ratón, 2004.

(17) H. Mjahed, G. Cado, F. Boulmedais, B. Senger, P. Schaaf, V. Ball, J.-C. Voegel, *Journal of Materials Chemistry* **2011,** *21*, 8416.

HYBRID SYSTEMS CARBON NANOMATERIALS/POLYELECTROLYTES

Chapter 5
Hybrid Nanofiltration Membranes Based on Multiwalled Carbon Nanotubes and Polyelectrolytes.

5.1 Introduction

In recent years there has been growing interest in the use of PEMs for nanofiltration and reverse osmosis applications.[1–8] In LbL, thickness and composition in the vertical direction can be defined with nanometer precision.[9–13] PEM thicknesses vary normally from a few to hundreds of nanometers with a high density of charged functional groups, positively and negatively charged, provided by the polyelectrolyte components.[14,15] These characteristics: nanoscale thickness and high functional group density, combined with their ease of fabrication, make PEMs very attractive for the fabrication of nanofiltration membranes. Several articles[3,4,6,7,16,17] have explored the possibilities of PEMs for nanofiltration and reverse osmosis using different combinations of polyelectrolytes with very high retention for specific ions.[18–21] For practical applications as nanofiltration and reverse osmosis membranes PEMs must be assembled on top of membrane supports, which are either polymeric or ceramic. The support entails pores necessary for the passage of the solutions to be filtrated. If the pores are smaller or have a comparable size with the polyelectrolyte molecules, which are normally assembled at ionic strengths between 100 and 800 mM NaCl in a coiled state the LbL assembly

takes place without difficulty. In these assembly conditions a dense and compact multilayer structure is normally obtained. Adamczyk et al.[22] found for example that PDADMAC (Mw = 160 $kgmol^{-1}$) at 0.5 M NaCl has a hydrodynamic diameter of 26.2 nm. If pores are larger than the size of polyelectrolyte molecules these will penetrate the pore and assemble on the pore walls, which are charged. After a few deposition cycles of polyelectrolytes, the pores will be filled with the polyelectrolyte as PEMs will assembly on the walls of the pores.[23,24] The size of the pores will decrease since the diameter will be reduced by the PEMs being assembled or the pore can even be fully blocked. If the polymer flows through the pores more polyelectrolyte layers will be necessary to bridge over the pores. With the size of the pore being reduced flow will also be reduced or stopped, hindering the use of the membrane. This will be the case for ceramic SiC membranes which display a broad distribution of pores ranging from a few nanometers in some cases to more than 50 nm. Ideally for an optimal nanofiltration membrane a dense PEM structure should be achieved on top of the pores without depositing on the pore walls, which would cause the reduction of pore size and flow through the pore. To overcome this problem of the size and the filling of the pores, as well as to avoid the deposition of a large number of layers to cover the pore we have fabricated an intermediate layer between the substrate and the PEMs based on MWCNTs. This intermediate layer will cover the pores of the SiC support and on top of these layers we have assembled the polyelectrolyte multilayer membrane. The MWCNTs have also been assembled in a "Layer by Layer"

fashion, using positively and negatively charged CNTs, which were later crosslinked by annealing. CNTs were oxdised and later modified with polycations to have negatively and positively charged CNTs respectively that could be alternately assembled by electrostatic interactions. Since CNTs are on average significantly longer than the pore diameter they will deposit on top without penetrating the pore. The CNTs layers will then form a mesh that does not allow the polyelectrolytes to go through the pore during the PEM assembly. In this way the PEM acting as the nanofiltration membrane will be separated from the pores by a MWCNTs multilayer. In these conditions the pores will not be filled with polymer during the PEM assembly. Moreover, this spacer will increase the path of water flow and thus allow lateral movement of water between the PEM and SiC pores, creating a funnel effect with a consequent increase in flow. We will show that by fabricating a hybrid membrane based on PEMs deposited on a MWCNT multilayer on top of ceramic silicon carbide (SiC) modules the performance of the PEMs, flow and retention, will be significantly increased compared with the situation without MWCNTs, leading to new operational possibilities in nanofiltration for PEMs.

5.2 Materials and Methods

PAH [Mw= 1.5 $kgmol^{-1}$], PSS [Mw=1000 $kgmol^{-1}$], PDADMAC [Mw=100-200 $kgmol^{-1}$], sodium chloride (Reag. Ph Eur), magnesium chloride hexahydrate (Ph Eur), sulfuric acid (95-97%), nitric acid fuming 100%, magnesium sulfate heptahydrate (Ph Eur), sodium hydroxide and multi walled carbon nanotubes 95% purity, 30 nm of diameter and 1-5 microns of length (Data from the

distributor). Ceramic SiC monotubular modules with a length of 250 mm, an inner diameter 6 mm, and an outer diameter of 10 mm and flat sheets were provided by Liqtech International, Denmark. According to company technical specifications the pore size is around 40 nm in diameter. The water used is ultra pure with a resistivity at 25ºC of 18.2 MΩ cm^{-1}.

5.2.1 MWNTs Functionalization

For the LBL assembly of the MWCNTs these were first oxidised in a mixture of H_2SO_4:HNO_3 (3/1 v/v) at reflux at 80-85 ºC for 90 minutes and then cleaned with water in an Amicon cell (pore size 200 nm) until neutral pH was achieved.[25] The carboxylated nanotubes (MWCNT-COOH) were stable in water and display a zeta potential of -23 mV at neutral pH. Once oxidised the MWCNTs were coated with PAH by electrostatic interactions. The CNTs become positively charged with a zeta potential of +39 mV also at neutral pH. For the PAH coating, previously oxidised MWCNTs were dispersed in a solution of 1 $mgml^{-1}$ PAH in 0.5 M NaCl for 30 minutes and then centrifuged at 35.000 rpm for 1 hour to remove excess of PAH and then washed with pure water 3 times.

5.2.2 Assembly of the MWCNTs Intermediate Layer

For the coating of planar SiC membranes a drop of the MWCNTs solution was placed on top and left it incubating for 15 minutes, as the surface is porous the water was filtered through it and the CNTs remained on top. Afterwards the SiC surface was washed with water 3 times before placing it in a beaker with fresh water and shaking it in order to remove the excess MWCNTs. Then, the

procedure was repeated a few times, alternating positively and negatively charged CNTs. The sample was left to dry overnight at room temperature and afterwards, annealed in an oven at 150°C for half an hour in order to crosslink the MWCNT layer. This crosslinking reaction creates amide bonds between the amines of the PAH and the carboxylic groups present in the oxidised MWNTS and will contribute to making it more stable.[25] On the SiC flat surfaces PDADMAC and PSS (1 $mgml^{-1}$ 0.5 M NaCl both solutions) were assembled by alternately dipping the sample in the polyelectrolyte solutions. After every assembly step the sample was rinsed 3 times with water.

For the assembly of the MWCNTs intermediate layer on top of the internal face of a ceramic SiC tubular module, the module was first enclosed inside a chamber specifically designed for this application and fixed with two o-rings at its borders, see Fig. 5.1. This chamber has three exits: 1- an inlet, 2- an outlet, and 3- a permeate exit from were only the liquid already filtered exits. The solution is pumped along the circuit by a pump.

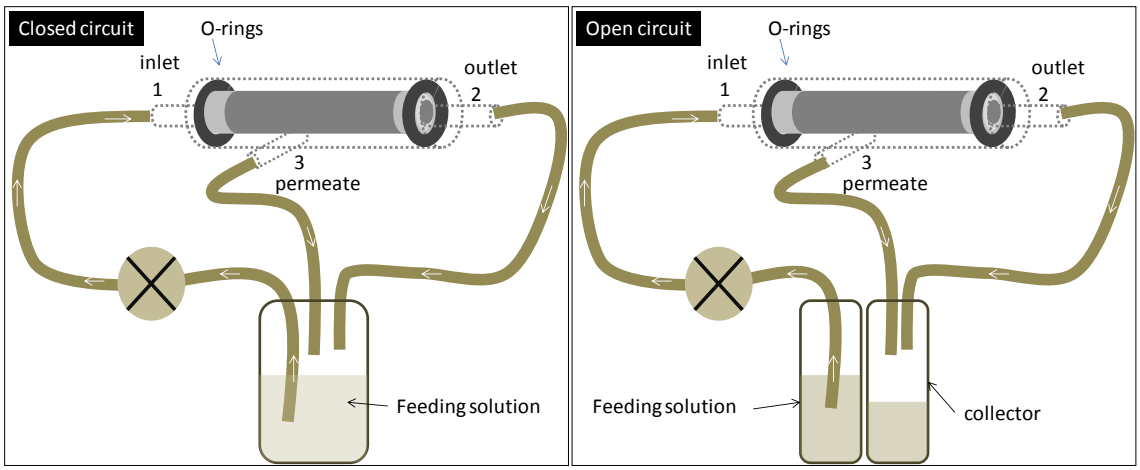

Figure 5.1. Sketch of the closed and open circuit system built for the assembly of the MWCNT reinforcing layer.

The assembly of each layer was done in two steps: a) first the corresponding positive or negative MWCNT solution (100 ml at 250 $\mu g ml^{-1}$) was pumped during 1 min in a closed circuit mode, afterwards the pump was stopped and the coating solution was left for 15 min inside the tube. b) The feeding solution was replaced with 400 ml of water and pumped during 15 minutes in a closed circuit (recirculating), the circuit was opened and the 400 ml of the water was collected from the exit, and finally another 400 ml was pumped in an open circuit mode. This procedure was alternately repeated as many times as number of layers were intended to be built. The monotube was removed from the chamber, left drying overnight at room temperature and then annealed in an oven at 150°C for half an hour in order to crosslink the MWCNT layer as for the planar surfaces. The permeability of the support at different pressures was measured after each deposition to confirm the assembly of the charged MWCNTs.

5.2.3 Polyelectrolyte Multilayer Coatings

SiC monotube membranes were coated with PDADMAC/PSS multilayer films in a custom cross-flow filtration setup. Aqueous polyelectrolyte solutions of PDADMAC and PSS were prepared with a polymer and NaCl concentrations of 1 mg ml^{-1} and 0.8 M respectively. The membranes were alternately coated with PDADMAC and PSS by filling the inner SiC monotube volume with the

polyelectrolyte solution, operating the filtration setup at a constant transmembrane pressure of 2.0 bar for 10 min (first PDADMAC layer for 5 min) without cross-flow, and subsequently rinsing with water for 3 min at a transmembrane pressure of 0.1 bar and a cross-flow of 50 lh^{-1}. The sequence was continued until a desired number of layers were deposited on the membrane.

5.2.4 Filtration Experiments

Pure water permeability (PWP) measurements and salt solution filtrations were conducted in a custom cross-flow filtration setup. PWPs were calculated from at least three pure water fluxes measured within a transmembrane pressure range of 0.3 – 2.0 bar, at a 0.5 ms^{-1} cross-flow velocity and 20 ˚C. A 5 mM $MgSO_4$ salt solution and a mixed salt solution containing 5 mM of NaCl and 5 mM of $MgCl_2$ were used to characterize membrane performance. Salt solution filtrations were conducted at various permeate fluxes within a transmembrane pressure range of 1.5 – 9.5 bar, and always at 0.83 ms^{-1} cross-flow velocity (Reynolds ≈ 5000) and 20 °C. Feed, permeate and retentate samples were collected for ion chromatography and conductivity measurements.

5.2.5 Ion Chromatography and Conductivity Measurements

Sodium and magnesium concentrations were analyzed from feed permeate and retentate samples with an ion chromatography system. An 11 mM sulfuric acid solution was used as the eluent. Conductivities were measured from feed, permeate and retentate samples at 25 °C.

5.2.6 Scanning Electron Microscopy

Scanning electron micrographs were obtained operating at 8kV acceleration voltage. Before imaging, dry membrane samples were cut open and sputtered with a thin layer of gold in an Edwards Scancoat Six sputter coater.

5.3 Results and Discussion.

The MWCNT assembly was first performed in SiC planar surfaces as explained in materials and methods. In Fig. 5.2 a) we can observe the topology of the SiC support. The surface has a grainy structure; grains are irregular in size and between them pores can be recognized.

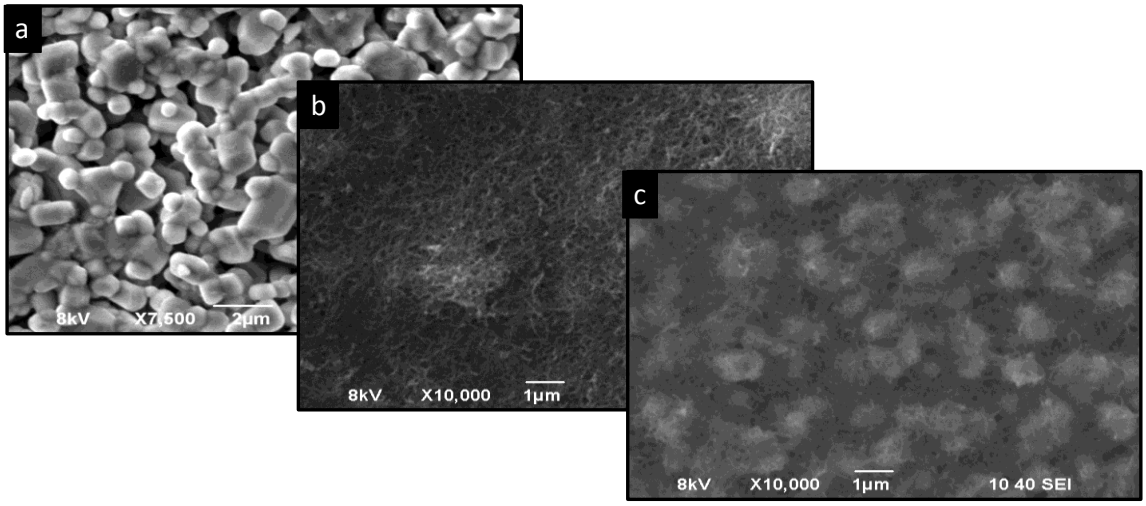

Figure 5.2. a) SEM image of the surface of a flat SiC membrane. b) SEM image of SiC support after being covered with 10 layers of MWNCTs. c) SEM image of a SiC support after being covered with MWCNTs and 10 layers of PDADMAC/PSS 1 $mgml^{-1}$ 0.8 M NaCl.

The SEM image in Fig. 5.2 b) shows the SiC surface coated with 5 bilayers of MWCNTs. The MWCNTs layer has been fabricated alternating layers of

oxidised and PAH coated CNTs as explained in the experimental part. The coating is continuous and dense; areas free of CNTs cannot be observed. The characteristic fibrillar shape of the CNTs can be easily recognized on the surface as well as pores smaller than those in the bare SiC surface. On top of the MWCNT layer we deposited a multilayer of PDADMAC and PSS resulting in a complete coating of the surface, Fig. 5.2 c). CNTs can be still recognized in some areas but not on the whole surface. Most of the surfaces present the grainy structure characteristic of PDADMAC/PSS films. We have chosen PDADMAC/PSS films as these are more suitable for practical applications of PEMs.[26]

The coating was then performed on the SiC tubular membranes as described in the experimental section. Once the assembly was completed the tubes were cut in the middle and the cross section was visualized by SEM, Fig. 5.3.

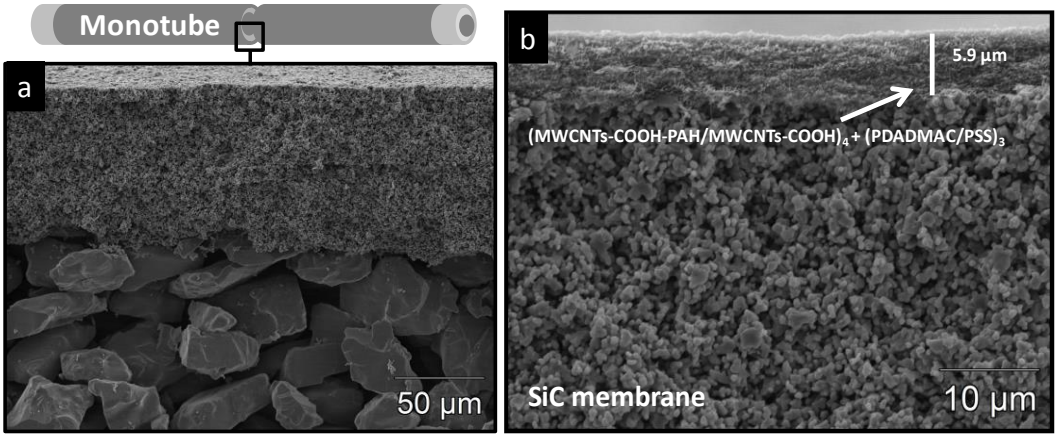

Figure 5.3. a) SEM micrographs from a cross section of the inner part of a SiC monotube modified with $(PDADMAC/PSS)_5$. b) Cross section of the inner part of a SiC monotube coated with $(MWCNTs\text{-}COOH\text{-}PAH/MWCNTs\text{-}COOH)_4$ reinforcing layer + $(PDADMAC/PSS)_5$ PEM.

The SiC support has a grainy structure with smaller grains in the inner surface than in the outer surface. In Fig. 3a the cross section of a SiC membrane coated with 5 bilayers of PDADMAC/PSS is observed. The presence of the PEM on top of the membrane cannot be confirmed from the lateral images. The MWCNTs assembly on top of the SiC support forms a thick layer of approximately 6 micrometer as it can be visualized in Fig. 3b. The layer is continuous on the SiC surface and as expected the CNTs are not penetrating in the pores.

5.3.1 Evaluation of Membrane Performance, Water Permeability and Rejection to $MgSO_4$

The pure water permeability (PWP) and ion rejection were measured for the SiC modules with the MWCNT coating and PEMs. In a first instance the PWP and the rejection to $MgSO_4$ were measured for the bare SiC without any modification as control and the SiC membrane with a variable number of (PDADMAC/PSS) bilayers.

As it can be seen in Table 5.1 the permeability of the SiC membrane decreases significantly from 10.300 to 5.3 l $m^{-2}h^{-1}bar^{-1}$ when a 5 bilayers PDADMAC/PSS PEM are assembled on top. PWP remains almost constant with the number of layers assembled; only a small decrease is observed with the addition of each bilayer due to the increase in density and thickness of the PEM. Once the MWCNT spacer is placed between the support and the PEM, the permeability increases a 42 % with respect to the same PEM without MWCNTs. Such an

increase in the flux represents a large improvement in the membrane performance.

For the PDADMAC/PSS PEMs assembled on the SiC support without CNTs the rejection to $MgSO_4$ increases from 48.2 % to a 59.1 % with an increasing number of bilayers forming the PEM, from 3 to 5. Most interesting the rejection increases to 84.4 % for 3 bilayers of PDADMAC/PSS when these are assembled on top of the MWCNT multilayer, a 75 % more efficient than the same number of layers without CNTs and a 42 % more efficient than having 5 bilayers of polyelectrolytes instead of 3.

Table 5.1. Pure water permeability and ion rejection for 5mM $MgSO_4$. $MgSO_4$ filtrations were operated at a cross-flow velocity of 0.83 ms^{-1} (Reynolds ≈ 5000) and a permeate flux of 15 ± 2 $lm^{-2}h^{-1}$. All experiments were conducted at 20 °C.

CNT support	PEM coating	PWP, $lm^{-2}h^{-1}bar^{-1}$	R ($MgSO_4$), %
(MWCNT-COOH-PAH) /$(MWCNT\text{-}COOH)_4$	$(PDADMAC/PSS)_3$	8.7 ± 0.2	84.4 ± 0.6
No	$(PDADMAC/PSS)_3$	6,1 ± 0.2	48.2 ± 0.5
No	$(PDADMAC/PSS)_4$	5.7 ± 0.2	56.1 ± 0.4
No	$(PDADMAC/PSS)_5$	5.3 ± 0.2	59.1 ± 0.4
No	No	10300 ± 400	<1

5.3.2 Ion Rejection Dependence on Flux

Two different experiments were performed to study ion rejection. In a first instance the effect of permeate flux on rejection of Mg^{2+} at a 5 mM $MgSO_4$ solution was analyzed. The rejection to Mg^{2+} increases slightly while the solution flux is increased through variations in the operation pressure, see Fig.

5.4 a). In the case of the membrane without MWCNTs, even if the number of bilayers of the PEM is bigger, the rejection to Mg^{2+} is lower than with MWCNTs, and also we can see that at a flux of around 45 $lm^{-2}h^{-1}$ rejection decreases.

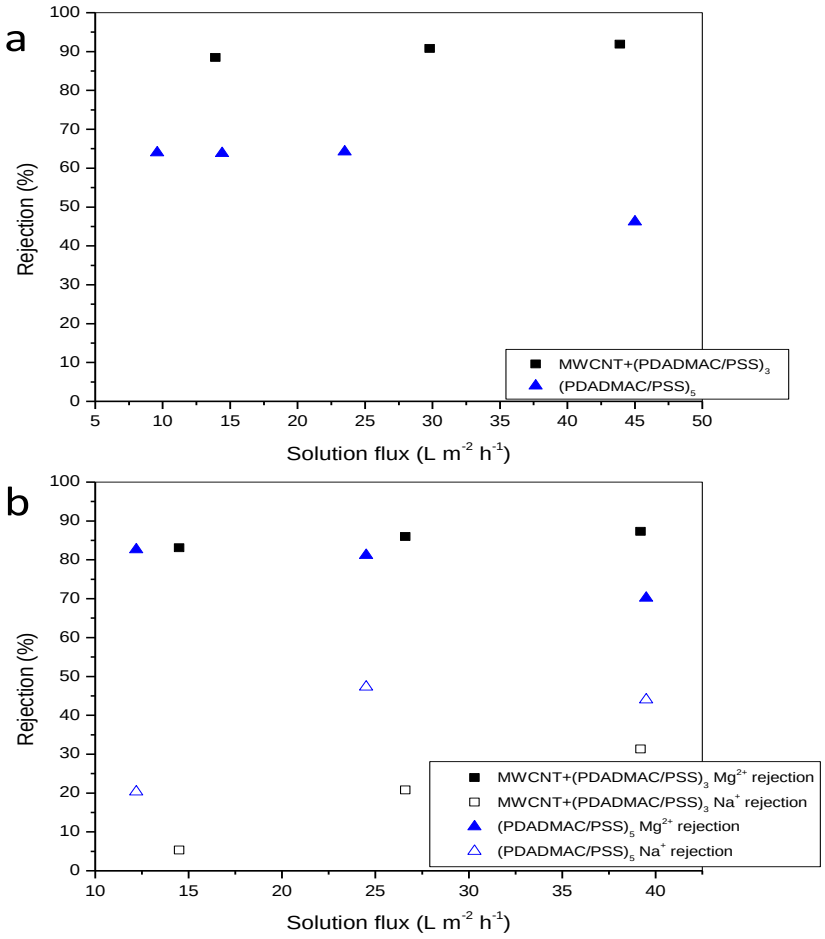

Figure 5.4. a) Mg^{2+} rejection dependence on flux for a 5 mM MgSO4 solution. b) Na^{+} and Mg^{2+} rejection dependence on flux for a mixed salt solution with 5 mM of NaCl and 5 mM of $MgCl_2$. All filtration experiments were conducted at a cross-flow velocity of 0.83 ms^{-1} (Reynolds ≈ 5000) and at 20 °C. The membranes analyzed are: $(PDADMAC/PSS)_5$ and $MWCNT+(PDADMAC/PSS)_3$.

As can be seen in Fig. 5.4 b) there is a bigger rejection for divalent ions of Mg^{2+}, than for monovalent ions of Na^{+}. There is only a slight change in the Mg^{2+} rejection for the PEMs on top of MWCNTs when the counter ion for Mg^{2+} changes from sulfate and chloride. Nevertheless when we look at the PEM without MWCNTs the Mg^{2+} with Cl^{-} as counter ions is significantly more rejected than for the solution with sulfate. When we compare the rejection of Mg^{2+} with sulfate as co-ion for membranes supported on MWCNTs and free of them we observe that the rejection for the ones on MWCNTs is much larger.

Divalent sulfate (by electroneutrality magnesium in Fig. 5.4 a) is better retained than monovalent chloride (sodium in Fig. 5.4 b). As the Fig. 5.4 a) and 4b show the difference in monovalent (NaCl salt) and divalent ions ($MgSO_4$ salt) retention was significantly higher with MWCNTs supported PEM membrane.

The curves in Fig. 5.4 also reveal that after a certain flux the rejection for both divalent and monovalent ions tend to decrease. However when the PEM is on top of the MWCNT layer the rejection remains constant or increases with increasing flux for the fluxes that we have applied in this work, up to 45 l m^{-2} h^{-1}. As we can observe in the curves for $MgSO_4$ the rejection for the PEMs on MWCNTs increases from 89 to 92 % approximately when going from a flux of 15 to 45 l $m^{-2}h^{-1}$. For the PEMs without the MWCNT and for fluxes between 10 and 25 $lm^{-2}h^{-1}$ rejection remains constant around a 65 % but at 45 $lm^{-2}h^{-1}$ decreases to less than 50 %. The effect is also clear for NaCl and $MgCl_2$.

From the Fig. 5.4 b) we can also observe that the rejection for Mg^{2+} is much larger than for Na^{+}. Though this is the case for PDADMAC/PSS with and without the MWCNT support. The effect is more pronounced on the MWCNT supported PEMs with a 56 % more rejection for the Mg^{+2} than the Na^{+} at 40 l m^{-2} h^{-1}, with a maximum difference at a low flux of around 14 l m^{-2} h^{-1} of 78%. This difference in rejection is larger than the observed for the PEMs without the MWCNT. At 40 l m^{-2} h^{-1} they show a difference in rejection of 26 % for Mg^{2+} and Na^{+}.

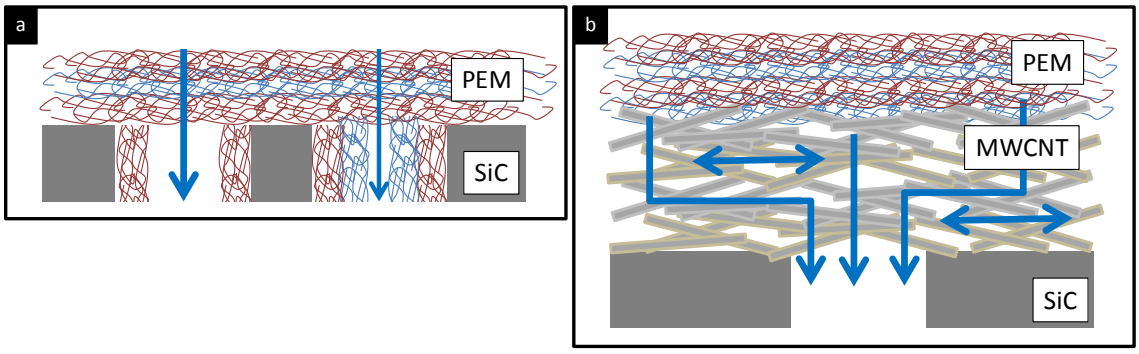

Figure 5.5. a) Sketch of the internal surface of a SiC monotube, covered with a PEM assembled Layer by Layer on top. b) Sketch of the internal part of a SiC monotube, covered with a multilayer of MWCNT with a PEM on top. The arrows represent the flux of permeating water.

In Fig. 5.5 we show two sketches with both assemblies of PEMs on top of the supporting membrane with and without the MCNTs intermediate layer. In Fig. 5.5 a) we can observe the sketch of the PEM assembled on top of the SiC support without the CNTs. In the sketch the PEM is covering the internal walls of the pores reducing the pore size. The flux passing through the pore will be also restricted to the solution going through the area of the PEMs that it is

deposited on top of the pore. In Fig. 5.5 b) the sketch shows the MWCNTs assembled on the porous support. On top of the MWCNTs multilayer a PEM has been deposited. It can be appreciated that the PEM is separated from the support by the MWCNTS multilayer, which act as a spacer. The flux going through the pores comes from the volume between the PEMs and the MWCNTs spacer acting as a funnel. In this situation the solution going through the pores is collected from larger membrane areas with the subsequent increase in the volume passing through the pore as compared with the situation of the PEM assembled onto the pores without the CNTs layers.

Pure water permeability decreases after placing polyelectrolytes on top, remaining almost constant independently of the number of layers assembled, only a small decrease is observed with the addition of each bilayer due to the increase in density and thickness of the PEM. After the MWCNT spacer is placed between the support and the PEM, the permeability increases such an increase in the flux represents a large improvement in the membrane performance, confirming our assumption. A comparison with the PWP of commercial nanofiltration membranes as NF270= 15.3 $lm^{-2}hr^{-1}bar^{-1}$ and NF90= 7.2 $lm^{-2}hr^{-1}bar^{-1}$ from Dow Chemicals (Midland, MI),[27] measured in similar conditions, shows that our MWCNTs+PEM SiC modified membranes give values of flux slightly lower than the commercial ones but still much higher than those of the PEMs without CNTs.

Rejection to $MgSO_4$ increases while we increase the number of polyelectrolytes assembled on top of the bare SiC support, until a maximum of around a 60 %

for the maximum number of layers tested. Once we place the MWCNTs spacer in between, rejection increases dramatically, reaching levels above 80 %.

We can conclude that there is a considerable improvement in terms of rejection when the reinforcing layer is placed in between the SiC and the PEM.

Analysing the effect of permeate flux on rejection of Mg^{2+} at a 5 mM $MgSO_4$ solution we observed as we previously said that rejection to Mg^{2+} increases slightly while the solution flux is increased through variations in the operation pressure. In this case there is a decoupling between ion flux and water flux, water flux increases while ion flux can be electrically and/or sterically hindered, resulting in a dilution effect and therefore in a lower ion concentration in the permeate and then ion rejection might be higher. At the same time due to this increase in the operation pressure there is a more significant transport of ions to the surface of the membrane enhancing the concentration polarization and reducing rejection. In our case the effect of dilution is slightly higher than the effect on the concentration polarization therefore the rejection increases.[28] In the case of the membrane without MWCNTs, even if the number of bilayers of the PEM is larger, the rejection to Mg^{2+} is lower than with MWCNTs, and also it can be observed that at a flux of around 45 l m^{-2} h^{-1} rejection decreases and the effect of the concentration polarization is bigger than the effect of dilution that was the predominant at lower fluxes.

Nanofiltration membranes have mainly two mechanisms for separation: sieving in the case of uncharged particles bigger than the membrane pore size and electric repulsion due to Donnan and dielectric effects in the case of charged particles or ions [29]. The interaction of charged molecules and ions with the functional groups present in the membrane is very important in determining their transport through the membrane or their rejection. We observed that there is a larger rejection for divalent ions of Mg^{2+}, than for monovalent ions of Na^{+}. Divalent cations have more charge and therefore they show less passage through the charged PEM than the monovalent one. This is understandable as the divalent ions are more charged than monovalent resulting in a stronger repulsion. There is only a slight change in the Mg^{2+} rejection for the PEMs on top of MWCNTs when the counter ion for Mg^{2+} changes from sulfate and chloride. Nevertheless when we look at the PEM without MWCNTs the Mg^{2+} with Cl^{-} as counter ions is significantly more rejected than for the solution with sulfate. This can probably be explained by a higher affinity of the Cl^{-} ions for the quaternary ammonium groups in PDADMAC.[30] When we compare the rejection of Mg^{2+} with sulfate as co-ion for membranes supported on MWCNTs and free of them we observe that the rejection for the ones on MWCNTs is much larger, most likely because of a more dense structure formed on the MWCNTs with less defects than for the case of the PEM without the MWCNTs support.

Since the PDADMAC/PSS membrane is negatively charged due to sulfonate groups of the uppermost PSS layer. Therefore, it can be assumed that the

charge of anions determines mostly the retention. Divalent sulfate is better retained than monovalent chloride, retention was significantly higher with MWCNTs supported PEM membrane. We can assume that the charge density on the PEM layer is higher when MWCNT support was used than without MWCNTs. As a result the retention decrease caused by higher diffusion, when concentration polarization was higher at higher flux, was compensated for higher electrostatic repulsion of MWCNT+PEM membranes. The higher retention of MWCNT supported PEM membranes might also be caused by denser membrane structure with fewer defects. Most likely the PEMs supported on the MWCNTs display both a higher charge density and a denser structure as layer coverage and density of functional groups are closely related issues for PEMs.

It can be observed too that for the membrane without spacer after a certain flux the rejection for both divalent and monovalent ions tend to decrease, while when the PEM is on top of the MWCNT layer the rejection remains constant or increases with increasing flux for the fluxes that we have applied in this work. The reason for the different response to the increase in flux must be due to the improved characteristics of the PEM supported on the MWCNT layers, with fewer defects than the PEMs without the MWCNTs.

Rejection for Mg^{2+} is much larger than for Na^{+}, in both cases with and without the MWCNT support. The effect is more pronounced on the MWCNT supported PEMs, the large difference in rejection for the PEMs on MWCNTs for mono and divalent ions make them very appealing for ion separation.

5.3.3 Comparison with other type of formulations

In order to create the MWCNT spacer not only the formulation explained before was used. Different types of functionalitations were tested until a stable spacer was created.

Amongst all the trials performed only four types of formulation reached the prototyping step in which the assembly was done and tested in the SiC monotubes. Between all of them only the formulation presented before was stable enough and withstands all the tested performed and the results were consistent with the repetitions. The rest three at some point of the tests flasks of MWCNTs were released from the spacer and its performance dropped dramatically. However some of them during their operative lifetime performed even better than the selected one and therefore it is interesting to present these experiments too.

Four formulations were assembled:

1- $[(\text{MWCNT-PSS-PAH})/(\text{MWCNT-PSS-PAH-PMAA})]_4$

2- $[(\text{MWCNT-COOH-PAH})/(\text{MWCNT-COOH})]_4$

3- $(\text{MWCNT-COOH-PAH})+[(\text{MWCNT-COOH/Laponite-PAH})]_4$

4- $[(\text{MWCNT-PSS-PAH})/(\text{MWCNT-PSS-PAH-PMAA})]_3$

In the case of 1 and 4 both are the same formulation but they differ in the number of bilayers. In this case the MWCNTs were not previously oxidated as we have explained previously; they were functionalized in a Layer by Layer fashion by wrapping the polyelectrolytes around them. As last layer PAH was

used as positive agent and poly(methacrylic acid) (PMAA) as negative one in order to have amines and carboxylic groups available for the posterior amidation by annealing.

Formulation 2 is the one explained during this chapter previously.

In formulation three a precursor layer of PAH adsorbed onto oxidated MWCNTs was used. The same used in formulation 2. But afterwards this component was changed for Laponite functionalized with PAH. Laponite was dissolved 1mg ml^{-1} in water at neutral pH, afterwards NaCl was added until a concentration of 0.5M was reached and finally PAH (Mw=15 Kg mol^{-1}) for having 1mg ml^{-1} of polyelectrolyte. After 1 hour the solution was rinsed 3 times with water by centrifugation in cycles of 9000 rpm during 15 minutes.

The assembly onto the inner part of the SiC monotube was performed as it has been explained before for formulation 2. In Fig. 5.6 SEM micrographs can be observed with the difference thickness of spacer obtained for each formulation. All of the formulations were annealed after the deposition. After the spacer a deposition of 3 bilayers of (PDADMAC/PSS) was assembled on top.

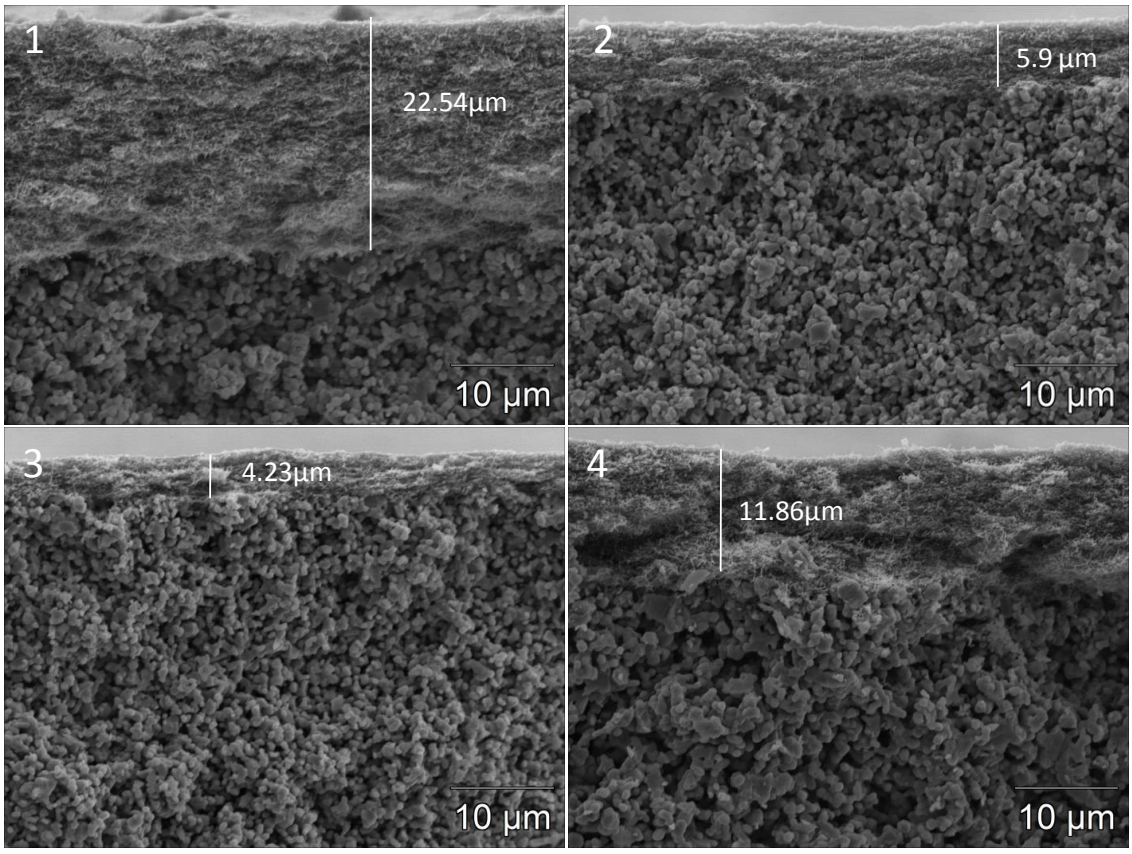

Figure 5.6. SEM micrographs for a) [(MWCNT-PSS-PAH)/(MWCNT-PSS-PAH-PMAA)]$_4$+(PDADMAC/PSS)$_3$, b) [(MWCNT-COOH-PAH)/(MWCNT-COOH)]$_4$ + (PDADMAC/PSS)$_3$, c) (MWCNT-COOH-PAH)+[(MWCNT-COOH/ Laponite-PAH)]$_4$ + (PDADMAC/PSS)$_3$ and d) [(MWCNT-PSS-PAH)/(MWCNT-PSS-PAH-PMAA)]$_3$ (PDADMAC/PSS)$_3$ onto the inner part of SiC monotubes.

It can be observed that thicknesses of the spacer differ greatly due to the composition. Higher spacers were obtained with the not previously oxidated MWCNTs, around 4 times bigger for the same amount of bilayers. Regarding the values of permeability, see Table 5.2, the not previously oxidated MWCNTs gives higher values of PWP than the oxidated ones. The lower values are for

the ones with Laponite, due to the laminar shape of the Laponite sheets can disturb the path of the water through the spacer reducing the permeability.

Table 5.2. Pure water permeability and ion rejection for 5 mM $MgSO_4$. $MgSO_4$ filtrations were operated at a cross-flow velocity of 0.83 ms^{-1} (Reynolds ≈ 5000) and a permeate flux of 15 ± 2 $lm^{-2}h^{-1}$. All experiments were conducted at 20 °C.

	CNT support	PEM coating	PWP, l m^{-2} h^{-1} bar^{-1}	Rejection $MgSO_4$, %
1	$[(MWCNT\text{-}PSS\text{-}PAH)/(MWCNT\text{-}PSS\text{-}PAH\text{-}PMAA)]_4$	$(PDADMAC/PSS)_3$	10.1 ± 0.2	88.5 ± 0,4
2	$[(MWCNT\text{-}COOH\text{-}PAH)/(MWCNT\text{-}COOH)]_4$	$(PDADMAC/PSS)_3$	8.7 ± 0.2	84.4 ± 0.6
3	(MWCNT-COOH-PAH)+ $[(MWCNT\text{-}COOH/\ Laponite\text{-}PAH)]_4$	$(PDADMAC/PSS)_3$	4.4 ± 0.2	86.6 ± 0. 4
4	$[(MWCNT\text{-}PSS\text{-}PAH)/(MWCNT\text{-}PSS\text{-}PAH\text{-}PMAA)]_3$	$(PDADMAC/PSS)_3$	14.2 ± 1,0	89.6 ± 0.5
No	No	$(PDADMAC/PSS)_3$	6.1 ± 0.2	48.2 ± 0.5
No	No	$(PDADMAC/PSS)_4$	5.7 ± 0.2	56.1 ± 0.4
No	No	$(PDADMAC/PSS)_5$	5.3 ± 0.3	59.1 ± 0.4
No	No	No	10.300 ± 400	<1

Rejection values to $MgSO_4$ are more or less in the same range for all four formulations, higher rejections were obtained for the non oxidated ones. The best performance regarding these values is for formulation 4 which is half thicker than formulation 1 and it gives the higher PWP and rejection values of all of them. In fact this values of PWP of 14.2 $lm^{-2}hr^{-1}bar^{-1}$are as high as commercial nanofiltration membranes as NF270= 15.3 $lm^{-2}hr^{-1}bar^{-1}$ and higher than NF90= 7.2 $lm^{-2}hr^{-1}bar^{-1}$ from Dow Chemicals (Midland, MI), measured in similar conditions.

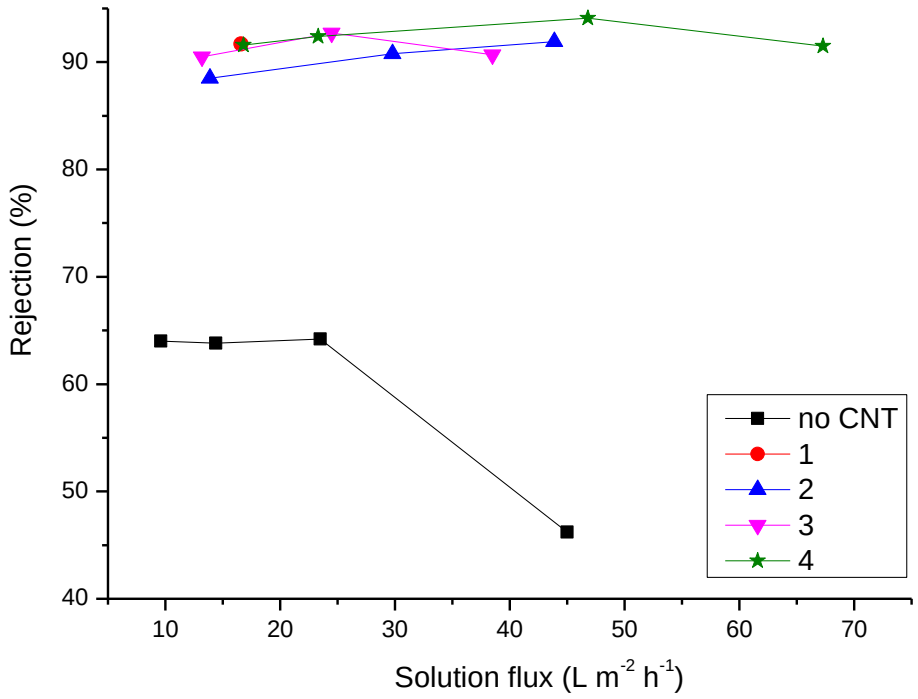

Figure 5.7. Mg^{2+} rejection dependence on flux for a 5 mM MgSO4 solution. All filtration experiments were conducted at a cross-flow velocity of 0.83 ms^{-1} (Reynolds ≈ 5000) and at 20 °C.

Analyzing rejection dependence on flux to $MgSO_4$ for all formulations it can be seen that all four formulations gives performances much better than without spacer. The higher rejection values are for formulation 4 giving a rejection of 94% at a flux of 46.8 $lm^{-2}h^{-1}$, see Fig. 5.7.

Regarding the difference in the rejection between divalent and monovalent ions, as it was seen before for formulation 2 during the chapter, there is a higher rejection for divalent ions than for monovalent ones in the four cases. In all cases the bigger differences are for low fluxes; while we increase the flux even if the rejection to divalent ions remains more or less constant in the case of

monovalent ions it gets higher, and then the difference between rejections for both type of ions decreases.

It can be seen also that for low fluxes we obtain negative values of rejection in the case of NaCl, it can be due to some remnant NaCl in the PEM that it was used for the assembly of the PEM. At these low values there can be some release of this NaCl to the solution disturbing the data obtained, see Fig. 3.8.

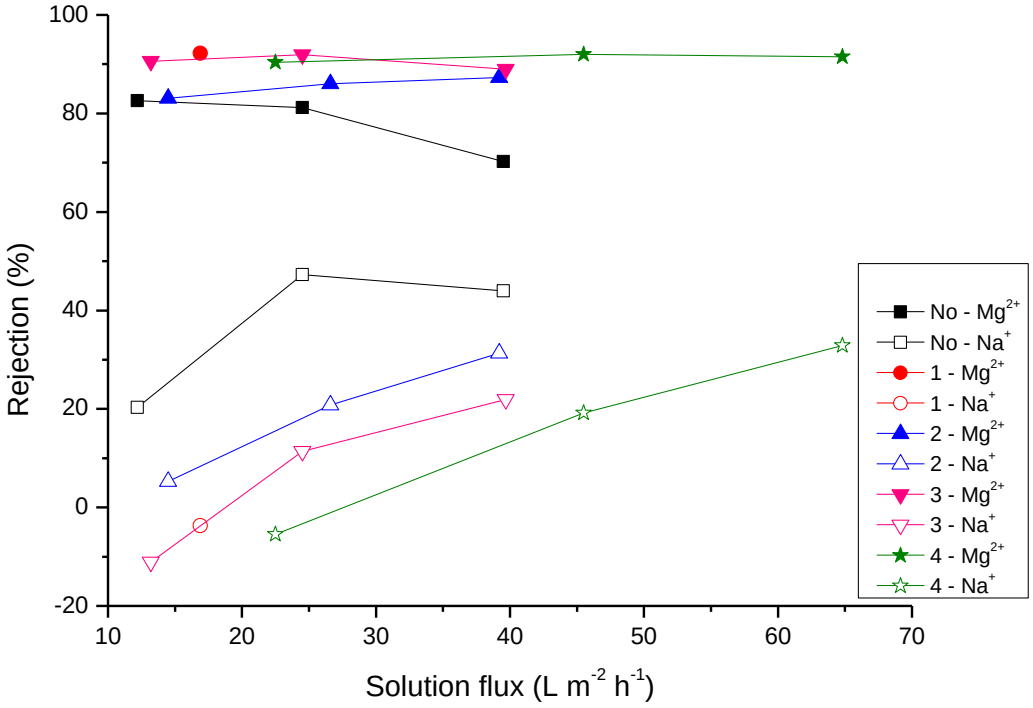

Figure 5.8. Na^{+} and Mg^{2+} rejection dependence on flux for a mixed salt solution with 5 mM of NaCl and 5 mM of $MgCl_2$. All filtration experiments were conducted at a cross-flow velocity of 0.83 ms^{-1} (Reynolds ≈ 5000) and at 20 °C.

Comparing the general outcome of the four formulations it seems that the best performance is for the fourth formulation, anyway as we have already mention this membrane started to show issues of instability after more than one use,

flakes of carbon nanotubes were released and values started dropping down. Only the second formulation remained constant with the use and time.

5.4 Conclusions

A hybrid nanofiltration membrane has been fabricated based on the assembly of a PDADMAC/PSS polyelectrolyte multilayer on top of a multilayer of MWCNTs. The MWCNTs layers act as a spacer between the membrane support and the polyelectrolyte multilayer. The spacer results on a dense polyelectrolyte multilayer assembly that cover the pores present in the MWCNT layer. The assembly of the PEMs on top the support without the MWCNT layer fails to cover the pores present on the membrane substrate for the same or larger number of layers assembled in the PEM as on top of the MWCNTs. The spacing of the PEM from substrate has the additional advantage of increasing the flux through the pores of the support as the volume going through a pore is collected from a larger area of the PEM with the MWCNTs acting as a funnel. The performance of the PEM supported on the MWCNT is significantly better than the PEM without CNTs. A PEM of 3 bilayer PDADMAC/PSS on a MWCNT spacer showed a rejection for $MgSO_4$ around 84 % while in the best of the case without MWCNT for a PEM of 5 bilayers a rejection of 59 % was observed. The PEMs on MWCNT show a large rejection difference for mono and divalent ions making them very appealing for separating ion mixtures.

The assembly of the PEMs on top of the MWCNTs as intermediate layer results in the formation of denser PEM membrane with a high charge density as needed for the divalent salt rejection and for a high stability with increasing flux, indeed with only 3 polyelectrolyte bilayers a significantly higher performance is achieved than with 5 bilayers on a SiC membrane without a MWCNT support.

A comparison with other type of formulations was done, the only formulation that remained stable and unaltered during the whole process was [(MWCNT-COOH-PAH)/(MWCNT-COOH)]$_4$ + (PDADMAC/PSS)$_3$, the rest of formulations were not suitable for their use due to instability issues.

The work presented in this chapter resulted in the following publication:

Irigoyen, J.; Laakso, T.; Politakos, N.; Dahne, L.; Pihlajamäki, A.; Mänttäri, M.; Moya, S. E. *Macromol. Chem. Phys.* **2016**, *217*(6), 804-811.

I would like to acknowledge Timo Laakso and Arto Pihlajamäki for the evaluation of the membrane performance regarding permeability and ion rejection measurements.

5.5 References

(1) Geise, G. M.; Lee, H.-S.; Miller, D. J.; Freeman, B. D.; McGrath, J. E.; Paul, D. R. *J. Polym. Sci. Part B Polym. Phys.* **2010**, *48* (15), 1685–1718.

(2) Ali, M.; Yameen, B.; Cervera, J.; Ramírez, P.; Neumann, R.; Ensinger, W.; Knoll, W.; Azzaroni, O. *J. Am. Chem. Soc.* **2010**, *132* (24), 8338–8348.

(3) Stanton, B. W.; Harris, J. J.; Miller, M. D.; Bruening, M. L. *Langmuir* **2003**, *19* (17), 7038–7042.

(4) Jin, W.; Toutianoush, A.; Tieke, B. *Langmuir* **2003**, *19* (7), 2550–2553.

(5) Shan, W.; Bacchin, P.; Aimar, P.; Bruening, M. L.; Tarabara, V. V. *J. Memb. Sci.* **2010**, *349* (1-2), 268–278.

(6) Miller, M. D.; Bruening, M. L. *Langmuir* **2004**, *20* (26), 11545–11551.

(7) Ouyang, L.; Malaisamy, R.; Bruening, M. L. *J. Memb. Sci.* **2008**, *310* (1-2), 76–84.

(8) Tripathi, B. P.; Dubey, N. C.; Stamm, M. *J. Hazard. Mater.* **2013**, *252-253*, 401–412.

(9) Decher, G. *Science (80-.).* **1997**, *277* (5330), 1232–1237.

(10) Lavalle, P.; Gergely, C.; Cuisinier, F. J. G.; Decher, G.; Schaaf, P.; Voegel, J. C.; Picart, C. *Macromolecules* **2002**, *35* (11), 4458–4465.

(11) Irigoyen, J.; Han, L.; Llarena, I.; Mao, Z.; Gao, C.; Moya, S. E. *Macromol. Rapid Commun.* **2012**, *33* (22), 1964–1969.

(12) Decher, G.; Hong, J. D.; Schmitt, J. *Thin Solid Films* **1992**, *210–211* (0), 831–835.

(13) Dubas, S. T.; Schlenoff, J. B. *Macromolecules* **1999**, *32* (24), 8153–8160.

(14) Arys, X.; Laschewsky, A.; Jonas, A. M. *Macromolecules* **2001**, *34* (10), 3318–3330.

(15) Alonso, T.; Irigoyen, J.; Iturri, J. J.; Larena, I. L.; Moya, S. E. *Soft Matter* **2013**, *9* (6), 1920–1928.

(16) Ramos, J.; Stahl, S.; Richter, R.; Moya, S. *Macromolecules* **2010**, *43* (21), 9063–9070.

(17) Deng, H. Y.; Xu, Y. Y.; Zhu, B. K.; Wei, X. Z.; Liu, F.; Cui, Z. Y. *J. Memb. Sci.* **2008**, *323* (1), 125–133.

(18) Cheng, C.; Yaroshchuk, A.; Bruening, M. L. *Langmuir* **2013**, *29* (6), 1885–1892.

(19) Armstrong, J. A.; Bernal, E. E. L.; Yaroshchuk, A.; Bruening, M. L. *Langmuir* **2013**, *29* (32), 10287–10296.

(20) Bruening, M. In *Multilayer Thin Films*; Wiley-VCH Verlag GmbH & Co. KGaA, 2002; pp 487–510.

(21) Joseph, N.; Ahmadiannamini, P.; Hoogenboom, R.; Vankelecom, I. *Polym. Chem.* **2014**, *5* (6), 1817–1831.

(22) Batys, P.; Michna, A.; Adamczyk, Z.; Jamro, K. *J. Colloid Interface Sci.* **2014**, *435*, 182–190.

(23) Raoufi, M.; Tranchida, D.; Schönherr, H. *Langmuir* **2012**, *28* (26), 10091–10096.

(24) Roy, C. J.; Dupont-Gillain, C.; Demoustier-Champagne, S.; Jonas, a. M.; Landoulsi, J. *Langmuir* **2010**, *26* (5), 3350–3355.

(25) Lee, S. W.; Kim, B.-S.; Chen, S.; Shao-Horn, Y.; Hammond, P. T. *J. Am. Chem. Soc.* **2009,** *131* (2), 671–679.

(26) Gregurec, D.; Olszyna, M.; Politakos, N.; Yate, L.; Dahne, L.; Moya, S. E. *Colloid Polym. Sci.* **2014**, *293* (2), 381–388.

(27) Sanyal, O.; Sommerfeld, A. N.; Lee, I. *Sep. Purif. Technol.* **2015**, *145*, 113–119.

(28) Fang, J.; Deng, B. *J. Memb. Sci.* **2014**, *453*, 42–51.

(29) Pérez-González, A.; Ibáñez, R.; Gómez, P.; Urtiaga, a. M.; Ortiz, I.; Irabien, J. a. *J. Memb. Sci.* **2015**, *473*, 16–27.

(30) Azzaroni, O.; Moya, S.; Farhan, T.; Brown, A. A.; Huck, W. T. S. *Macromolecules* **2005**, *38* (24), 10192–10199.

Chapter 6
Hybrid Graphene Oxide/Polyelectrolyte Capsules on Erythrocite Cell Templates.

6.1 Introduction

Graphene is undoubtedly one of the most exiting materials generated in the last decade however there is a significant drawback for the practical application of graphene. Most studies of graphene have been performed on graphite oxide or its exfoliated form, GO, because it is difficult to work with layered graphene in wet chemical applications due to dispersability issues and its tendency to form multi-layered agglomerates.[1–3] Because of these difficulties, these derivatives of graphene have the potential to be reduced to what is called a reduced form of graphene oxide, rGO, which can lead to materials with properties more like G than GO.[4–7]

The use of GO sheets in the formation of hierarchical structures and assemblies is a subject of current interest, and if done by procedures involving wet chemical techniques, offers much potential for the development of advanced and composite layered materials.

The assembly of GO in thin films on the basis of its surface charge can be accomplished using the LbL technique. Although the technique was originally developed for the alternating assembly of PEs of opposite charge, LbL can be and has been extended to include particles, 2D layered materials,

nanostructures, lipid vesicles, etc., which provide charged surfaces, or, which can have complementary interactions with another material that can lead to a subsequent or alternating assembly.[8] There are examples in literature of the assembly of GO with polycations using the LbL technique as a promising tool for the incorporation of GO into nanoscale organized thin films and the subsequent electrochemical reduction of the GO to rGO.[9,10]

Using the LbL technique, we explored the assembly of exfoliated GO into 3D structures and developed micron-sized capsules on the basis of GO and polyelectrolytes using chicken erythrocyte cells as templates. Template cells have been used in the past as capsule templates on the basis of a simple protocol, which includes the oxidation of the cell components to leave a thin polymer film capsule that mimics the dimensions and topological features of the cell template.[11–13] We show that by incorporating GO within the LbL assembly on top of the erythrocytes, 3D closed films containing walls of PE/GO and empty volume can be produced.

Capsules based on GO have potential applications in drug delivery, especially for topical applications, as the LbL capsules provide low degradability and high stability through the GO. The use of GO in the fabrication of capsules for drug delivery was reported by Hong et al. and by Kurapati et al., the last one with a focus on drug delivery.[14,15] The authors, however, use a different protocol and templates for their fabrication. In the present work, we produce continuous GO capsules with the shape of cells and show the presence and location of the GO by raman confocal microscopy and TEM. Another potential application of these

capsules is for the production of dense PE/GO films with a high concentration of GO, which was achievable in the present study by employing a high concentration of exfoliated GO during the layer by layer assembly. This is due to the coating protocol employed in which the cells are suspended in a GO solution and then centrifuged. Under these conditions, a high concentration of GO is achieved on the cell surface leading to a continuous coating.

Once dried, the capsules collapse by losing internal volume and form planar films with nanoscale thicknesses. Such films could be used to build additional hierarchical structures or for integration into devices; moreover, by the judicious choice of reagents, the GO may be further reduced to form rGO to alter particularly the electronic, mechanical and optical properties of the films.

6.2 Materials and Methods

PAH [Mw=15 $kgmol^{-1}$], PSS [Mw=70 $kgmol^{-1}$], sodium hypochlorite with active chlorine 13%, phosphate buffered saline 10x (PBS), glutaraldehyde solution grade II 25 % in water, Hank´s balanced salt solution 10x, sodium chloride, graphite powder (< 45 µm, ≥ 99.99% trace metals basis), Lymphocytes isolation solution (Ficoll) and full blood chicken collected in Alsever's anticoagulant solution.

6.2.1 Erythrocytes

Erythrocytes were separated from the chicken blood and the rest of the plasma components by centrifugation. Chicken blood conserved in Alsever´s solution was diluted with (Ca, Mg) Hank´s solution and carefully poured onto a Ficoll

solution to avoid mixing. Afterwards the resulting solution was centrifuged at 800 G speed during 30 minutes at 4 ^{o}C depositing the Erythrocytes at the bottom and the rest of the plasma in different phases above them. Only the Erythrocytes were obtained and cleaned twice with Hank´s solution by centrifugation under the same conditions as before. Cells were then fixed during 1 hour at 4 ^{o}C with glutaraldehyde at a concentration of 2.5 % in filtered PBS buffer. After fixation, they were centrifuged and washed in 0.9 % NaCl several times at 10 ^{o}C and kept refrigerated.

6.2.2 Graphene Oxide

GO was prepared by strong acid oxidation of graphite using the Hummer's method as modified in where the dispersion was water washed to neutral pH.[16,17] Following this, we washed with dilute HCl followed again by water washes to neutral pH. The graphene oxide was exfoliated via ultra-sonication and microwave irradiation. FT-IR spectra were taken with a Nexus 470 Spectrometer over 4000-400 cm^{-1} using multiple scans and 4 cm^{-1} resolution in transmission mode.

6.2.3 Layer by Layer Assembly

The LbL assembly of GO and polyelectrolytes was performed on the fixed erythrocytes. Previous to the GO assembly, two bilayers of PSS/PAH were assembled. The polyelectrolytes were assembled at a concentration of 1 $mgml^{-1}$ in 0.5 M NaCl. Two washings were performed with water between each layer assembly by centrifugation (67.08 G during 2 min). The first assembled layer on top of the cells was always PSS since it was already shown that it assemblies

better using a polyanion rather than a polycation on the erythrocytes, despite the negative charge of the cells.[18] After the fourth layer was assembled, GO is deposited in a concentration of 0.1 or 0.2 $mgml^{-1}$ in water (pH 10). The assembly of GO is performed without NaCl as the salt would screen the charges of the GO and lead to aggregation. The incubation time for polyelectrolytes and GO was always two minutes. After GO deposition, the cells were also washed in water by centrifugation. GO was assembled alternating with PAH or with three polyelectrolyte layers; PAH/PSS/PAH, until a total number of 11 layers was achieved in both cases. Also, another sample with just 9 layers of PEs, without GO, was assembled as a control, following the same procedure described above.

6.2.4 Capsule Fabrication

Once the GO/polyelectrolyte multilayer was assembled on top of the cells, they were exposed to aqueous 1 % NaOCl. The oxidizing solution degrades the cells by breaking their protein constituents through oxidation. After NaOCl treatment, samples were washed first in NaCl and then in water for several cycles to remove the products of oxidation.

6.2.5 Transmission Electron Microscopy

An aliquot of 5µl of each sample was deposited on grids of carbon film 400 Mesh Cu, (50/bx) and left to evaporate. The grid was previously stained with uranyl acetate. The images were acquired with a CCD camera of samples prepared from water dispersions cast on lacey carbon grids.

6.2.6 X-Ray Difraction

XRD data for GO was obtained operating at 35 KV and 25 mA and Cu Kα radiation.

6.2.7 Raman Spectroscopy and Confocal Raman Microscopy

Raman analysis was performed with a 100x objective, a 532 nm laser excitation and 1800 mm^{-1} grating. The system was calibrated to the spectral line of crystalline silicon at 520.7 cm^{-1}. A drop of a diluted solution containing the capsules was placed onto a silicon wafer and left evaporating overnight.

6.2.8 Atomic Force Microscopy

The samples were imaged in contact mode in air, using a TESP-V2 silicon probe with a k= 42 Nm^{-1}. A drop of a diluted solution with the capsules was placed on a glass substrate with a thin layer of Au deposited on top. The sample was left evaporating and afterwards imaged.

6.3 Results and Discussion

GO was prepared by the strong acid oxidation of powdered graphite by a modified Hummer's method; characterization data are shown in Fig. 6.1.[16,17] Multiple TEM images formed from exfoliated GO in water and dried on lacey carbon grids show micron size, few-layer GO sheets with some gentle folds and ripples (Fig. 6.1a and b). The SAED inset in b shows diffraction spots indicative of hexagonal patterns.[19] Raman spectroscopy (Fig. 6.1c) shows the expected prominent peaks for GO at 1349 and 1601 cm^{-1}, with a D/G ratio of 0.8. The D resonance corresponds to the vibration of sp^2 carbon while G corresponds to sp^3

carbon and defects associated with vacancies and grain boundaries.[20] The peaks at higher wavenumbers are also characteristic of graphene oxide. XRD results Fig. 1d indicate the absence of graphite and show the prominent (002) peak at 12.0 degrees 2θ, indicating an inter-planar GO sheet distance of 0.737 nm.[21] Prominent fourier transform infrared (FT-IR) bands for GO were observed at 3415, 1723, 1623, 1394 and 1050 cm^{-1} as reported, for example, in.[22]

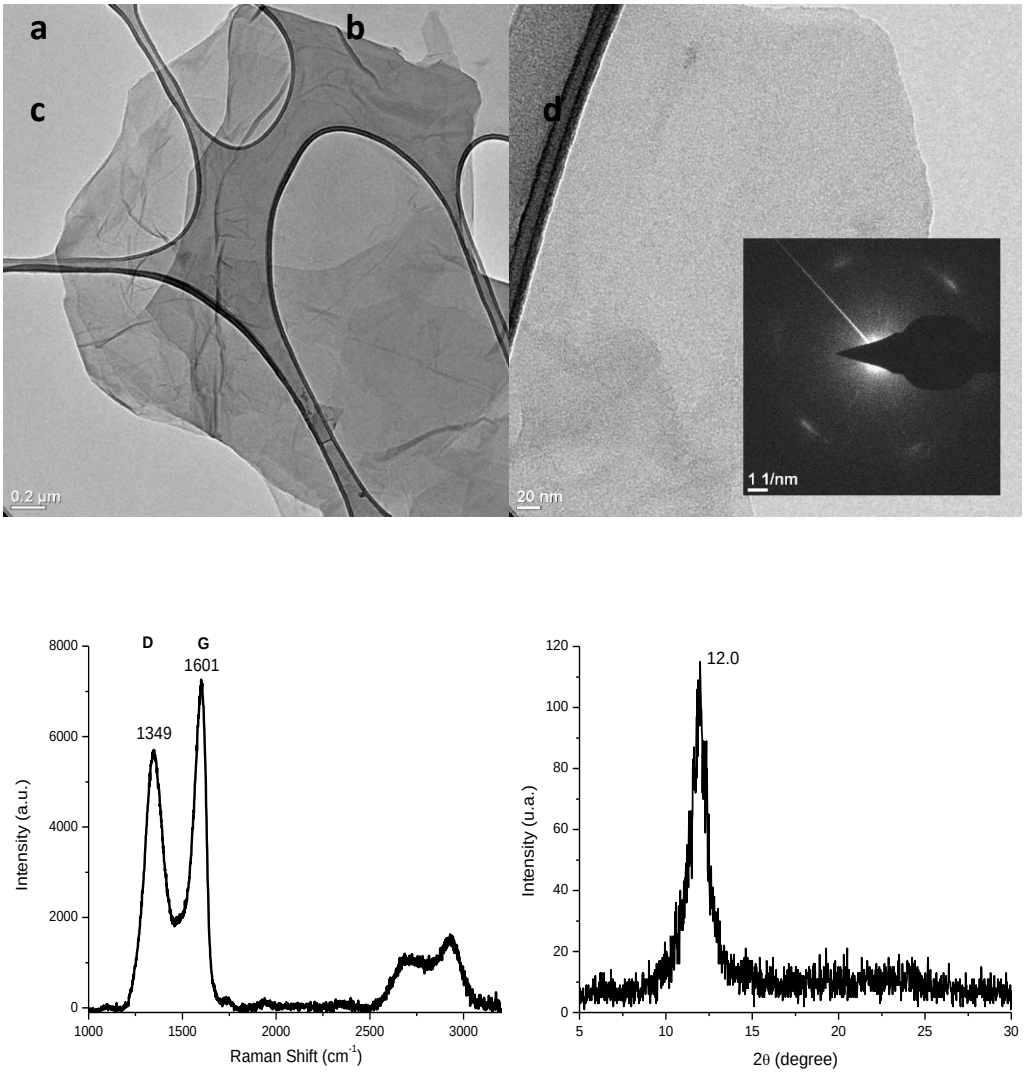

Figure 6.1. GO data; a) and b) TEM images of graphene oxide on lacey carbon, inset: SAED showing diffraction spots of hexagonal patterns; c) Raman

spectrum with 532 nm excitation d) XRD pattern showing (002) with d= 0.737 nm.

A scheme of the Layer by Layer assembly applied on the erythrocytes for the deposition of GO and polymers, as well as for the subsequent NaOCl oxidation and capsule generation, is represented in Fig. 6.2. In the first step, the red blood cells are crosslinked with glutaraldehyde. The crosslinking is necessary to insure that the polyelectrolytes will not disrupt the erythrocyte membrane. Erythrocytes were chosen because of their simple structure that lacks a nucleus, which makes the degradation of the whole cell content with NaOCl solution easier. Before the coating with GO, four layers of PSS/PAH were assembled on top of the cell. Despite the erythrocytes have a slightly negative charged surface the first assembled layer was PSS, which is also negative. We have observed earlier that the PSS assembles better as first layer on the cells causing significantly less aggregation of the cells.[10] The coating of the cells with an initial film of PSS/PAH is done to ensure a homogenously charged surface prior to the GO deposition. The assembly of the polyelectrolytes in the first layers and between the GO was done in 0.5 M NaCl as in these salt conditions the polymers assemble in a denser and compact structure, due to the optimal coiled conformation of the PEs at this ionic strength.

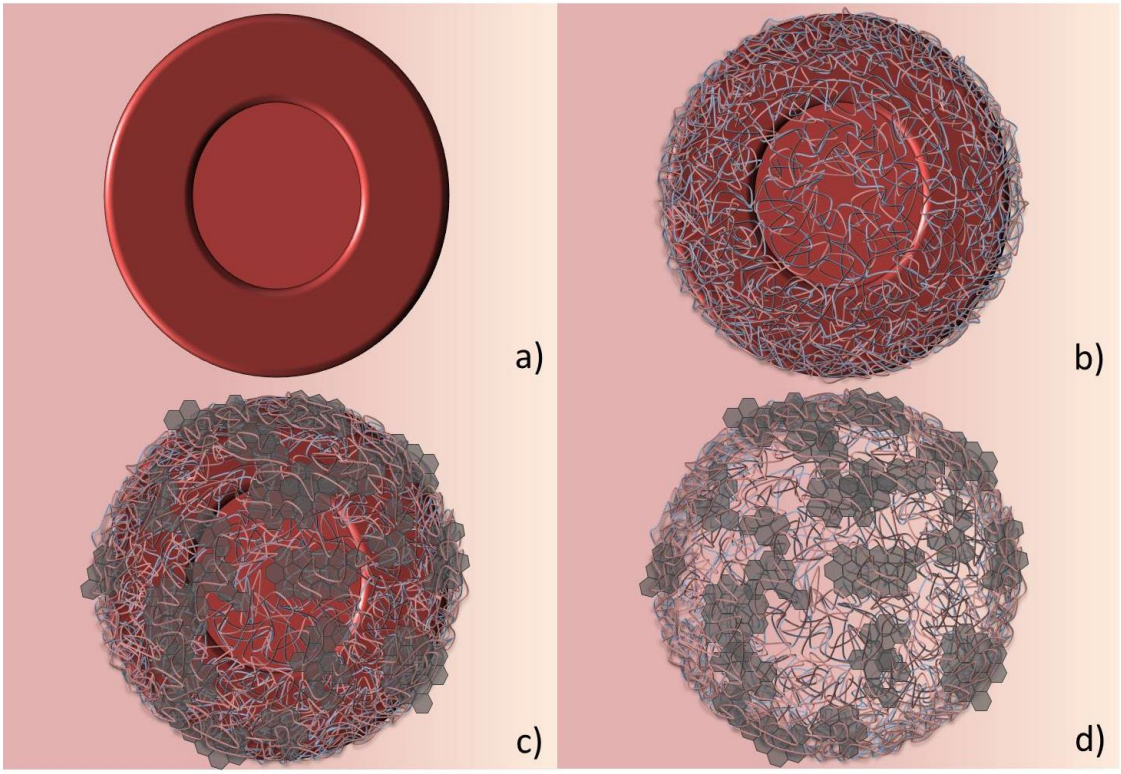

Figure 6.2. Schematic illustrations of a) the glutaraldehyde fixed red blood cells, b) the fixed erythrocytes coated with 4 layers of PSS/PAH, c) the fixed cells in (b) coated with additional GO/polyelectrolyte layers and d) the hybrid GO/polyelectrolyte capsule after NaOCl oxidation of the cell. *(Illustration courtesy of Eleftheria Diamanti).*

The assembly of exfoliated GO was done in water at pH 10 to avoid the screening of the charges on the GO. If present, screening the GO charges could lead to a stronger interaction between GO sheets in solution leading to aggregation. Charge screening would also eventually reduce the electrostatic interaction between the GO and the polyelectrolyte on the cell, which would be unfavourable for assembly. Between each GO deposition, we deposited either one layer of PAH or three layers of PAH/PSS/PAH. Since the assembly of one layer of PAH between the GO layers may not be sufficient to lead to a complete

coating of the surface and full recharging, we additionally prepared capsules assembling three polyelectrolyte layers in between the GO layers. The addition of three polyelectrolyte layers on top of the GO layer makes the procedure more time consuming but we observe a major improvement in the stability of the coated cell, thus reducing aggregation.

The removal of the cell interior by NaOCl is based on the oxidation of the cell content. The cell interior is mainly formed by proteins, which are oxidized defragmented in presence of NaOCl and are easily eliminated during centrifugation and washing cycles with NaCl and water. Oxidation also affects the PAH within the layers but a thin polymer film remains as was shown previously.[23] The possible oxidation of the GO with NaOCl would increase the percentage of negative charge on the GO surface.

The morphology and structural characteristics of the capsules were first studied by TEM which also provided proof of the core removal. Fig. 3a shows an image of the capsules prepared as a control, which do not contain GO. They clearly retain the shape of the erythrocytes used as templates. The capsules contain only water and collapse in the dry state to ellipsoid shaped films. The drying process is responsible for the appearance of edges on the capsule surface.

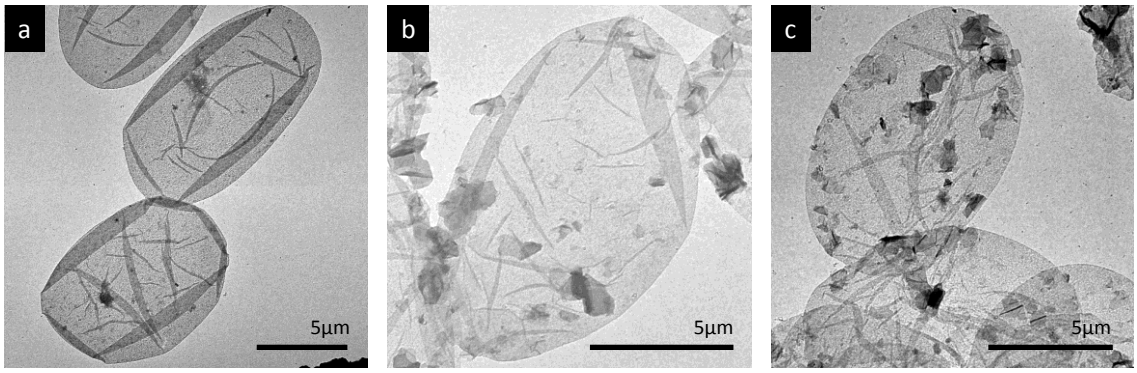

Figure 6.3. TEM micrographs of a) sample 1: $(PSS/PAH)_{4.5}^{0.5M}$, b) sample 2: $(PSS/PAH)_2^{0.5M}$ + [GO/$(PAH/PSS/PAH)^{0.5M}$ /GO] + $(PSS/PAH)^{0.5M}$, c) sample 3 (PSS/PAH)20.5M + $[GO/PAH]_{2.5}$ + $(PSS/PAH)^{0.5M}$ using a concentration of 0.1 mg/ml^{-1} of GO during the assembly.

In Fig. 6.3b and c we observe two examples of capsules fabricated with GO at a 0.1 $mgml^{-1}$ concentration with 1 PAH layer and three PAH/PSS/PAH layers in between the GO. As for the polyelectrolyte capsules, the GO capsules also retain the shape and size of the cells used as templates. The GO capsules are also empty as they are in a collapse state after drying. On the capsule wall we can recognize the presence of a structure of patches, with dimensions between a few hundred of nanometers and 1 micron. GO is recognized in the structure but embedded within the polyelectrolyte materials. The patches have the characteristic µm range size of the GO sheets. GO is present on some random spots in the capsule, the rest of the capsule structure is very similar to the control capsules. The patches have the characteristic µm range size of the GO sheets.

We decided to increase the concentration of GO to 0.2 $mgml^{-1}$ in order to increase the GO present on the coating. For this GO concentration TEM imaging reveals that indeed the GO coating has become visible all over the surface of the capsules as can be appreciated in Fig. 6.4.

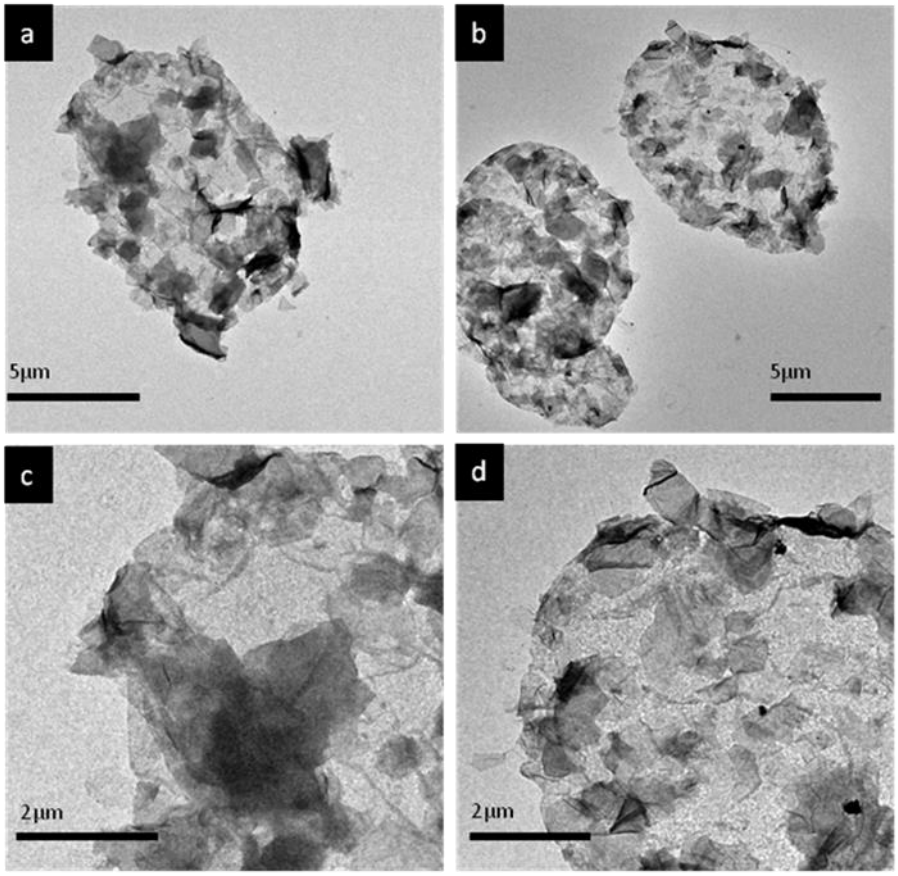

Figure 6.4. TEM micrographs of a) sample 2: $(PSS/PAH)_2^{0.5M}$ + $[GO/(PAH/PSS/PAH)^{0.5M}/GO]$ + $(PSS/PAH)^{0.5M}$, b) sample 3: $(PSS/PAH)_2^{0.5M}$ + $[GO/PAH]_{2.5}$ + $(PSS/PAH)^{0.5M}$, c-d) magnification of samples 1, 2 respectively. GO concentration was 0.2 $mgml^{-1}$.

In Fig. 6.4 a) and b) the capsules are prepared as in Fig. 6.3 a) and b) but with a GO concentration of 0.2 $mgml^{-1}$ instead of 1 $mgml^{-1}$. Fig. 6.4 c) and d) are magnifications of a selected area from the corresponding capsules represented

in Fig. 6.4 a and b, respectively. The GO sheets can be recognized all over the surface. Presumably, there is more GO deposited in the areas that show more contrast. The presence of these darker areas could imply that there may be GO stacking on top of previously assembled GO but still separated by PEs. The TEM images also confirm that by increasing the GO concentration, there is a complete coverage of the capsules with GO, which is not observed at the 1 mg ml^{-1} concentration. The TEM images also proves the formation of a complete and continuous coating of the capsule surface with GO with only three layers of GO being assembled, which, interestingly, is not obtained for the same number of layers on a planar surface. The use of a layer of PAH or three polyelectrolyte layers between the GO assemblies does not seem to affect the integrity of the capsules. Accordingly, we proceeded with the assembly with just one intermediate polyelectrolyte layer, which results in a reduced number of steps during the assembly for ease of fabrication.

Although the GO sheets can be recognized by their characteristic shape, we performed confocal Raman microscopy imaging to provide additional proof that the patches on the capsule wall correspond to GO. A representative scan on one capsule is shown in Fig. 6.5 a.

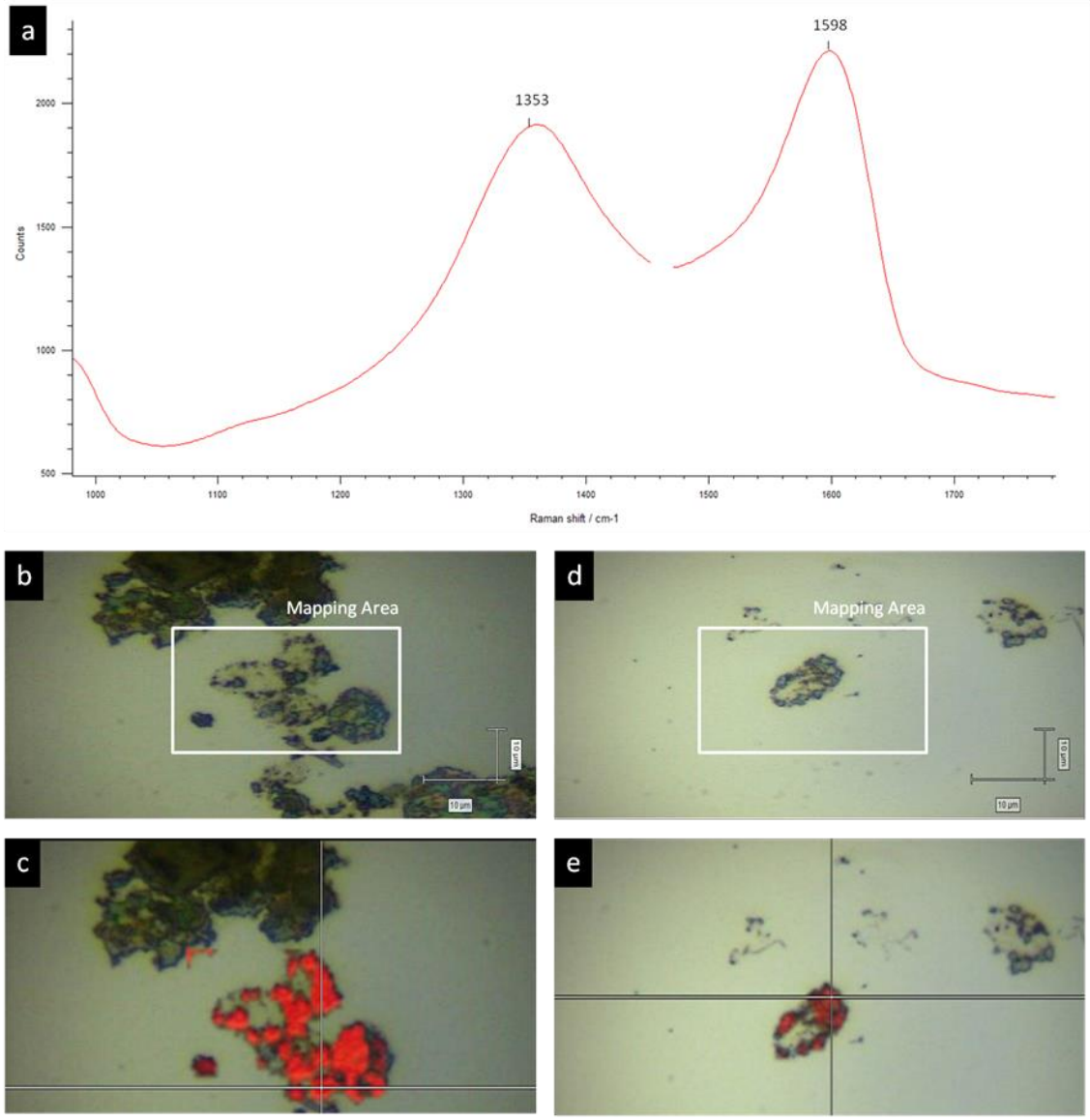

Figure 6.5. Raman of the GO-capsules. a) Raman spectra of GO sheets, G band located at 1598 cm^{-1} and D band at 1353 cm^{-1}. b) Image of the sample 2: $(PSS/PAH)_2^{0.5M}$ + [GO/$(PAH/PSS/PAH)^{0.5M}$ /GO] + $(PSS/PAH)^{0.5M}$ capsules onto Si wafer with the selected area to be analysed. c) Mapping by intensity of the G band at 1598 cm^{-1} of the area selected in b. d) Image of sample 3 $(PSS/PAH)_2^{0.5M}$ + $[GO/PAH]_{2.5}$ + $(PSS/PAH)^{0.5M}$ capsules onto Si wafer with the selected area to be analysed. e) Mapping by intensity of the G band at 1598 cm^{-1} of the area selected in d.

The surface of the capsule was scanned point by point. At each point, the Raman spectra revealed the presence of characteristic and strong bands at 1353 and 1598 cm^{-1}, which are typical for the GO and graphene structures and which cannot be detected in the capsules prepared solely with polyelectrolytes. The peaks in the Raman spectra of the capsules correspond to the G and D bands observed in the pristine GO (*vide supra*), with the typical shift in the G band to higher frequencies for GO with respect to graphite.[20]

In order to determine the thickness of the capsule walls we performed AFM imaging of the capsules in the collapsed state. From the AFM images, see in Fig. 6 a, an estimated maximal thickness of about 30 nm could be determined for the capsules, implying a thickness in the order of 10-19 nm for the walls of the capsule in the dry state. These values are obtained assuming that the thickness of the collapsed capsule is twice the thickness of the capsule wall since the capsule loose internal volume when drying. These values are taking from the maximal and minimal thickness measured for the capsule. AFM imaging also confirmed the stability of the capsules, which retain their shape and integrity after collapsing in air, Fig. 6.6 b.

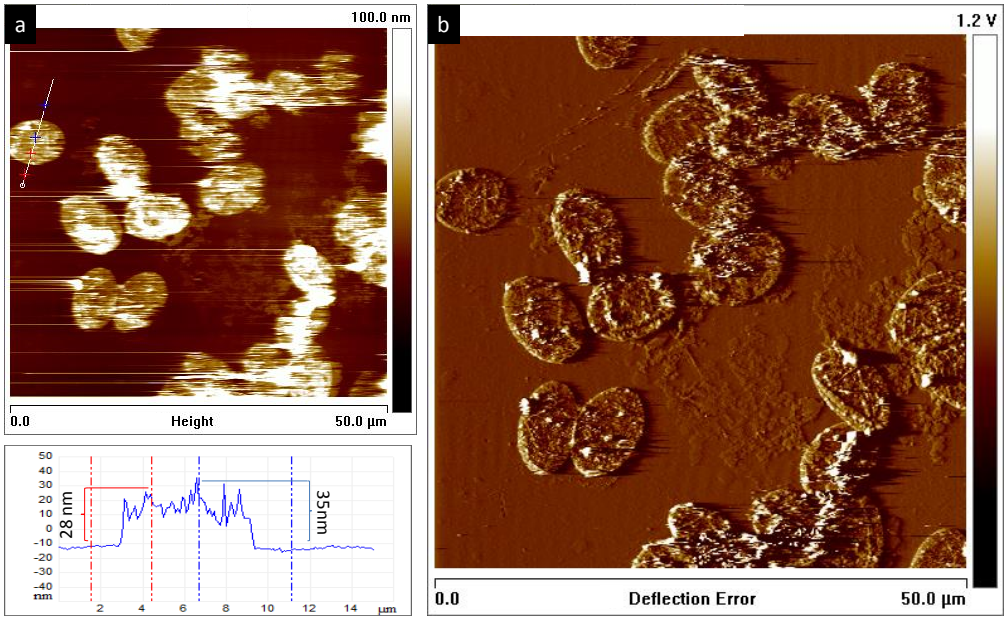

Figure 6.6. Atomic force microscope images of dried hybrid PE/GO capsules. a) Height image of a 50 x 50 µm image, with a profile corresponding to the line drawn in the image. b) Deflection image of the same area analysed in a).

6.4 Conclusions

We have shown that 3D micron sized objects in the form of capsules can be fabricated on the basis of the LbL assembly of GO and polyelectrolytes on top of fixed erythrocyte cells as templates. TEM imaging revealed a surface structure composed of GO sheets when the GO assembly was performed with a high GO concentration. The presence of GO was confirmed by Raman spectro-microscopy that revealed the presence of the GO in the capsule structure. AFM revealed that the capsule walls are thin films with a thickness of ~ 15 nm. Our result shows an alternative method for the fabrication of capsules entailing GO in a dense arrangement that could eventually have applications in drug delivery and optoelectronics by developing hybrid thin polymer films containing graphene oxide or its reduced form rGO.

The work presented in this chapter resulted in the following publication:

Irigoyen, J.; Politakos, N.; Diamanti, E.; Rojas, E.; Marradi, M.; Ledezma, R.; Arizmendi, L.; Rodríguez, J. A.; Ziolo, R. F.; Moya, S. E. *Beilstein J. Nanotechnol.* **2015**, *6*, 2310–2318.

6.5 References

(1) Tasis, D.; Papagelis, K.; Spiliopoulos, P.; Galiotis, C. *Mater. Lett.* **2013**, *94*, 47–50.

(2) Nicolosi, V.; Chhowalla, M.; Kanatzidis, M. G.; Strano, M. S.; Coleman, J. N. *Science (80-.).* **2013**, *340* (6139), 1226419.

(3) Hernandez, Y.; Lotya, M.; Rickard, D.; Bergin, S. D.; Coleman, J. N. *Langmuir* **2010**, *26* (5), 3208–3213.

(4) Dreyer, D. R.; Park, S.; Bielawski, C. W.; Ruoff, R. S. *Chem. Soc. Rev.* **2010**, *39* (1), 228–240.

(5) Si, Y.; Samulski, E. T. *Nano Lett.* **2008**, *8* (6), 1679–1682.

(6) Hassouna, F.; Kashyap, S.; Laachachi, a.; Ball, V.; Chapron, D.; Toniazzo, V.; Ruch, D. *J. Colloid Interface Sci.* **2012**, *377* (1), 489–496.

(7) Gao, X.; Jang, J.; Nagase, S. *J. Phys. Chem. C* **2010**, *114* (2), 832–842.

(8) Decher, G. *Science (80-.).* **1997**, *277* (5330), 1232–1237.

(9) Yang, M.; Hou, Y.; Kotov, N. a. *Nano Today* **2012**, *7* (5), 430–447.

(10) Kotov, N. A.; Dekany, I.; Fendler, J. H. *Adv. Mater.* **1996**, *8* (8), 637–641.

(11) Donath, E.; Moya, S.; Neu, B.; Sukhorukov, G. B.; Georgieva, R.; Voigt, A.; Baumler, H.; Kiesewetter, H.; Mohwald, H. *Chemistry* **2002**, *8* (23), 5481–5485.

(12) Moya, S. E.; Georgieva, R.; Bäumler, H.; Richter, W.; Donath, E. *Med. Biol. Eng. Comput.* **2003**, *41* (4), 504–508.

(13) Georgieva, R.; Moya, S.; Hin, M.; Mitlöhner, R.; Donath, E.; Kiesewetter, H.; Möhwald, H.; Bäumler, H. *Biomacromolecules* **2002**, *3* (3), 517–524.

(14) Hong, J.; Char, K.; Kim, B.-S. *J. Phys. Chem. Lett.* **2010**, *1* (24), 3442–3445.

(15) Kurapati, R.; Raichur, A. *M. Chem. Commun.* **2012**, *48* (48), 6013.

(16) Hummers, W. S.; Offeman, R. E. *J. Am. Chem. Soc.* **1958**, *80* (6), 1339.

(17) Kovtyukhova, N. I.; Ollivier, P. J.; Martin, B. R.; Mallouk, T. E.; Chizhik, S. A.; Buzaneva, E. V; Gorchinskiy, A. D. *Chem. Mater.* **1999**, *11* (3), 771–778.

(18) Gao, C.; Leporatti, S.; Moya, S.; Donath, E.; Möhwald, H. *Chem. – A Eur. J.* **2003**, *9* (4), 915–920.

(19) Kim, T.; Chang Kang, H.; Thanh Tung, T.; Don Lee, J.; Kim, H.; Seok Yang, W.; Gyu Yoon, H.; Suh, K. S. *RSC Adv.* **2012**, *2* (23), 8808–8812.

(20) Kudin, K. N.; Ozbas, B.; Schniepp, H. C.; Prud'homme, R. K.; Aksay, I. A.; Car, R. *Nano Lett.* **2008**, *8* (1), 36–41.

(21) Jeong, H.-K.; Lee, Y. P.; Lahaye, R. J. W. E.; Park, M.-H.; An, K. H.; Kim, I. J.; Yang, C.-W.; Park, C. Y.; Ruoff, R. S.; Lee, Y. H. *J. Am. Chem. Soc.* **2008**, *130* (4), 1362–1366.

(22) Lee, D. W.; De Los Santos V., L.; Seo, J. W.; Felix, L. L.; Bustamante D., A.; Cole, J. M.; Barnes, C. H. W. *J. Phys. Chem. B* **2010**, *114* (17), 5723–5728.

(23) Moya, S.; Dähne, L.; Voigt, A.; Leporatti, S.; Donath, E.; Möhwald, H. *Colloids Surfaces A Physicochem. Eng. Asp.* **2001**, *183-185* (0), 27–40.

Conclusions

The main goal of this thesis is the study of multilayered assembled structures of polyelectrolytes solely or combined with carbon nanomaterials in order to use them for specific applications such as nanofiltration membranes and smart surfaces. Physico-chemical studies of PEM stability in different media, the assembly of the multilayers in extreme ionic strength conditions and study of different growth regimes by choosing different pairs of polycations and polyanions have been additionally performed.

Combined polyelectrolyte and carbon nanomaterial hybrid materials have been also created. Carbon nanotubes have been used to fabricate an intermediate layer acting as a spacer between commercial porous supports and PEMs for applications in nanofiltration. A novel approach to combine polyelectrolytes with graphene oxide producing capsules using erythrocytes as templates with a tuneable content in carbon has also been performed.

MULTILAYERED POLYELECTROLYTE MEMBRANES

In chapter 2, the differences in the assembly between two different polycations, PDADMAC showing a supralinear growth and PVBTMAC which displays a linear growth have been discussed. The assembly of PVBTMAC/PSS creates denser and less hydrated PEMs than the PDADMAC/PSS assembly. PBVTMAC/PSS PEMs are also more hydrophilic and they act as better insulators. Their permeability seems not to vary with the number of layers after

a certain number of layers have been assembled and their insulating behaviour increases in a regular fashion with the number of layers assembled. The PDADMAC/PSS PEMs on the other hand grow in a supralinear fashion, creating sponge-like multilayers especially when more than 11 layers are assembled. The nature of these multilayers is more hydrophobic than those of PVBTMAC/PSS. PDADMAC/PSS systems also act as insulators and are more efficient with increasing numbers of layers. A particular phenomenon has been observed during the electrochemical experiments performed, when more than 11 layers have been assembled, there is complex formation between the quaternary amines of the PDADMAC and the ferro species used as an electrochemical probe, the multilayer behaves as an electron regulating interface affecting how charge transfer along the membrane is produced and its capacity as an insulator. Even if the multilayer is thicker than the PVBTMAC/PSS one, the current reduction is more effective in the latter.

In chapter 3, di-block PEMs with a top removable block have been fabricated. We have prepared different polyelectrolyte combinations: (PAH/PSS)-(PDADMAC/PAA), (PAH/PSS)-(PDADMAC/PSS) and (PEI/PSS)-(PEI/PAA) showing that, depending on the particular combination of polyelectrolyte chosen, different procedures can be applied to remove the top layers: pH variations, and treatment with the TTAB and SDS surfactants.

The removal of the top layers does not affect, in most cases, the 1st block of the PEM, which is fabricated upon polyelectrolytes that are resistant to the stimuli

that leads to the removal of the top block. There is a certain interdigitation between the stacks, making the removal of the top blocks less pronounced than the removal of top block if it were standing alone without the supporting stack. Foulant present on top of the PEM, as shown for BSA, can be removed together with the top layers applying the corresponding stimuli. Surprisingly, the removal of the top block is enhanced in the presence of BSA and in the case of the di-block PEI/PSS with PEI/PAA on top the presence of BSA leads to complete removal of the PEMs after SDS treatment.

Once the layers have been removed they can be rebuilt free from foulants. The whole procedure from the regeneration to the removal can be repeated several times.

If applied to a filtration membrane the removal and reassembly could extend the operative life of the membrane.

In chapter 4, PEMs with the ability to collapse, displaying a variation in thickness of 200 nm, approximately a 46 % reduction in its thickness, have been fabricated by assembling PDADPMAC/PSS at 3 M NaCl. PEM assembly at 3 M NaCl with the chains highly coiled results in a high content of water entrapped between polyelectrolyte chains. PDADMAC assembles at these conditions with a higher water content with respect to PSS as has been measured by combined ellipsometry-qcm. When reducing the ionic strength to that of pure water the chains expand and flatten, thus occupying lateral space and removing the water between chains. As a consequence, the thickness of the PEM is reduced. An

increase in the ionic strength to 3 M NaCl reverses the process and the film stands up and regains the lost water. Such a PEM film could have interesting applications, such as nanoactuators or controllable barrier applications where polyelectrolyte brushes are frequently applied, with the advantage that the response of the PEMs to varying ionic strength would be opposite to that observed by a brush. Additionally, the thickness of the film can be easily controlled over a few hundred nanometres by controlling the number of polyelectrolyte layers assembled.

HYBRID POLYELECTROLYTE-CARBON NANOMATERIALS

In chapter 5, a hybrid nanofiltration membrane has been fabricated based on the assembly of a PDADMAC/PSS polyelectrolyte multilayer on top of a multilayer of MWCNTs. The MWCNTs layer act as a spacer layer between the membrane support and the polyelectrolyte multilayer. The spacer results in a dense polyelectrolyte multilayer assembly that covers the pores present in the MWCNT layer. The assembly of the PEMs on top the support without the MWCNT layer fails to cover the pores present on the membrane substrate for the same or greater numbers of layers assembled in the PEM as on top of the MWCNTs. The spacing of the PEM from substrate has the additional advantage of increasing the flux through the pores of the support as the volume going through a pore is collected from a larger area of the PEM with the MWCNTs acting as a funnel. The performance of the PEM supported on the MWCNT layer is significantly better than the PEM without CNTs. A PEM of 3

bilayers of PDADMAC/PSS on a MWCNT spacer showed a rejection for $MgSO_4$ of around 84 % while in the best case without MWCNT for a PEM of 5 bilayers a rejection of 59 % was observed. The PEMs on MWCNT show a large rejection difference for mono and divalent ions making them very appealing for separating ion mixtures.

The assembly of the PEMs on top of the MWCNTs as an intermediate layer results in the formation of denser PEM membranes with a high charge density as needed for the divalent salt rejection and for a high stability with increasing flux, indeed with only 3 polyelectrolyte bilayers a significantly higher performance is achieved compared to with 5 bilayers on a SiC membrane without a MWCNT support.

In the last chapter, we have shown that 3D micron sized objects in the form of capsules can be fabricated on the basis of the LbL assembly of GO and polyelectrolytes on top of fixed erythrocyte cells as templates. TEM imaging revealed a surface structure composed of GO sheets when the GO assembly was performed with a high GO concentration. The presence of GO was confirmed by Raman spectro-microscopy that revealed the presence of the GO in the capsule structure. AFM revealed that the capsule walls are thin films with a thickness of ~ 15 nm. Our results show an alternative method for the fabrication of capsules involving GO in a dense arrangement that could eventually have applications in drug delivery and optoelectronics by

developing hybrid thin polymer films containing graphene oxide or its reduced form rGO.

List of Publications

(1) García, T. A.; Gervasi, C. A.; Rodríguez Presa, M. J.; **Irigoyen Otamendi, J.**; Moya, S. E.; Azzaroni, O. *J. Phys. Chem. C* **2012**, *116* (26), 13944–13953.

(2) **Irigoyen, J.**; Han, L.; Llarena, I.; Mao, Z.; Gao, C.; Moya, S. E. *Macromol. Rapid Commun.* **2012**, *33* (22), 1964–1969.

(3) Alonso, T.; **Irigoyen, J.**; Iturri, J. J.; Larena, I. L.; Moya, S. E. *Soft Matter* **2013**, *9* (6), 1920–1928.

(4) **Irigoyen, J.**; Arekalyan, V. B.; Navoyan, Z.; Iturri, J.; Moya, S. E.; Donath, E. *Soft Matter* **2013**, *9* (48), 11609–11617.

(5) Moya, S. E.; **Irigoyen, J.** *J. Polym. Sci. Part B Polym. Phys.* **2013**, *51* (14), 1068–1072.

(6) Coustet, M.; **Irigoyen, J.**; Garcia, T. A.; Murray, R. A.; Romero, G.; Susana Cortizo, M.; Knoll, W.; Azzaroni, O.; Moya, S. E. *J. Colloid Interface Sci.* **2014**, *421*, 132–140.

(7) **Irigoyen, J.**; Politakos, N.; Murray, R. A.; Moya, S. E. *Macromol. Chem. Phys.* **2014**, *215* (16), 1543–1550.

(8) Gu, H.; Ciganda, R.; Castel, P.; Vax, A.; Gregurec, D.; **Irigoyen, J.**; Moya, S.; Salmon, L.; Zhao, P.; Ruiz, J.; Hernández, R.; Astruc, D. *Chem. – A Eur. J.* **2015**, *21* (50), 18177–18186.

(9) **Irigoyen, J.**; Iturri, J.; Camacho, J. L.; Donath, E.; Moya, S. *MRS Online Proc. Libr. Arch.* **2015**, *1754*, 53–58.

(10) **Irigoyen, J.**; Politakos, N.; Diamanti, E.; Rojas, E.; Marradi, M.; Ledezma,

R.; Arizmendi, L.; Rodríguez, J. A.; Ziolo, R. F.; Moya, S. E. *Beilstein J. Nanotechnol.* **2015**, *6*, 2310–2318.

(11) Marmisollé, W. A.; **Irigoyen, J.**; Gregurec, D.; Moya, S.; Azzaroni, O. *Adv. Funct. Mater.* **2015**.

(12) Qiu, Y.; Rojas, E.; Murray, R. A.; **Irigoyen, J.**; Gregurec, D.; Castro-Hartmann, P.; Fledderman, J.; Estrela-Lopis, I.; Donath, E.; Moya, S. E. *Nanoscale* **2015**, *7* (15), 6588–6598.

(13) Rapakousiou, A.; Deraedt, C.; **Irigoyen, J.**; Wang, Y.; Pinaud, N.; Salmon, L.; Ruiz, J.; Moya, S.; Astruc, D. *Inorg. Chem.* **2015**, *54* (5), 2284–2299.

(14) **Irigoyen, J.**; Laakso, T.; Politakos, N.; Dahne, L.; Pihlajamäki, A.; Mänttäri, M.; Moya, S. E. *Macromol. Chem. Phys.* **2016**, *217*(6), 804-811.

(15) Wang, C.; Ciganda, R.; Salmon, L.; Gregurec, D.; **Irigoyen, J.**; Moya, S.; Ruiz, J.; Astruc, D. *Angew. Chemie Int. Ed.* **2016**, *55* (9), 3091–3095.

(16) Muzzio, N. E.; Gregurec, D.; Diamanti, E.; **Irigoyen, J**.; Pasquale, M. a.; Azzaroni, O.; Moya, S. E. *Adv. Mater. Interfaces* **2016**, accepted in press.

(17) Diamanti, E.; Muzzio, N.; Gregurec, D.; **Irigoyen, J**.; Pasquale, M.; Azzaroni, O.; Brinkmann, M.; Moya, S. E. *Colloids Surfaces B Biointerfaces* **2016**, accepted in press.

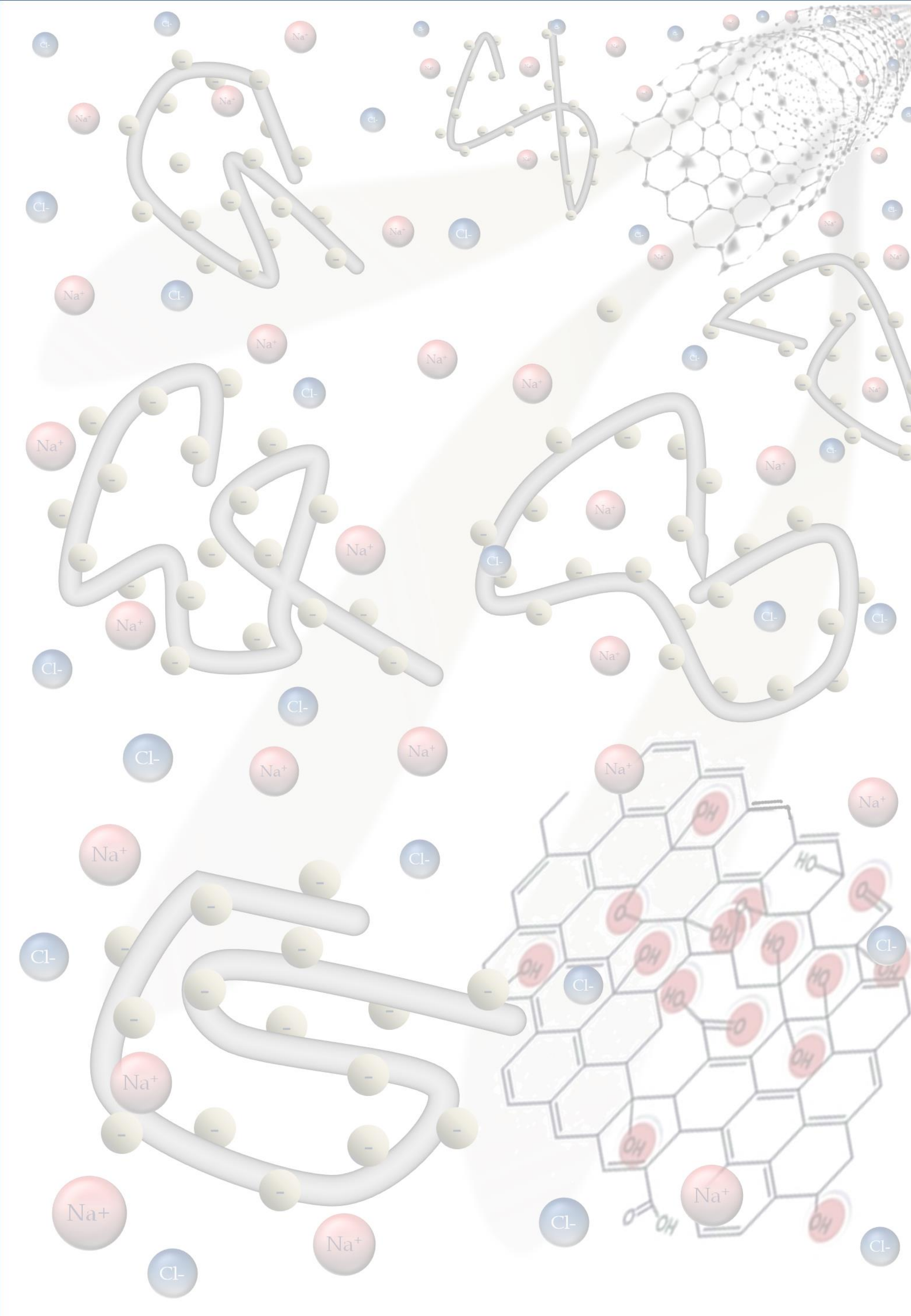
Na$^+$
Cl-
Na+
OH
HO